UNIVERSITY OF CALIFORNIA,
IRVINE

Scanning Tunneling Investigation of Olefin Dehydrogenation on Platinum Single Crystal and $Pt/Al_2O_3/NiAl(110)$ Model Catalysts

DISSERTATION

submitted in partial satisfaction of the requirements
for the degree of

DOCTOR OF PHILOSOPHY

in Chemistry

by

Safa S-S Khan

Dissertation Committee:
Professor John C. Hemminger, Chair
Professor Barbara Finlayson-Pitts
Professor Sergey Nizkorodov

2015

DEDICATION

To

my parents, husband, son, siblings, in-laws and friends

for being my light when it is dark,

for being my anchor when it is stormy,

for being my compass when I am lost,

for being my advocate when my voice is absent.

You all have taught me to be a better person and have guided me to success.

TABLE OF CONTENTS

LIST OF FIGURES

LIST OF TABLES

ACKNOWLEDGMENTS

It takes a village to raise a child. Analogously, it takes an entire school system to raise a doctor. I cannot thank every individual who has helped me and guided me along the way – that would be a book in itself. Firstly, I thank my advisor, John C. Hemminger. His patience and support have helped me complete my degree. No matter how ignorant or naïve my questions may have been, he has always guided me without malice and always with care.

Thank you to Hemminger past and present group members for supporting me and giving me invaluable advice on graduate school and running experiments. Notably, I give thanks to Ana De La Ree and Guofeng Sun for patiently training me on our chamber and on imaging with STM. Without them, I would have had a much more difficult time learning how to troubleshoot all the disasters and breakdowns that occur on regular basis. I also would like to especially thank Wenbo Yan and Jayde Kwon for their guidance and support.

Thanks to Wilson Ho for helping me learn the finer points of troubleshooting STM failures. He turned nightmares into successes.

I would like to thank my committee members. Thanks to Sergey Nizkorodov for treating me like his own student and making me feel welcome in the department. Thanks to Barbara Finlayson-Pitts for her guidance and being an example of what women can do against many odds.

Thank you Melissa Sweet and Patricia Terrell for helping organize all of my conference trips and all of the special events that make for a well rounded graduate school experience.

I would also like to give a special thanks to Cyril McCormick and Lee Moritz. You two have helped save many of the components to my chamber.

Thank you to both NASA and Department of Education GAANN program for providing me with fellowships that have made this entire process much easier. I would also like to thank the Department of Energy (DOE) for funding my projects.

I thank my family, especially my husband, parents, in-laws, and son. They have helped me stay sane during all the tough times. They kept me smiling and laughing when times were trying.

Most importantly, thank you God for giving me the opportunity to finish my PhD.

CURRICULUM VITAE

Safa Shakir-Shatnawi Khan

EDUCATION

University of California, Irvine, Irvine, CA
Ph.D. in Chemistry (Emphasis in Atmospheric/Physical Chemistry) January 2015
Masters in Chemistry June 2010

University of Washington, Seattle, WA
Bachelor of Science in Chemistry June 2008
Bachelor of Science in Biology: Physiology June 2008
Bachelor of Arts in Near Eastern Studies: Languages and Civilizations June 2008

University of California, Davis, Davis, CA 2003 – 2005

RESEARCH EXPERIENCE

Graduate Student Researcher - Department of Chemistry, UC Irvine 2008-present

- Analyzed the mechanistic details of heterogeneous catalyst reactions of hydrocarbons on platinum under the supervision of John Hemminger, PhD.
- Perfected a multitude of techniques, such as STM (Surface Tunneling Microscope) and AES (Auger Electron Spectroscopy).
- Wrote the manual to the FTMS-STM Instrument.

Research Investigator - Department of Atmospheric Sciences, University of Washington 2007-2008

- Investigated the origin and column values of tropospheric BrO in Antarctica under the supervision of Chemist Joel Thornton, PhD.
- Utilized MATLAB, a technical computing language to compare results with Global Ozone Monitoring Experiment (GOME).

Clinical Research Investigator - King County EMS, University of Washington 2006-2007

- Worked closely with Hendrika Meischke, PhD, on an exposition regarding white coat hypertension in the pre-hospital setting.
- White coat hypertension is a common cause of clinical hypertension and given the paucity of data on this topic our team analyzed and presented the available information in a clinical literature review (published).

Lab Assistant III - Veterinary Medicine, Department of Health and Reproduction, UC Davis 2004-2005

- Organized and carried out various experiments as part of a team to verify the destruction of pathogens in East Bay Municipal Utilities District in modified sewage treatment procedures using polio and hepatitis B as examples of pathogens.
- Mastered cell culturing, staining and RT-PCR.
- Gained the experience and expertise *in vitro* bacterial cell culture.

Research Investigator - Center for Neuroscience, UC Davis 2003-2005

- Conducted research under the supervision of Natalie Kacinik, PhD, and Kathleen Baynes, PhD, on aphasias of the brain and how linguistic disorders are mentally represented.
- Worked with fMRI scans, and preparing lists of experimental stimuli/data.

TEACHING EXPERIENCE

Pedagogical Training - University of California, Irvine Present

- Engaged in a quarter long class that surveyed chemical education literature on active learning in traditional lecture, hybrid classroom environments, and online learning. The course also covered different teaching formats.

Teaching Assistant - University of California, Irvine 2009 and 2012

- Prepared and taught lectures for both the discussion and lab sections for general chemistry.
- Planned lessons and assignments for classes of up to 35 students.
- Graded papers and exams.

Teaching Assistant - AirUCI Summer Teaching Program 2011

- Taught laser-induced breakdown spectroscopy (LIBS) to high-school science teachers.
- Helped develop the lab manual for this class.

CPR Instructor - Seattle, WA and Davis, CA 2004-2008

- Taught CPR to the members of Al-Shifa Clinic in Seattle and health care professionals in Davis.

ACADEMIC AND PROFESSIONAL SERVICE

Member - Iota Sigma Pi, National Honor Society of Women in Chemistry 2009-Present

- Retained membership in this society that promotes interest in chemistry among women and helps stimulate accomplishment and advancement in academic, business and social life.
- Volunteered for a community outreach program where children in the local area learn science and conduct experiments.

Founding Board Member - Crescent Free Clinic of Orange County 2008-Present

- Trained and mentored undergraduates to run a free healthcare clinic for the underserved communities of Orange County.

Founding Director of Volunteer Services – Al-Shifa Clinic, University of Washington 2005-2008

- Founded the only open University of Washington student-run free clinic.
- Led 18 undergraduates divided into 3 teams and managed clinic financing, education and prevention, and outreach.

Layout Manager & Writer - Ergo Sum, UC Davis 2004-2005

- Taught writers how to format articles for this journal of bioethics and the philosophy of Science.
- Supervised the layout of this unique campus-wide published journal.

Founding President - Help and Education Leading to Prevention (HELP) Club, UC Davis 2004-2005

- Directed this organization to help the homeless populations of Sacramento and Yolo counties.

Secretary - Neurobiology, Physiology, and Behavior Club, UC Davis 2004-2005

- Expanded the community service events for the club, such as Relay for Life, Homeless Thanksgiving dinner, and many others.

Secretary - Middle East and South Asia Student Coalition, UC Davis 2004-2005

- Worked on ensuring that minority groups are fairly represented in the UC education system.

PUBLICATIONS

Khan SS, Hemminger JC. The Dehydrogenation of Ethylene on $Pt/Al_2O_3/NiAl(110)$ (*J. Phys. Chem. C*, in progress, 2015).

Khan SS, Sun G, De La Ree A, Hemminger JC. The Conversion of Small Hydrocarbons to Carbon Clusters on Platinum (*J. Phys. Chem. C*, in progress, 2015).

Khan, TV, Akhondi A, **Khan SS**. Intranasal Naloxone as Initial Treatment for Opioid Overdose in the Pre-hospital Setting. *EMS Professional,1(3)*:34-37 (2009).

Khan, TV, **Khan SS,** Akhondi A, Khan TW. White Coat Hypertension: Relevance to Clinical and Emergency Medical Services Personnel. *EMS Professional,1(2)*:16-21 (2009).

Khan, TV, **Khan SS,** Akhondi A, Khan TW. White Coat Hypertension: Relevance to Clinical and Emergency Medical Services Personnel. *Medscape General Medicine, 9(1)*: 52, 3-13-2007.

PRESENTATIONS

Khan SS, Hemminger JC. The conversion of olefins to carbon clusters on $Pt/Al_2O_3/NiAl(110)$, NASA Ames JPFP Symposium, San Jose, CA, July 22-26 2013.

Khan SS, Hemminger JC. The Investigation of Ethylenediamine Conversion to Cyanogen on Nickel, NASA MUST Symposium, Hyatt Orlando Airport Hotel, Orlando, Fl, July 19-22 2012.

Khan SS, Sun G, De La Ree A, Hemminger JC. The Conversion of Small Hydrocarbons to Carbon Clusters on Platinum, AVS 59th International Symposium and Exhibition, Tampa, Fl, Oct 31st 2012.

Khan SS, Sun G, De La Ree A, Hemminger JC. Poster Presentation of The Conversion of Small Hydrocarbons to Carbon Clusters on Platinum, SCCAVS Exhibition, Los Angeles, CA, Oct 3rd 2012.

Khan SS, Sun G, De La Ree A, Hemminger JC. The Conversion of Small Hydrocarbons to Carbon Clusters on Platinum, NASA Ames STEM Symposium, DoubleTree Hotel, San Jose, CA, July 25-29 2011.

AWARDS

- NASA Harriett G. Jenkins Pre-doctoral Fellowship (2010-2013) - NASA
- Graduate Assistance in Areas of National Need (GAANN) Fellowship (2008-2009) – US Department of Education
- Excellence in Academic Community Service Leadership – Al Shifa Clinic (2009)
- Dean's Honors List – The Dean of The College of Agricultural and Environmental Sciences at UC Davis (2004)

ABSTRACT OF THE DISSERTATION

Scanning Tunneling Investigation of Olefin Dehydrogenation on Platinum Single Crystal and $Pt/Al_2O_3/NiAl(110)$ Model Catalysts

By

Safa S-S Khan

Doctor of Philosophy in Chemistry

University of California, Irvine, 2014

Professor John C. Hemminger, Chair

Propylene and butylene thermal dehydrogenation have been studied on Pt(111) single crystal using Scanning Tunneling Microscopy (STM). Propylene and butylene were heated to 1000 K on the Pt single crystal. Both olefins formed uniform sized carbon clusters, with less than a monolayer coverage on the Pt surface. With cycles of continued dosing and heating, particles grew in number but not size. The catalytic activity stopped by the third saturation dose, leaving areas of bare Pt. Carbon clusters generated from the dehydrogenated propylene and butylene were approximately 1 Å in height and 12 Å in diameter. Propylene and butylene clusters contained an average of 44 and 51 carbon atoms per cluster respectively.

The reactions of Pt nanoparticles on $Al_2O_3/NiAl(110)$ were compared with those on the Pt single crystal. An Al_2O_3 thin film was formed with similar properties to previous alumina reported in literature. The Pt nanoparticles formed were circular, flat, and uniform in size (13 Å) and shape, corresponding to approximately 20 atoms. The Pt nanoparticles deposited only onto crystalline Al_2O_3 surfaces. Ethylene was then dosed onto the Pt. At 1000 K, ethylene deposited only onto the Pt nanoparticles and not onto the oxide layer. The thermally dehydrogenated

ethylene covered the Pt nanoparticles and particles grew to a maximum of 20 Å. Particle density did not increase at an annealing temperature of 1000 K. At 1100 K the density of particles increased and decorated the step edges.

Another set of experiments examined the dehydrogenation of ethylenediamine at 300-500 K on Ni(111). The goal of this study was to form cyanogen. The end result was unidentifiable via imaging by STM and cyanogen formation was not observed.

CHAPTER 1

Introduction

1.1 Background and Overview of the Thesis

To date, no accurate models predict reactions at the atomic surface interface. Predicative capabilities for surface reactions are not yet understood and the rules of surface science are mainly limited to empirical work. Surface properties are important factors in a large variety of fields including generating materials that have desired electronic properties and in generating materials with a high degree of stability. Understanding the fundamentals of surface molecular interactions allows for the design of new nanoscale materials. One of the main goals of this project is to study model heterogeneous catalyst systems in order to provide fundamental knowledge that can be applied towards theoretical studies and technological applications. Catalysts are highly important to industry as they reduce the energy requirement for a reaction to occur.[1] Thus lower temperatures and pressures are required for chemical processes.[2]

This project takes advantage of the superior atomic resolution imaging ability of scanning tunneling microscopy (STM) to reveal the surface morphology of reactions over model catalysts at the atomic level. All experiments are held under ultra high vacuum (UHV) in order to provide for a controlled environment. Chapter 2 discusses the experimental techniques used in the thesis as well as the general theory and experimental setup for UHV, auger electron spectroscopy (AES), and STM. Chapter 2 also gives a brief description and cleaning method for the model catalyst single crystal samples: Platinum(111), Nickel(111) and Nickel Aluminum(110).

Chapters 3 and 4 describe the formation of platinum over aluminum oxide on nickel aluminum ($Pt/Al_2O_3/NiAl(110)$). Pt is one of the most used and important heterogeneous catalysts in industry from chemical refinery to fuel cell storage.[3-7] The Pt particles are deposited

over an oxide support, as this provides stability to the adsorbed nanoparticles.[3,4] Ultrathin oxide supports are used in research as they have similar properties to the bulk oxide, yet they are not electronically insulating allowing for electron dependent techniques such as STM.[8,9] Chapter 3 provides a detailed literature background for Al_2O_3 thin films. The literature results are compared to our thin films. The morphology, structure, and defects of the thin film are discussed in detail. Chapter 4 discusses the evaporation of Pt and the formation of Pt nanoparticles onto Al_2O_3/NiAl(110). The size, structure and binding preference of our Pt nanoparticles are compared to literature.

Hydrocarbon chemistry over Pt surfaces are important to industry and science and are being utilized for a number of projects, such as pollution control, biodegradable detergents and chemical synthesis.[10,11] One of the main goals of this project is to study the morphology of the Pt surface before and after dehydrogenation at various temperatures. By understanding the surface better, we hope to be able to control it better during reactions. Chapters 5 and 6 describe various olefin reactions. Olefins are dosed and thermally dehydrogenated on both Pt nanoparticles and a Pt single crystal. Specifically, Chapter 5 gives an analysis of propylene and butylene dosed onto Pt(111). This chapter compares these results to previous studies with ethylene on Pt(111). In Chapter 6, we compare our study of ethylene dehydrogenation on Pt nanoparticles to the olefin studies on the Pt single crystal. It is important to compare both the bulk Pt and Pt nanoparticles, as catalytic nanoparticles have different activity compared to their bulk counterparts due to their varying size, structure and shape.[2] Nanoparticles can lower the cost of production in industry as less expensive catalyst material is required.[2]

Chapter 7 briefly discusses an experiment of ethylenediamine dosed onto Ni(111). The goal of this study was to determine if cyanogen can be formed from the dehydrogenation of

ethylenediamine on a Ni crystal. Cyanogen is theorized to act as an air filter to capture various hydrocarbons.[12]

Finally, Chapter 8 concludes the thesis with a summary and future outlook.

1.2 References

(1) C. H. Bartholomew; Farrauto, R. J., *Fundamentals of Industrial Catalytic Processes*. 2nd ed. 2011, New York, NY: Wiley & Sons.s

(2) Applegate, J. R.; Pearlman, H.; Bakrania, S. D., *Catalysis of Methanol-Air Mixture Using Platinum Nanoparticles for Microscale Combustion.* Journal of Nanomaterials. **2012**: p. 8.

(3) Libuda, J.; Baumer, M.; Freund, H. J., *Structural Characterization of Platinum Deposits Supported on Ordered Alumina Films.* Journal of Vacuum Science & Technology a-Vacuum Surfaces and Films, 1994. **12**(4): p. 2259.

(4) Dandapat, A.; Jana, D.; De, G., *Synthesis of Thick Mesoporous Alumina Films, Loading of Pt Nanoparticles, and Use of the Composite Film as a Reusable Catalyst.* ACS Applied Materials & Interfaces, 2009. **1**(4): p. 833.

(5) Jiang, C.; Hara, K.; Fukuoka, A., *Low-Temperature Oxidation of Ethylene over Platinum Nanoparticles Supported on Mesoporous Silica.* Chem. Int. Ed, 2013. **52**: p. 6265.

(6) Namgee Junga; Dong Young Chungb; Jaeyune Ryua; Sung Jong Yooa; Yung-Eun Sungb, *Pt-based nanoarchitecture and catalyst design for fuel cell applications.* NanoToday, 2014. **9**: p. 433.

(7) Lin, Y.-C.; Huber, G. W., *The critical role of heterogeneous catalysis in lignocellulosic biomass conversion.* Energy Environ. Sci., 2008. **2**: p. 68.

(8) R.M. Jaeger; H. Kuhlenbeck; Freund, H.-J., *Formation of a well-ordered aluminium oxide overlayer by oxidation of NiAl(110).* Surface Science, 1991. **259**: p. 235.

(9) Cuenya, B., *Synthesis and catalytic properties of metal nanoparticles: Size, shape, support, composition, and oxidation state effects.* Thin Solid Films, 2010. **518**: p. 3127.

(10) Akia, M.; Alavi, S. M.; Yan, Z.-F., *Promoted Platinum Dehydrogentaion Catalyst on a Nano-Sized Gamma Alumina Support.* Petroleum and Coal, 2010. **52**(4): p. 280.

(11) Gawthrope, D. E.; Wilson, K.; Lee, A. F., *Propene combustion over a model Pt/Al2O3/NiAl{110} catalyst.* Physical Chemistry Chemical Physics, 2003. **5**(15): p. 3299.

(12) Kingsley, J. R.; Dahlgren, D.; Hemminger, J. C., *Coadsorption Chemistry Of H-2 And C2n2 On Pt(111) - A Common Intermediate In The Hydrogenation Of Cyanogen And The Dehydrogenation Of Ethylenediamine On Pt(111).* Surface Science, 1984. **139**(2-3): p. 417.

CHAPTER 2

Introduction to Instrumentation and Experimentation: Theory and Background

2.1 Introduction to Instrumentation

Surface science refers to the study of the physical and chemical properties at the interface of two different phases.[1] Specifically, we study the heterogenic catalytic reactions which occur between solid and gas phase. The term surface science is fairly recent in history and came only into prevalence in the 1960s.[1] Groundbreaking surface science work on adsorption by Langmuir and on low energy electron diffraction by Davisson and Germer occurred in the 1920s.[1] However, the field of surface science did not become prominent until the 1960's with the introduction and development of ultra high vacuum (UHV) technology.[1] UHV provides a controlled environment, which allows for a variety of new techniques to be created and old techniques to be advanced. Most importantly to our project, scanning tunneling microscopy (STM), a technique that images atoms, performs best when held under UHV conditions.[2] STM was introduced to the world by IBM in 1982 and revolutionized the understanding and control of science at the nano-scale, thereby winning its inventors Binning and Rohrer the Nobel Prize in 1986.[2]

Our experiments were performed in a homebuilt instrument maintained at UHV with a base pressure of less than 1×10^{-10} Torr. There are three chambers: fast entry load lock, preparation chamber and STM chamber as shown in Figures 2.1 and 2.2. To acquire UHV pressures, a well sealed chamber connected to a network of pumps is required. As shown in Figure 2.3 our chamber utilizes two ion pumps with titanium sublimation pumps, two turbo molecular pumps and two rotary mechanical pumps. The majority of the time, the chamber is

held in vacuum solely with the ion pumps. Furthermore, it is necessary to heat the chamber to temperatures of 150^{o}C to remove water and other gases from the interior chamber walls.[3,4]

We have gas dosers in both the preparation and STM chambers. The majority of gas dosing is performed in the preparation chamber to maintain a clean STM chamber. A clean STM chamber is crucial, as we store up to three tips and three samples in our STM chamber at a time. The Pt evaporation and argon bombardment occurs in the preparation chamber as well. A quartz crystal microbalance (QCM) and deposition flux monitor are utilized in the preparation chamber to monitor the evaporation from the Pt rod. This chapter provides a brief summary with the most vital experimental information and background. Topics covered in this chapter include: sample and sample holder information, UHV, STM and AES theory and experimental conditions. Chapters 3 and 4 provide a detailed description for the making of Pt nanoparticles and Al_2O_3 thin films.

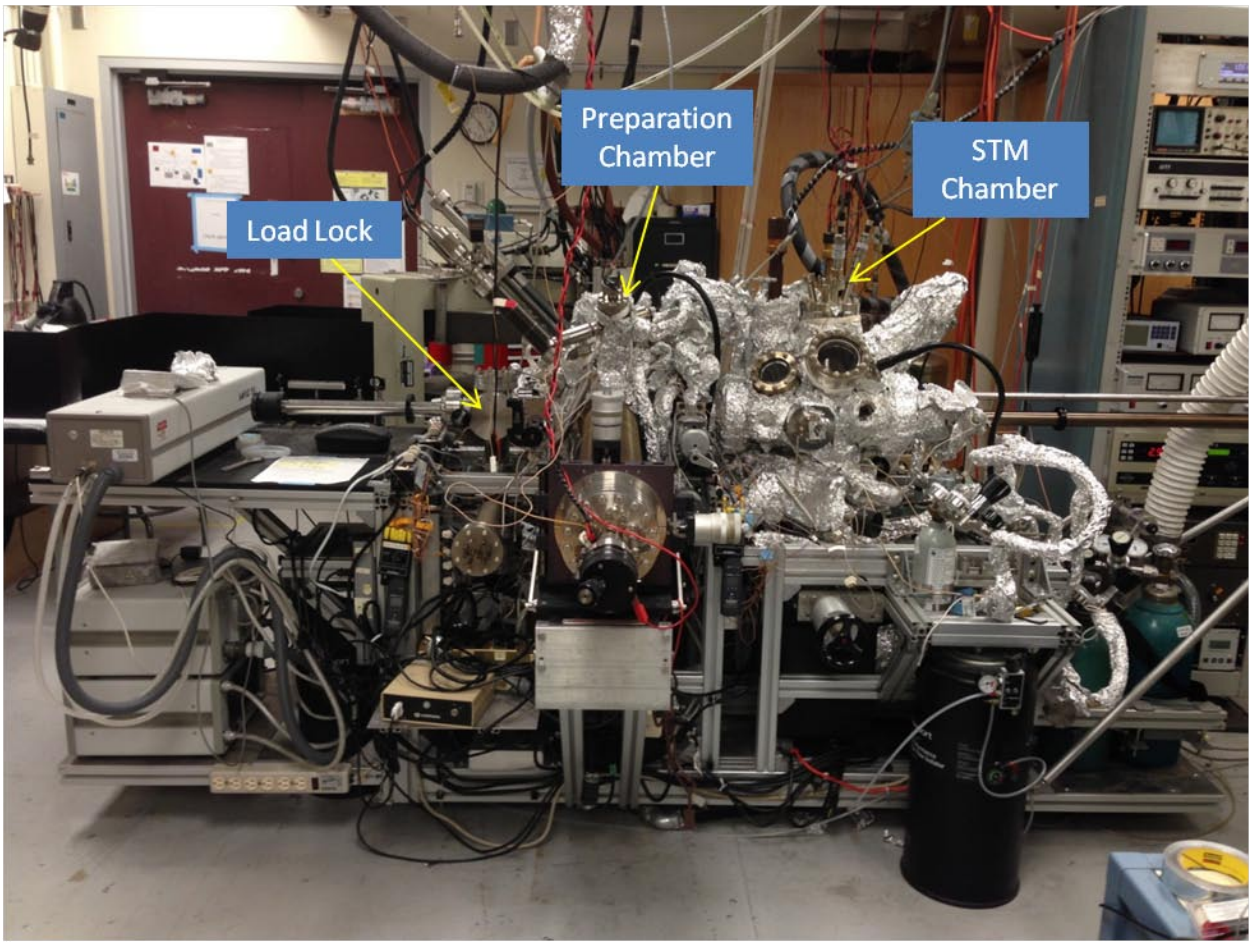

Figure 2.1 A photograph of the instrument used for the experiments. Three chambers consisting of the preparation chamber, load lock and STM were utilized.

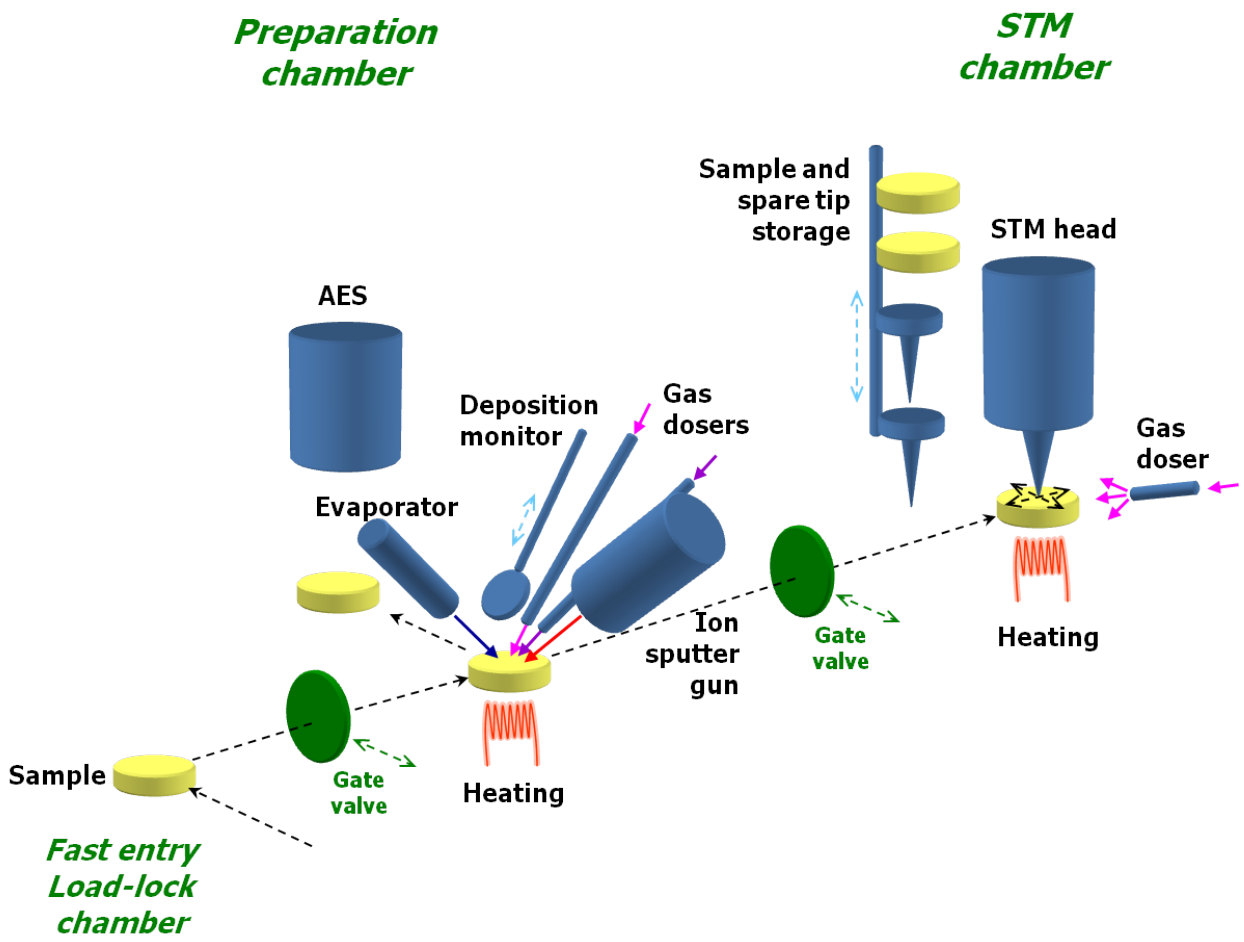

Figure 2.2 Schematic of the chamber showing the essential parts used herein: load lock, AES, gas dosers, evaporator, deposition monitor, STM and heating.

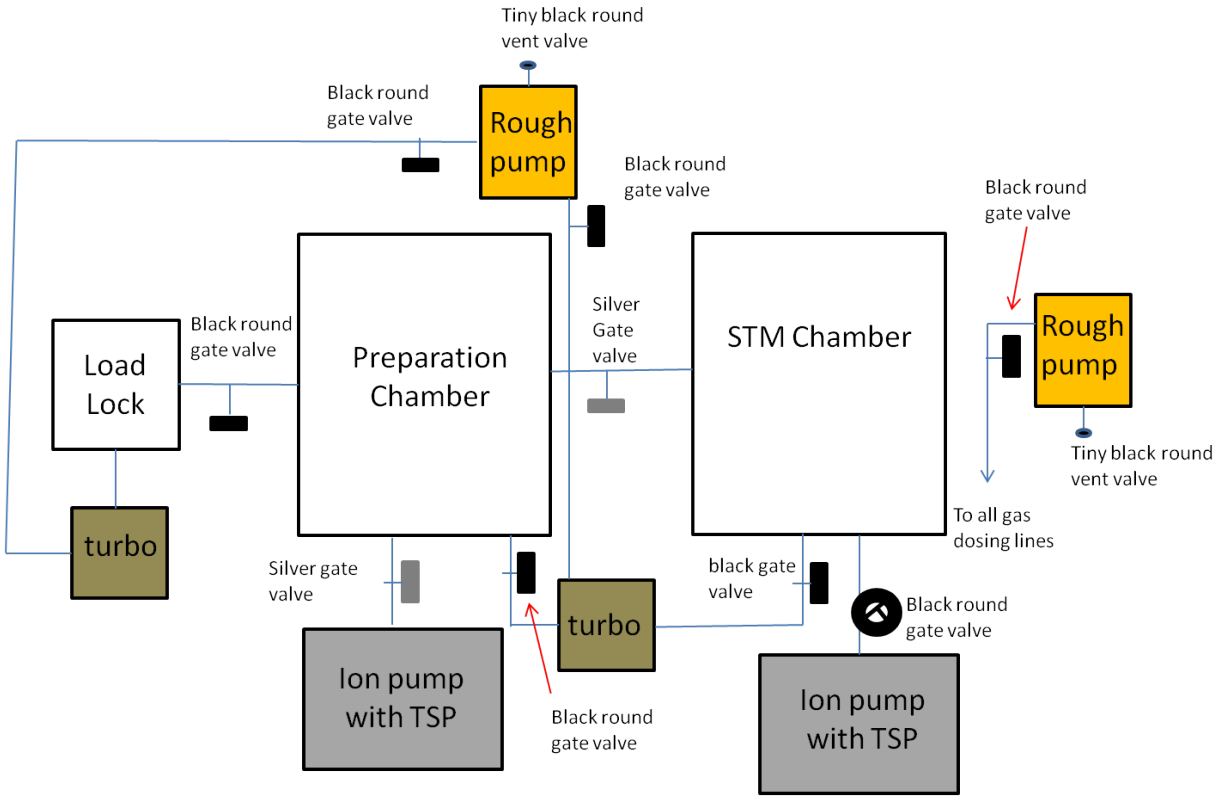

Figure 2.3 Schematic showing the connections, gate valves and vacuum pumps used to maintain UHV in our instrument. The load lock, STM and preparation chambers are separated via gate valves. The preparation and STM chambers each have an ion pump with a titanium sublimation pump (TSP). Both the preparation and STM chambers share one turbomolecular pump (or turbo pump) and the load lock has its own turbo pump. All three chambers share one rotary mechanical pump (or rough pump). Finally, the gas dosing lines are pumped using a separate rough pump.

2.2 Ultra High Vacuum and Surface Science Theory

The most important and critical technique used in the experiments described herein is UHV. UHV refers to pressures of 10^{-9} to 10^{-12} Torr, typically found in specially designed chambers. UHV is important for maintaining a clean sample, preventing contamination and providing a clear path for electrons to flow relatively unhindered.[5,6] A clear path for electrons is crucial for surface science techniques such as Auger Electron Spectroscopy and ion

bombardment. The mean free path, λ, describes the average distance that a particle, electron, atom or molecule can travel in the gas phase before it collides with a molecule. UHV increases the mean free path length.

The molecule-molecule mean free path, $\lambda_{molecule}$, is derived from the ideal gas law and a hard sphere collision model in a cylindrical volume and is calculated using the *r*, molecular radius (m), *k*, Boltzmann constant, and *T*, temperature (K) and *P*, pressure (N m^{-2}).

$$\lambda_{\text{molecule}} = \frac{kT}{4\sqrt{2}\pi r^2 P} \tag{2.1}$$

The mean free path for electrons is slightly different as the radius of the cylinder is reduced to *r* instead of *2r*, since the electrons take up less space. Furthermore, we disregard the relative molecular velocity of $\sqrt{2}$. Taking into account these two differences the mean free path of the electrons, $\lambda_{electron}$, can be approximated from the molecule-molecule mean free path by multiplying Equation 2.1 by $4\sqrt{2}$.[7] Therefore the $\lambda_{\text{electron}}$ is longer compared to the $\lambda_{\text{molecule}}$. The mean free path equations show that pressures less than 10^{-4} Torr are required for collision free conditions. This is a pressure far greater than 10^{-9} Torr and does not justify the effort required to maintain UHV. Therefore, the primary purpose of UHV is in maintaining a clean sample and preventing contamination.[5,6]

A sample sitting under atmospheric pressure will form a monolayer of gases within 10^{-9} seconds. A monolayer is the maximum attainable surface coverage that is a single molecule thick on a surface. This monolayer of gases or contamination prevents a controlled, consistent adsorption of the molecule being studied. Langmuir, who won the Nobel prize in 1932 for his work in surface science,[8] is now associated with a unit to describe gas exposure – such that a Langmuir, *L*, is the product of pressure and time that a surface is covered with 1 monolayer.

$$1\ L = 1 \times 10^{-6}\ Torr\ s \tag{2.2}$$

Langmuir is important in order to identify the pressures required for a clean surface and the pressures required for dosing a sample. If pressures are 1×10^{-6} *Torr* the surface of a sample will be contaminated by 1 monolayer within 1 second. Therefore, every order of magnitude drop in pressure will produce an increase in an order of magnitude for the amount of time of contamination. Specifically, at 10^{-10} *Torr*, it is expected that 10^4 seconds are needed for a monolayer coverage to occur. This concept is derived by the incident molecular flux, *F* and the sticking coefficient. *F* is the flux of molecules sticking to a surface. The incident molecular flux is calculated based on the gas density,

$$F = ¼\, n\, \bar{v} \tag{2.3}$$

where, *n* is the molecular gas density and $\bar{v}$ is the average molecular velocity as shown in Equations 2.4 and 2.5,

$$n = \frac{N}{V} = \frac{P}{kT} \tag{2.4}$$

$$\bar{v} = \sqrt{\frac{8kT}{m\pi}} \tag{2.5}$$

where *N* is the number of molecules, *V* is the volume and *k* is Boltzmann's constant, *P* is pressure in Pascals, m is gas mass. Therefore, *F* can be rewritten as Equation 2.6, with *M* as the molecular weight in kg.

$$F = 2.63 \times 10^{24} \frac{P}{\sqrt{MT}} = \frac{number\ of\ molecules\ impacting\ the\ surface}{m^2 s} \tag{2.6}$$

Flux simply describes the number of gas molecules hitting the surface per unit time. However, the sticking coefficient, Θ, describes the ratio of the number that adsorb to the surface versus the number of molecules that hit the surface. Θ is dependent on a multitude of factors, including temperature, coverage, and inherent properties of the sample. At Θ=1 every molecule adsorbs; at Θ=0 there is no adsorption. The typical number of atoms on the surface is 10^{15}

atoms/cm^2. With this value and by assuming the sticking coefficient is 1, Langmuir's equation can be calculated.

2.2 Single Crystal Samples: Pt(111), NiAl(110), Ni(111)

All single crystal samples were processed and held under UHV conditions. Pt (111), NiAl(110) and Ni (111) single crystals are well studied model catalysts and are used in this project. Pt(111) served as a comparative model to $Pt/Al_2O_3/NiAl(110)$, which is also studied in this project. In basic terms, a catalyst is a material that increases the rate of reaction.[4] A heterogeneous catalyst is a catalyst that is in a different phase than the reactants.[4] Using heterogeneous catalysts is advantageous for certain reactions as it is easier to separate a solid catalyst from a liquid or gas.[4]

Before each experiment the Pt, Ni and NiAl crystals were cleaned. The NiAl single crystal sample was cleaned by cycles of oxygen dosing ($P = 2 \times 10^{-6}$ Torr, $T_{sample} = 540$ K, for 10 minutes), followed by annealing ($T_{sample} = 1320$ K for 15 minutes). Ni and Pt were cleaned by multiple cycles of argon bombardment (Table 1). Ion bombardment (ISE-10, Omicron) is used to clean the surface from elements that cannot be removed by oxygen cleaning, such as sulfur. Pt cleaning cycles included an oxygen treatment for 30 min at 700 K with oxygen partial pressure of 5.0×10^{-6} Torr. Oxygen cleaning was not performed on Ni since oxidation of the surface occurs at room temperature, but this does not occur on Pt until 800 K.[9-11] Oxygen cleaning removes carbon species from the surface by pumping it away as CO_2 (g).[12] Each cycle is completed by the annealing of the sample which produces a smooth surface with sharp step edges. The samples were heated and annealed by using electron bombardment (e-beam) heating by a tungsten filament approximately 2 mm below the sample. The temperature was monitored

using a chromel-alumel thermocouple sitting on the sample. AES and STM confirmed clean surfaces with flat terraces and sharp step edges.

Table 2.1 Argon bombardment parameters for each respective experiment.

Single Crystal	Beam Energy	Ion Beam current	Bombardment Time/Cycle	Bombardment Temperature	Anneal Time/Cycle	Annealing Temperature
Pt	0.600 kV	5 μA	30 min	300 K	10 min	1100 K
Ni	1 kV	10 μA	15 min	300 K	15 min	1000 K

Pt(111) took several months and hundreds of cycles to obtain a clean sample. Ni(111) and NiAl(110) were comparatively easy to clean and required only a month of cleaning. Once clean, NiAl(110) is easily maintained in a UHV chamber. Every so often, simply heating to 1320 K for 15 minutes can remove any oxidation. Due to the ease of cleaning NiAl(110), we used a second NiAl(110) as a backup sample in the STM chamber for cleaning or calibrating tips.

2.3 Sample Holder Design

In order to complete experiments, the NiAl sample was required to be heated at 1320 K for multiple 15 minute cycles while held under UHV conditions. Unfortunately, the stock STM sample holder purchased through RHK (Beetle, UHV 300 VT-STM) could not maintain this temperature. We redesigned the sample holder by incorporating a filament ~2 mm below the sample into the sample holder. The design is based on electron beam heating and is shown in Figures 2.4a and b. The sample and the connections are isolated from the chamber and each other by sapphire washers and ceramic holders respectively to maintain electron bombardment. The final filament is made with relatively thick W wire of 0.5 mm in diameter. The filament loop is ~ 3 mm in diameter and is shown in Figure 2.4a. A thermocouple is attached to the sample to monitor temperatures. This setup required a few months of time to perfect the heating to handle high voltages of 1000 V and high temperatures for lengths of time.

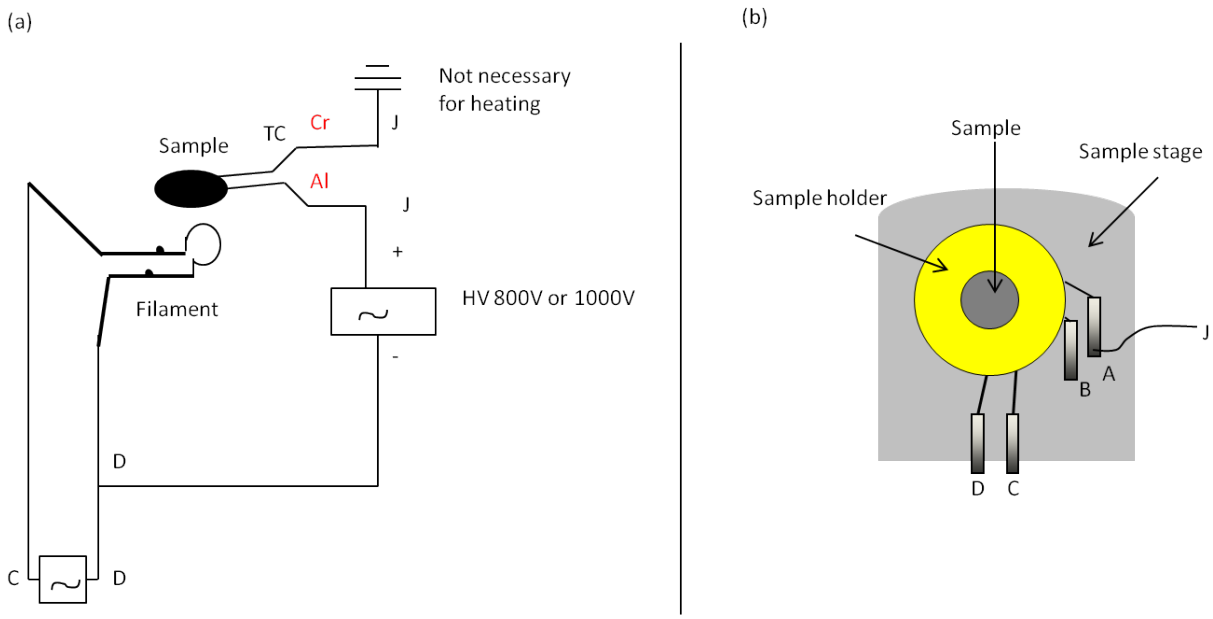

Figure 2.4 (a) The electron beam heating setup that runs currents of 3-3.5 A through the filament. A voltage is held between the filament and the sample of ~800-1000 V. The filament is made of W wire and the loop is ~3 mm in diameter. (b) The sample stage with the sample holder is shown to exemplify the connections for electron beam heating.

2.4 Scanning Tunneling Microscopy (STM) Theory

STM in essence provides a topographical image of a surface at an atomic scale. STM has resolutions reaching 0.01 nm vertically and 0.1 nm laterally.[13] STM can also be used for chemical spectroscopy at very low temperatures: 10 K or less.[13] Furthermore, with STM, atoms can be manipulated on a surface to create various structures. The STM has forever changed experimental and theoretical science and thereby won its creators Binning and Rohrer the Nobel Prize in 1986.[14]

The basic experimental setup of the STM is a mono-atomically sharp metal tip held less than 1 nm from a conductive surface held in liquid, vacuum or air (Figure 2.5). The tip scans along the surface and is sensitive to the density of states.[13] STM is a sum of three main concepts: 1) tunneling effect, 2) piezoelectric effect and 3) feedback loop.

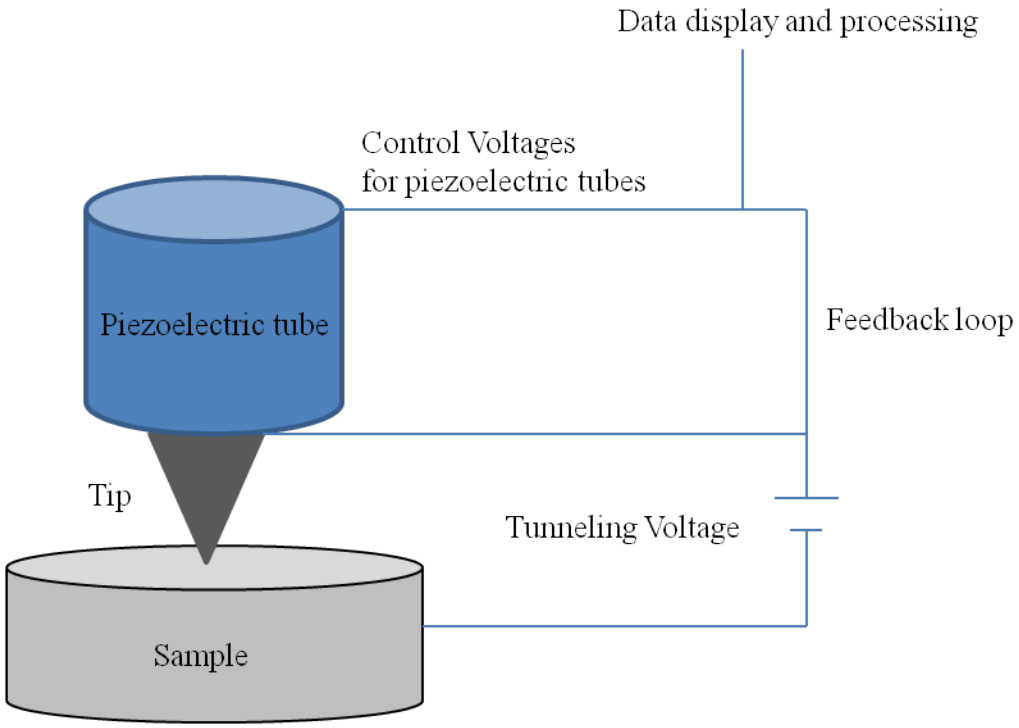

Figure 2.5 Basic setup of STM, including the feedback control system.

In classical mechanics, an electron cannot pass through an energy barrier, however in quantum mechanics an electron can "tunnel" through the barrier.[15] Specifically with UHV and STM, the barrier is the vacuum between the tip and the surface. An example of tunneling with STM and UHV is shown in Figure 2.6. The minimum energy required to remove an electron from the tip or the surface and tunnel through the vacuum is referred to as work function, Φ. When the bias between the tip and the sample are zero, their Fermi levels are equal and therefore tunneling will not occur.[16] When a bias voltage, V is applied, electrons can travel either from the tip to the sample or sample to the tip, depending on the polarity of the bias voltage.[13] By applying a positive bias voltage to the sample (tip grounded), the Fermi level of the sample is elevated by $E_F + eV$ in comparison to the tip.[16] This provides empty states in the tip now

available for tunneling into. The electrons at top of the elevated Fermi level will contribute to the majority of the tunneling.[16]

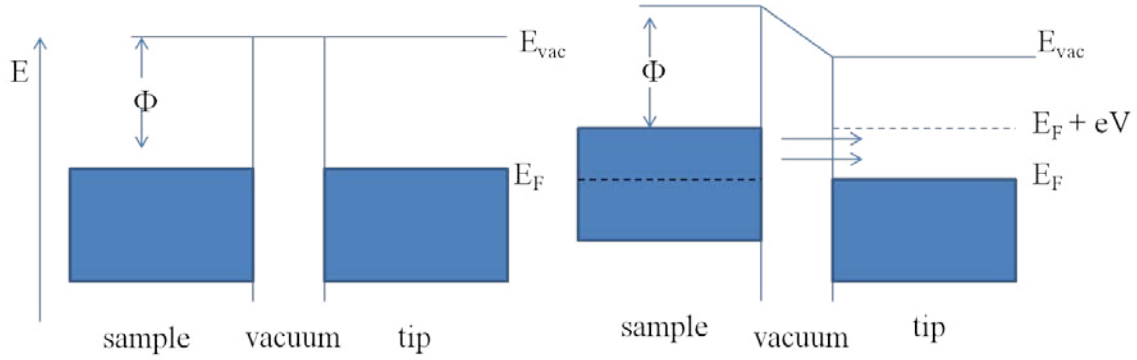

Figure 2.6 The basic principle of Scanning Tunneling Microscopy.

The tunneling current, *I* falls exponentially as the barrier thickness increases (see Equation 2.11).[17]

$$I \sim V_b \exp(-K\Phi^{1/2} d) \qquad (2.11)$$

Where V_b is the bias voltage, K is a constant, Φ is the work function with a typical value of 4 eV, and d is the distance between the sample and tip. This has important implications, in that very small changes in the distance between the tip and the sample produce large changes in the tunneling current. This allows the distance to be controlled minutely.

Therefore it is important to control the distance between the tip and the sample, which thereby controls the tunneling current. Piezoelectric actuator (or piezos) are the key to finely tuning the distance at values less than a nanometer.[15] Piezos are solids that take advantage of the piezoelectric effect where when compressed or elongated a current is created.[15] Conversely, when a current is applied to a piezoelectric solid they will deform.[15] This allows for the tip to be controlled on x, y and z axes with fine tuning.

The STM tip is connected to a piezo that is sensitive to the feedback loop. The feedback loop is designed to maintain a constant current between the tip and the sample. The feedback

loop monitors the tunneling current and makes adjustments to the tip via applied voltage to the piezos to maintain a constant current value.[15] This applied voltage provides data that can be plotted to give a 2D representation of the surface. In our experiments, we use the constant current mode, as it provides much more sensitive information. This approach prevents crashing to the surface when the height changes are large on a rough surface. However, this method is slow, so many opt to use the constant height mode. Constant height mode inhibits the feedback loop and keeps the distance between the tip and the sample constant while the current adjusts. The two modes are illustrated in Figure 2.7. The electronic structure of the surface affects the tunneling current, which then provides the topographical output of the surface.

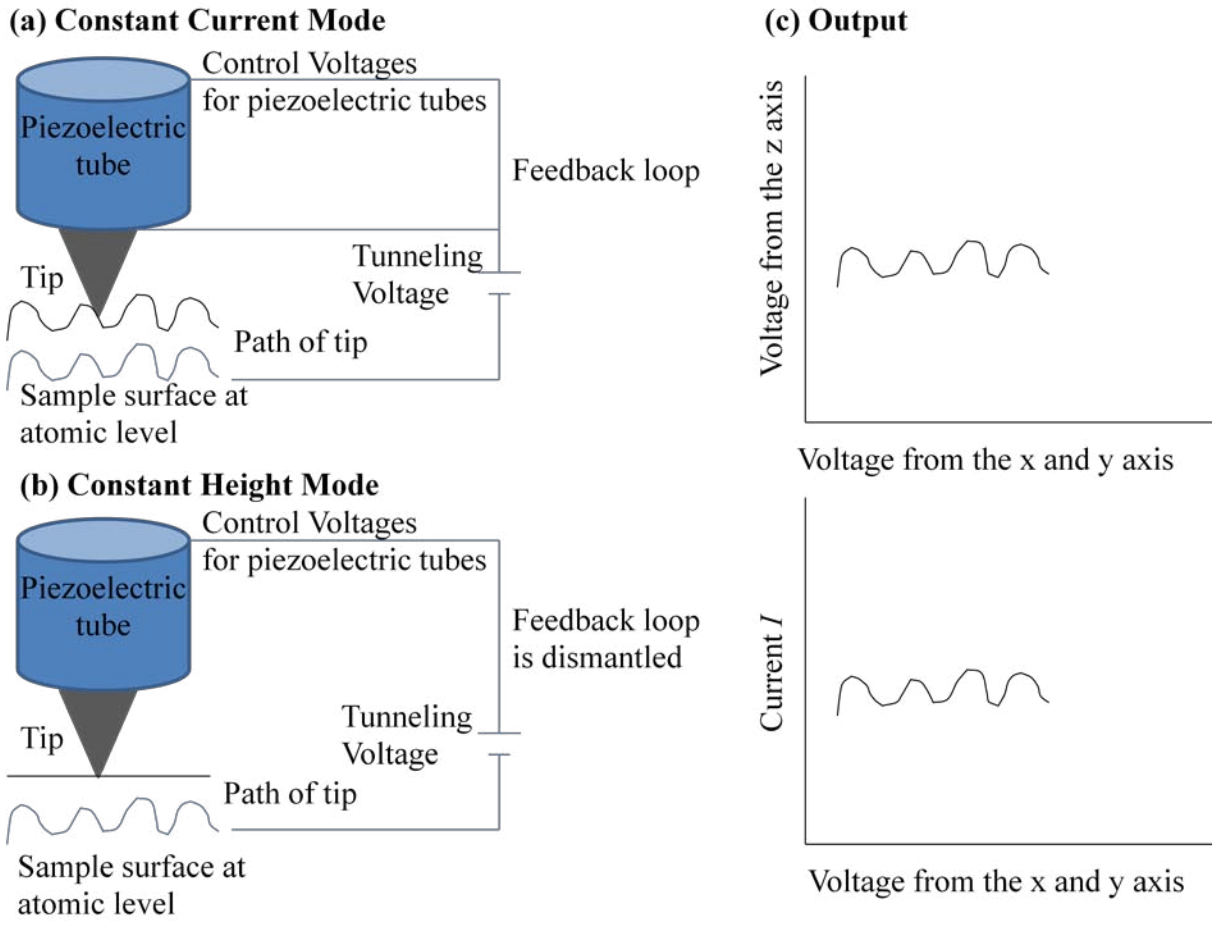

Figure 2.7 Comparison of constant current and constant height tip modes. (a) With the constant current mode the tip follows the path of the sample as the current is adjusted. (b) With the constant height mode, the path of the tip stays constant and the feedback loop is dismantled. (c) The output of both modes should be very similar.

2.6 Imaging Conditions

The STM used for experimentation herein, is the UHV 300 VT-STM from RHK Technology, Inc. This STM can run experiments in the range of 10 K to 1273 K. Imaging can be performed up to temperatures of 500 K. The range available for tunneling current is between 0.01-10 nA, however typically the tunneling current is held at ~1 nA. The bias voltage can be

held between ±0-10V. When choosing a bias voltage, the value is not critical for conductive surfaces like Pt or NiAl. Typically, we image at a range of 2 mV to 2 V bias. However, when working with semiconductive materials like the Al_2O_3/NiAl surface it is critical to choose a proper bias voltage. In particular, in bulk Al_2O_3 the band gap is 8 eV,[18] however with the thin film the band gap is slightly reduced to 6.7 eV.[19] The Fermi Level is about the middle of the band gap, and therefore a bias voltage minimum of U ± 3.4 V is needed for tunneling to occur from the oxide layer.[18] However, at high bias voltages (U > 2 V) the STM tips are not very stable and imaging is very difficult. The high bias voltage produces a field evaporation on the tip, causing the tip to restructure.[20] This instability of the tip can be seen in Figure 2.8a which is Al_2O_3 imaged at 4.13 V. We found that when the oxide layer is made very thin, imaging can be performed at lower bias voltages of ≤ 2 V, as shown in Figure 2.8b. Due to the comparable ease of imaging the oxide support with lower biases it has become common.[21-24] However, when imaging at a lower bias voltage electrons are tunneling between the tip and the metal support.[25] The oxide layer only serves to influence the potential barrier.[25] As a result, we found that adsorbed particles on the oxide layer appear taller by nearly 3 Å. This is due to the tip tunneling from the Pt nanoparticles to the metal support and not from the Pt to the oxide layer. Furthermore, we found that if we did not image at a minimum of 4 V we could not resolve the grain boundaries.

This became problematic for our data analysis. Therefore, we found that if we made the oxide layer thinner, where we annealed at 1200 K for 10 minutes, to the extent where the oxide layer was beginning to desorb we could image at higher bias voltages with a stable tip. Typically our imaging conditions for Al_2O_3/NiAl were held at a bias range between 4-6 V, as shown in Figure 2.8c.

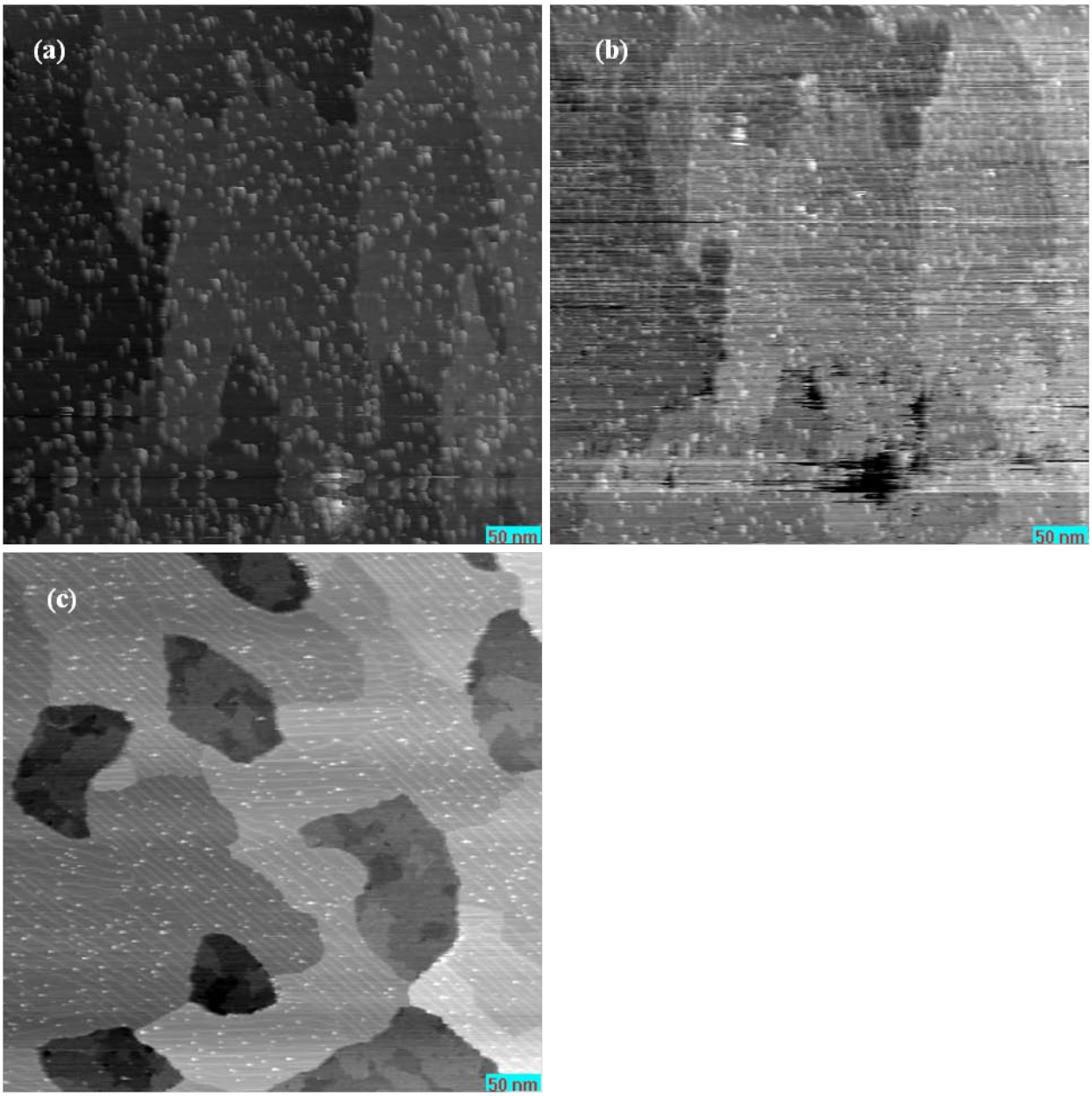

Figure 2.8 500 × 500 nm images that portray Pt/Al_2O_3/NiAl(110). Figure (a) and (b) are at the same location with the first imaged at 4.13 V and the second imaged at 2.5 V. Image (c) is the ultra-thin oxide layer imaged at 4.63 V. The ultra-thin oxide layer is patchy and has many areas that are not crystallized.

2.7 STM Tips

We make our STM tips with a wire of Platinum Iridium (Pt-Ir) mix of 80-90% and 10-20% respectively with 0.25 mm in diameter. Pt-Ir is preferred for use in air because platinum does not easily oxidize. The Ir in the alloy makes the tip much harder. A tip made with pure platinum would become blunt in a short time. The tip is made by clamping down on the wire at a 25° angle with wire cutters and then pulling the wire cutters free (Figure 2.9). This theoretically creates a monatomically sharp tip. Our chamber does not have the capability to heat tips, so we cannot use etched tips as they require heating to remove the oxide layer. After cutting, the tip is processed by approaching the tip to a sample until it is in tunneling conditions. Then the bias voltage is changed rapidly between the tip and the sample until contaminates drop off. Occasionally, a controlled crash of the tip to the sample is required to change the shape of the tip. Processing a tip can take up to 2-3 weeks for a new tip and a few hours for a tip that has been in use and held in UHV. Tips periodically need to be replaced as they become unusable with time.

Tip convolution is an important concept when analyzing STM data. Convolution occurs when the image shows features from the tip and the sample – the image is a convolution of the tip and surface.[26] For example, a double tip can produce double features on the sample. A broad tip can produce broad features. When a tip is well processed these types of issues do not occur. We retain a clean NiAl(110) in the chamber at all times, to periodically clean the tip during experimentation. By measuring a monatomic step on a clean Pt or NiAl surface, convolution associated from the tip can be approximated. Images were calibrated in the z-dimension using the NiAl crystal step height of 2.0 Å[6] and the Pt crystal step height of 2.3 Å.[27]

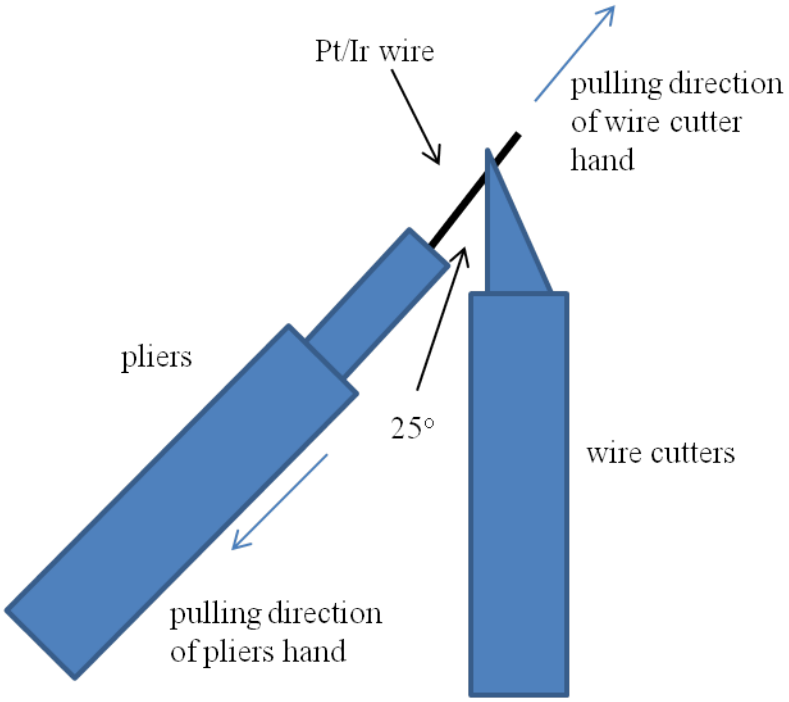

Figure 2.9 Schematic of how to cut STM tips. Wire cutters clamp down at a 25° on the Pt/Ir wire without cutting all the way through. The wire is then torn by pulling the wire cutters free by moving the hands in two different directions.

2.8 Auger Electron Spectroscopy Theory

Auger electron spectroscopy (AES) is an important technique for surface science for a multitude of reasons. AES can identify most atoms (excluding helium and hydrogen).[15,28] Most importantly, AES has one of the highest resolutions for surface spectroscopy.[29] Due to a focused electron beam, our AES (PHI model 10-155, single pass cylindrical mirror analyzer (CMA)) has a high-spatial resolution of less than 25 μm and an effective probe depth of 1 nm.[29,30] Also, this technique is highly advantageous since its procedure takes only a few minutes, while other surface science techniques can be extremely time consuming. The individual elemental components do not interfere with one another, therefore the spectra can be made into compiled

books and can be directly referred to.[6] AES is mainly used for identifying species present at the surface and for providing their relative amounts.

The AES system begins with the electron gun control, which provides beam voltage, filament current and emission voltage to the electron gun in the CMA. From the filament, electrons are emitted, focused and accelerated to form a beam. The electron beam (2-10 keV) hits the sample surface and is scattered, both elastically and in-elastically until it either escapes back through the surface or reaches thermal energies.[31] In this process the primary electrons from the electron beam ionize inner core electrons, creating vacancies in the inner level. An example of an electron created at the K level is shown in Figure 2.10 and Equation 2.12.[6,32]

$$C + e^{-} (2kV) \rightarrow C^{+} + 2e^{-} \qquad (2.12)$$

This vacancy is filled by another electron from a higher level, such as one of the L levels.[6] To note, hydrogen does not have outer electrons and helium has an insufficient amount and therefore neither can be detected by AES.[33] From there two processes are possible. One, from the transition (L→ K), energy can be released in the form of radiation. If the energy difference E_K-E_L is large enough, x-rays are emitted, providing the basis for x-ray fluorescence.[6] However, the energy can be transferred to another electron in the same level or a level close to it, as shown in Equation 2.13 and Figure 2.10.[6,32]

$$C^{+} \rightarrow C^{2+} + e^{-} \qquad (2.13)$$

The second ionized electron can gain enough energy to escape from the atom if the difference E_K-E_L is sufficiently large.[6] This escaping electron is called an Auger electron.

This process is usually written in terms of three levels involved, ABC. A is the level in which the vacancy is created by the electron beam; B is the level from which the electron which

filled the vacancy originates; and C, the level from which the Auger electron is emitted (E.g. KL_1L_2).

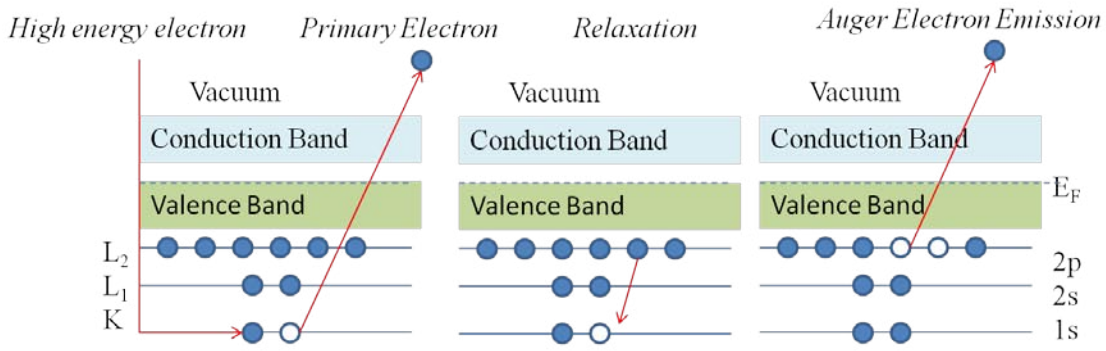

Figure 2.10 Auger electron emission for KL_1L_2.

The Auger electron energies are characteristic of the sample material and the ionization energy from C^+ to C^{2+}, consequentially the energy is independent of the incident electron energy.[6,32] The Auger electron's kinetic energy can be approximated based on the binding energies of the core electron (E_1), the relaxed electron (E_2) and the electron that the receives the released energy (E_3).[31,34] Finally, the kinetic energy is dependent on the work function, Φ of the analyzed material (Equation 2.14).[31,34] The work function's typical value is 4 eV, which is the amount of minimum energy required to remove an electron from the sample.[31]

$$KE_{Auger} = E_1 - E_2 - E_3 - \Phi \qquad (2.14)$$

For lower energy events leading to a photon or electron with energy less than 2 keV the Auger process is dominant with more than 95% of ionizations leading to the ejection of the Auger electron.[31] The kinetic energy of the electrons must be greater than the kinetic energy of the resulting Auger electrons that are to be analyzed, while not being so great that these electrons damage the spectrum.[35]

The spectrum can shift based on the surrounding chemical environment. However, each of the three electrons involved can be associated with multiple final states making it difficult to

determine the chemical environment.[35] A similar technique, x-ray photoelectron spectroscopy (XPS), reads the first electron emitted and therefore it is easier to identify the chemical environment.

Once the Auger electron is formed it moves through the solid and loses its energy through inelastic collisions with bound electrons (Figure 2.11). However, if the Auger electron is released close enough to the surface (5 to 25Å thick), it may escape from the surface with little to no energy loss.[31,33] This probing depth of approximately 1 nm is dependent on the ability of auger electrons to come off the surface with its kinetic energy intact.[32] Thus, the density of emitted Auger electrons depends on the mean free path (Equation 2.15).[6]

$$N(z) = N_o \exp(-z/\lambda) \tag{2.15}$$

N(z) is the density of auger electrons originating at a depth *z*, and N_o is the electron surface density. [6] For electrons with energy of 100 eV, the inelastic mean free path of electrons (λ) is approximately 2 monolayers thick and therefore the outer surface dominates the Auger signal.[31] For electrons with energy above 100 eV, λ is greater and the signal is not as surface specific, however ten monolayers is usually the limit for AES.[31] Unexpectedly, due to quantum mechanics the escape depth increases with decreasing auger energy in the region below 100 eV (Figure 2.11).[6]

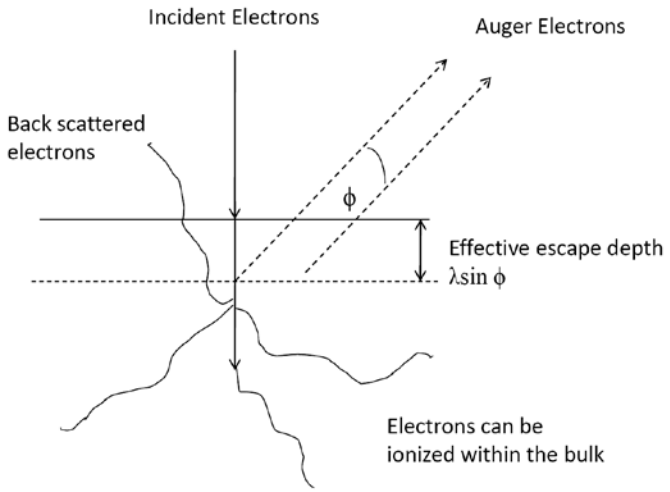

Figure 2.11 Auger electron production.

The escaped electrons are multiplied through a cylindrical mirror analyzer. Auger electrons are not the only electrons to escape the sample, backscattered primary electrons also can escape when the incident beam energy is substantially greater than the binding energy of the core level involved.[28] Also, many inelastic collisions produce low energy secondary electrons. These back scattered electrons and secondary electrons contribute to the spectrum. This makes it very difficult to read the peaks.

The total distribution function, N(E) versus E is differentiated to obtain a distribution function, dN(E)/dE versus E. Either of these representation provides identification "fingerprints" of the composition of the sample being investigated.[6] However, the derivative is more useful since the high, slowly varying background is removed . Because the background is usually sloping, even increasing the gain of the electron detection system and applying a zero offset is often not a great advantage.[28]

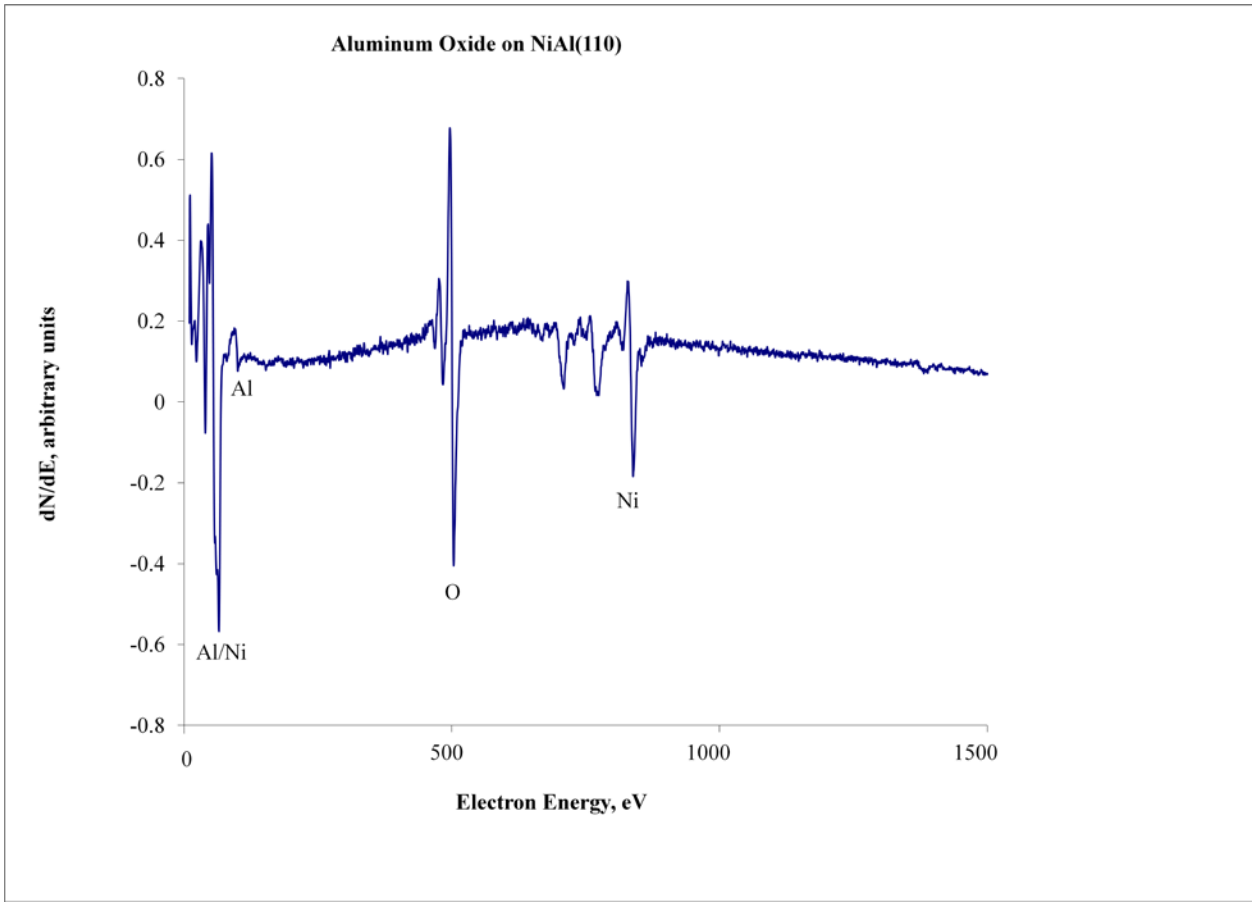

Figure 2.12 Auger spectra converted into differentiated form. AES of Al_2O_3/NiAl(110) after oxygen dosing of 1200 L at 550 K (1 Langmuir = 10^{-6} Torr s) for 10 min and annealing at 1200 K for 10 minutes.

2.9 Analyzing AES Data

An example of an Auger electron spectrum of Al_2O_3/NiAl(110) after oxygen dosing of 1200 L at 550 K (1 Langmuir = 10^{-6} Torr s) is given in Figure 2.12. Peak at 500 eV is representative of oxygen, peaks at 61 and 848 eV are representative of Ni, and peaks at 68 and 1396 eV are representative of Al.

AES is used primarily for elemental identification. However, it can give quantitative results. For example by performing peak intensity comparisons, we can determine relatively how much of a chemical is dosed. This is performed by taking the difference between the smallest

and the largest part of the peak, such as for oxygen. This difference is compared to another element's peak, such as for Ni.

2.10 References

(1) Hudson, J., *Surface Science an Introduction*. 1998, New York, NY: John Wiley & Sons, Inc.

(2) Thornton, S.; Rex, A., *Modern Physics for Scientists and Engineers*. 4th ed. 2013, Boston, MA: Cengage Learning.

(3) Marton, K., *Vacuum Physics and Technology*. Methods of Experimental Physics, ed. Weissler, G., Carlson, R. Vol. 14. 1979.

(4) Samorjai, G., *Introduction to Surface Chemistry and Catalysis*. 2nd ed. 2010, Honoken, New Jersey: John Wiley & Sons.

(5) Ibach, H., *Surfaces in Ultrahigh-Vacuum*, in *Physics of Surfaces and Interfaces*. 2006, Springer: New York.

(6) Yacobi, B. G.; Holt, D. B.; Kazmerski, L. L., *Microanalysis of solids* 1994: Springer.

(7) Heide, P. v. d., *Secondary Ion Mass Spectrometry: An Introduction to Principles and Practices*. 2014, Hoboken, New Jersey: John Wiley and Sons, Inc.

(8) Ross, J., *Heterogeneous Catalysis: Fundamentals and Applications*. 2012, Amsterdam, Netherlands: Elsevier.

(9) Ibach, H.; Bruchmann, D., *Observation of Surface Phonons on Ni(111) by Electron Energy-Loss Spectroscopy.* Physical Review Letters, 1980. **44**(1): p. 36.

(10) Deckers, S.; Habraken, F. H. P. M.; van der Weg, W. F.; Geus, J. W., *Oxidation of clean and Pt-covered Ni(111).* Applied Surface Science. **45**(3): p. 207.

(11) Steininger, H.; Lehwald, S.; Ibach, H., *Adsorption of oxygen on Pt(111).* Surface Science, 1982. **123**(1): p. 1.

(12) Groß, A., *Theoretical Surface Science: A Microscopic Perspective*. 2009, Berlin: Springer-Verlag.

(13) Bai, C., *Scanning Tunneling Microscopy and Its Applications*. 1992, Berlin: Springer-Verlag Berlin Heidelberg New York.

(14) John N. Lalena; Cleary, D. A., *Principles of Inorganic Materials Design*. 2010, New Jersey: John Wiley and Sons, Inc.

(15) Ahmad I; Voda A; Besancon G, *Controller Design and Analysis for High-Perforance STM*, in *Micro, Nanosystems and Systems on Chips: Modeling, Control and Estimation*, A, V., Editor. 2010, ISTE Ltd and John WIley & Sons, Inc: London, UK.

(16) SN Magonov; M-H Whangbo, *Surface Analysis with STM and AFM*. 2008, New York, NY.: VCH Publishers Inc.

(17) Seah, M. P., *Electron Energy and Ion Analysis*, in *Methods of surface analysis: techniques and applications*

Walls, J. M., Editor. 1989, Cambridge University Press Cambridge.

(18) Libuda, J.; Winkelmann, F.; Baumer, M.; Freund, H. J.; Bertrams, T.; Neddermeyer, H.; Muller, K., *STRUCTURE AND DEFECTS OF AN ORDERED ALUMINA FILM ON NIAL(110).* Surface Science, 1994. **318**(1-2): p. 61.

(19) Andersson, S.; Bruhwiler, P. A.; Sandell, A.; Frank, M.; Libuda, J.; Giertz, A.; Brena, B.; Maxwell, A. J.; Baumer, M.; Freund, H. J.; Martensson, N., *Metal-oxide interaction for metal clusters on a metal-supported thin alumina film.* Surface Science, 1999. **442**(1): p. L964.

(20) Kumagai, T., *Visualization of Hydrogen-Bond Dynamics: Water Based Model Systems on a Cu(111) Surface*. 2012, Tokyo, Japan: Springer.

(21) Luo, M. F.; Lin, W. R.; Wen, W. H.; Chang, B. W., *Methanol electro-oxidation and induced sintering on Pt nanoclusters supported on thin-film Al(2)O(3)/NiAl(100).* Surface Science, 2008. **602**(21): p. 3258.

(22) Luo, M. F.; Sartale, S. D.; Shiu, H. W.; Ten, M. H.; Huang, J. Y., *Scanning tunneling microscopy study of growth of Pt nanoclusters on thin film Al 2O 3/NiAl(100).* Surface Science, 2006. **600**(22): p. 4978.

(23) Luo, M. F.; Wen, W. H.; Lin, C. S.; Chiang, C. I.; Sartale, S. D.; Zei, M. S., *Structures of Co and Pt nanoclusters on a thin film of Al2O3/NiAl(100) from reflection high-energy electron diffraction and scanning-tunnelling microscopy.* Surface Science, 2007. **601**(10): p. 2139.

(24) Luo, M.-F.; Wang, C.-C.; Chao, C.-S.; Ho, C.-Y.; Wang, C.-T.; Lin, W.-R.; Lin, Y.-C.; Lai, Y.-L.; Hsu, Y.-J., *Temperature-dependent structuring of Au-Pt bimetallic nanoclusters on a thin film of Al2O3/NiAl(100).* Physical Chemistry Chemical Physics, 2007. **13**(4): p. 1531.

(25) Baumer, M.; Freund, H. J., *Metal deposits on well-ordered oxide films.* Progress in Surface Science, 1999. **61**(7-8): p. 127.

(26) Meyer, E.; Hug, H.; Bennewitz, R., *Scanning Probe Microscopy: The Lab on a Tip*. 2004, New York: Springer.

(27) MacLaren, J. M.; Pendry, J. B.; Rous, P. J.; Saldin, D. K.; Somorjai, G. A.; Van Hove, M. A.; Vvedensky, D. D., *Surface crystallographic information service. A handbook of*

surface structures. Surface crystallographic information service. A handbook of surface structures, 1987: p. viii+352.

(28) Chourasia, A. R.; Chopra, D. R., *Auger Electron Spectroscopy*, in *Handbook of Instrumental Techniques for Analytical Chemistry*, Settle, F., Editor. 1997, Prentice Hall. p. 791.

(29) Ecke, G.; Cimalla, V.; Tonisch, K.; Lebedev, V.; Romanus, H.; Ambacher, O.; Liday, J., *Analysis of Nanostructures by Means of Auger Electron Spectroscopy.* Journal of Electrical Engineering, 2007. **58**(6): p. 301.

(30) Perkin Elmer, *Instruction Manual Model 11-010 Electron Gun Control*, Eden Prairie.

(31) Bishop, H., *Auger Electron Spectroscopy*, in *Methods of surface analysis: techniques and applications*, Walls, J. M., Editor. 1989, Cambridge University Press Cambridge.

(32) Hemminger, J., Electrostatic Energy Analyzers lecture.

(33) Hoflund, G., *Spectroscopic Techniques: X-ray Photoelectron Spectroscopy (XPS), Auger Electron Spectroscopy (AES) adn Ion Scattering Spectroscopy (ISS)*, in *Handbook of surface and interface analysis: methods for problem-solving* Rivière, J. C., Myhra, S., Editors. 1998, CRC.

(34) Gabor L. Hornyak; H.F. Tibbals; Joydeep Dutta; Moore, J. J., *Introduction to Nanoscience and Nanotechnology*. 2009, Boca Raton, FL: Taylor & Francis Group.

(35) Perkin Elmer, *Instructions Manual Model 10-155/15-155 Cylindrical Mirror Analyzer*, Eden Prairie, MN: Physical Electronics Divison.

CHAPTER 3

Formation of Al_2O_3 Thin Films

3.1 Abstract

Al_2O_3/NiAl(110) was created and studied using scanning tunneling microscopy (STM) held under ultra-high vacuum (UHV) conditions. Alumina formation was a critical step for creating nanoparticles in later experiments. The NiAl(110) was oxidized at 550 K and then subsequently annealed to 1200 K. The resulting oxide layer was patchy with areas of both amorphous and crystalline Al_2O_3. The oxide layer that is formed was easily imaged. Domain boundaries were observed at bias voltages above 4 V and are 0.08 Å in height and 10 Å in width. The average distance between the boundaries was 60 Å. The step height between crystallized oxide layers was observed at 2.5 Å.

3.2 Introduction

Prior to the discovery of alumina (Al_2O_3) thin films, it was difficult to study bulk Al_2O_3 with techniques that require electrons and ions as alumina is an insulator.[1] In the early 1990s thin films formed by oxidizing NiAl(110) were discovered to be well ordered and were thin enough to avoid charge accumulation.[1,2] Alumina thin films grown on NiAl(110) have been imaged extensively[1,3-10] and studied with other experimental techniques such as electron energy loss spectroscopy (EELS), low energy electron diffraction (LEED) and x-ray photoelectron spectroscopy (XPS).[2,11-13] Experimental studies have indicated that the surface properties between bulk and thin film alumina are very similar, especially under UHV conditions.[13] This chapter provides a brief review of our thin film alumina and the current knowledge about thin films.

The thin films are believed to be formed in two Al-O layers about 5 Å thick, with the O terminated to the vacuum.[1,2,4,10,11,14,15] It has been shown by ion scattering spectroscopy and photo emission that the alumina film does not contain Ni.[16] The crystalline thin film alumina has been shown to have a longer unit cell than bulk alumina, with the film's rectangular unit cell dimensions of 10.6Å × 17.9 Å over the NiAl(110) unit cell of 2.89 Å x 4.08 Å.[4,15,17] The domain boundaries or a network of line defects are a common feature for crystallized alumina thin films and have been observed in the literature.[14,18,19] The domain boundaries are an irregular overlayer caused by a lattice mismatch between the NiAl and the oxide film, possibly caused by either an insertion of a row of oxygen or oxygen deficiencies.[14,18,19] These local areas or line defects are not charge neutral which causes band gap states and band bending.[18] The domain boundaries can be either straight or zigzag.[14,15]

Alumina bulk can exit in several different crystalline phases: α, γ, κ, χ, η, φ and δ.[20] Each phase has unique structure and properties.[20] The phase of thin film alumina is inconclusive and this can be in part due to the differing methods in forming the thin films. It has been difficult for researchers to determine the structure of thin film alumina since its unit cell is quite large for definitive labeling by LEED.[4] Furthermore, the large bias voltage required for imaging with STM has made it incredibly challenging to obtain high atomic resolution of the geometric positions of the atoms.[4] Some studies have shown that the properties of thin film alumina are similar to properties of transitional phase bulk oxides, such that the Al cations are tetrahedrally and octahedrally coordinated.[21,22] Other experimental studies indicate that the properties of the alumina thin film are structurally similar to those of bulk γ-alumina.[2,4,6,23] An XRD study has indicated that the thin film might be more κ-like.[12] A DFT and STM study, indicated that the alumina thin film is more α-like after annealing and that the film's stoichiometry differs greatly

from the bulk.[1] In the bulk alumina the charge is Al^{3+} and the oxygen is octahedrally and tetrahedrally coordinated with an Al_2O_3 stoichiometry.[1] This DFT and STM study found that with the thin films, the Al is bound to the NiAl metal, thus their charge is Al^{2+}.[1] Therefore, more Al atoms are required to keep the oxide charge neutral. In addition, they found that the actual stoichiometry of the film is $4(Al_4O_6Al_6O_7)$ or overall $Al_{10}O_{13}$.[1] This has not been verified by other studies and thin film alumina are still referred to as Al_2O_3. For brevity and simplicity, in this paper Al_2O_3 is used to refer to the thin film alumina.

The main goal for this project is to create a well ordered Al_2O_3 thin film that can be easily imaged with STM. The thin film should match the literature data in terms of its structure. In future projects the Al_2O_3 will be utilized as a support for Pt nanoparticles for thermal dehydrogenation of olefins, therefore the method in creating the thin film should be as simple as possible and reproducible.

3.3 Experimental Section

Growing thin film alumina has been the most challenging part of our experiment. Other published experimental parameters for making thin films did not work with our experimental setup for a variety of possible reasons. The exact temperature, type of heating and cooling system, distance of doser to sample, and other confounders may have played a role in this discrepancy. It took several months of trial and error to find the ideal parameters for our chamber to form well crystallized alumina that is easily imaged.

A NiAl(110) single crystal (MaTeck, 99.999% purity, ~9 mm in diameter by 1.5 mm thick) was continuously held in an Ultra High Vacuum (UHV) chamber. The NiAl single crystal sample was cleaned by cycles of oxygen dosing (P = 2 × 10^{-6} Torr, T_{sample} = 550 K, for 10 minutes), followed by annealing (T_{sample} = 1320 K for 15 minutes). Cleaning cycles were

repeated until Auger Electron Spectroscopy (AES, PHI model 10-155, single pass CMA) and STM (UHV 300 VT-STM, RHK Technology, Inc) confirmed a surface free of contaminants. STM images of the NiAl surface were obtained in constant current mode with tunneling currents of 1-2 nA and typical bias voltage of 0.5 V applied to the tip. Images were calibrated in the z-dimension using the NiAl crystal step height of 2.0 Å.[6]

We exposed the NiAl(110) surface to a saturation exposure of 1200 Langmuir of oxygen at 550 K (1 Langmuir = 10^{-6} Torr s) for 10 min. The sample was then annealed at 1200 K for 10 minutes. At lower annealing temperatures and shorter annealing times, we found that little to none of the surface was crystallized. However, if we annealed at temperatures higher than 1200 K the crystallized oxide layer began to desorb. The surface was imaged directly after forming the oxide layer using STM (UHV 300 VT-STM, RHK Technology, Inc). Typically our imaging conditions for Al_2O_3/NiAl were held at a bias range between 4-6 V and 1 nA tunneling current.

3.4 Results and Discussion

The morphology of the Al_2O_3 thin film is shown in Figure 3.2. Domain boundaries were only observed when we imaged above 4 V, indicating that they are due to the electronic properties between the metal substrate and the oxide layer. The domain boundaries are labeled in Figure 3.2a. The oxide layer typically runs ± 24^o to the [001] direction of the NiAl(110) substrate.[7,15] This difference of + or - 24 ^{o} is shown in Figure 3.1 and Figures 3.2c and d where the straight domain boundary lines run in two different directions. These bi-directional shifts are often referred to as two different domains, A and B. Domain A is labeled on Figure 3.2c and the domain boundaries run in the same direction as the step edges. Domain B is labeled on Figure 3c and the domain boundaries run perpendicular to the step edges. Approximately, 70% of the crystallized layer is domain A and the other 30% is domain B. Our crystallized oxide layer is

patchy. This can be seen in Figures 3.2a-d. Some areas show domain boundaries and are considered the crystallized oxide, while areas that do not have domain boundaries are considered amorphous. The two different areas were found to react differently within our experiment. The domain boundaries are 0.08 Å in height and 10 Å in width. The average distance between the boundaries is 60 Å. The step height between crystallized oxide layers was observed at 2.5 Å.

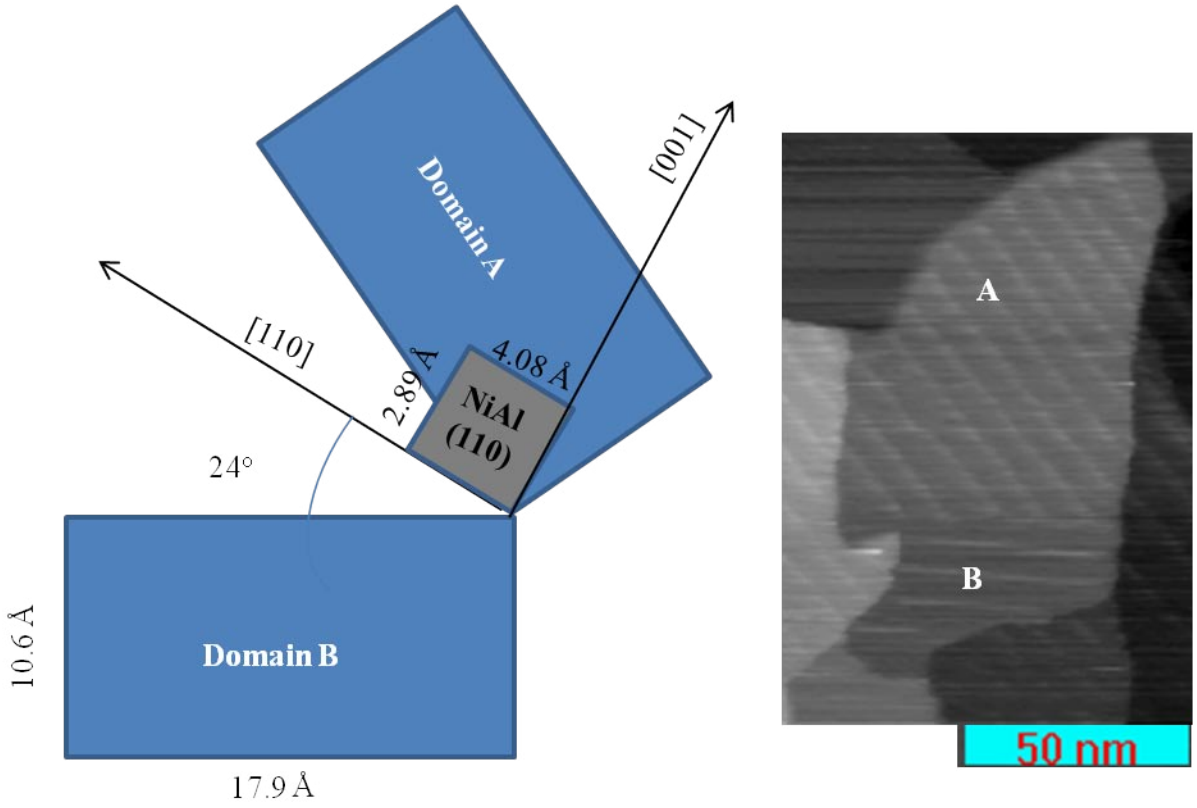

Figure 3.1 Orientation and unit cell size of the Al_2O_3 in relation to the substrate NiAl(110). Domains A and B are represented in both the schematic and the STM image.

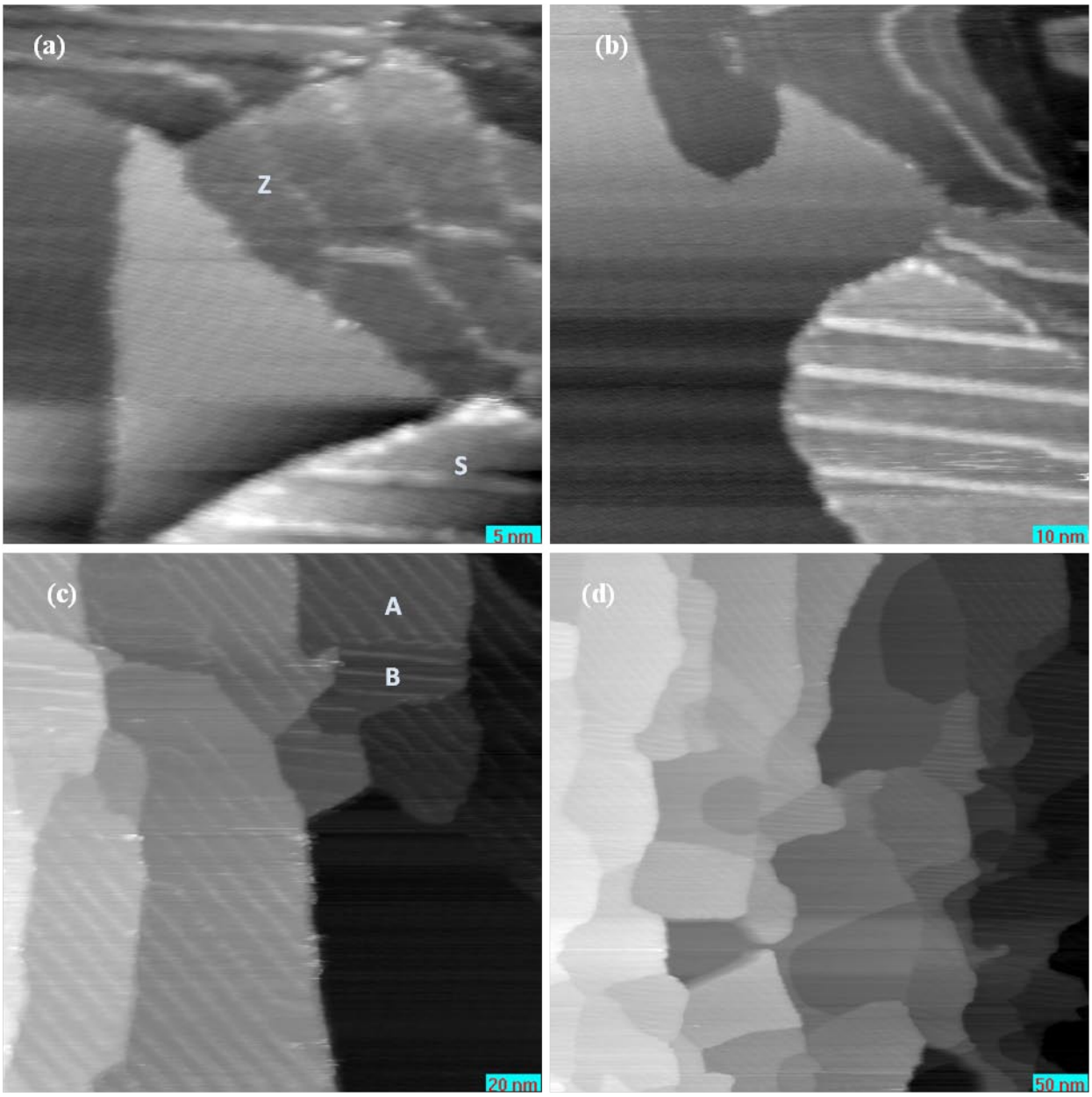

Figure 3.2 STM images of alumina thin layer formed by exposing NiAl(110) to 1200 Langmuir at 550 K for 10 min and then annealing to 1200 K for 10 min. (a) 50 × 50 nm image showing both zigzag (Z) and straight (S) domain boundaries in the crystallized oxide, (b) 100 × 100 nm image showing the straight domain boundaries next to areas that are amorphous, (c) 200 × 200 nm and (d) 500 × 500 nm images show how the crystalline oxide layer is patchy with domains A and B.

3.5 Conclusions

We were able to form a well ordered crystalline oxide layer with parameters somewhat similar to the well studied thin film alumina in literature. Our STM imaging observations closely matched what has already been observed in literature. Therefore, our Al_2O_3 thin film is adequate for further studies using platinum and olefin.

3.6 References

(1) Kresse, G.; Schmid, M.; Napetschnig, E.; Shishkin, M.; Kaehler, L.; Varga, P., *Structure of the Ultrathin Aluminum Oxide Film on NiAl(110).* Science, 2005. **308**(5727): p. 1440.

(2) Jaeger, R. M.; Kuhlenbeck, H.; Freund, H. J.; Wuttig, M.; Hoffmann, W.; Franchy, R.; Ibach, H., *Formation of a well-ordered aluminum oxide overlayer by oxidation of NiAl(110).* Surface Science, 1991. **259**(3): p. 235.

(3) Bertrams, T.; Brodde, A.; Hannemann, H.; Ventrice, C. A.; Wilhelmi, G.; Neddermeyer, H., *STM of Manipulated Structures - Characterization of metal-oxide films.* Applied Surface Science, 1994. **75**: p. 125.

(4) Ceballos, G.; Song, Z.; Pascual, J. I.; Rust, H. P.; Conrad, H.; Baumer, M.; Freund, H. J., *Structure investigation of the topmost layer of a thin ordered alumina film grown on NiAl(110) by low temperature scanning tunneling microscopy.* Chemical Physics Letters, 2002. **359**(1-2): p. 41.

(5) Simon, G. H.; Koenig, T.; Rust, H. P.; Heyde, M.; Freund, H. J., *Atomic structure of the ultrathin alumina on NiAl(110) and its antiphase domain boundaries as seen by frequency modulation dynamic force microscopy.* New Journal of Physics, 2009. **11**(9): p. 093009.

(6) Klimenkov, M.; Nepijko, S.; Kuhlenbeck, H.; Freund, H. J., *Transmission electron microscopic investigation of an ordered Al2O3 film on NiAl(110).* Surface Science, 1997. **385**(1): p. 66.

(7) Pang, C. L.; Raza, H.; Haycock, S. A.; Thornton, G., *Noncontact atomic force microscopy imaging of ultrathin Al2O3 on NiAl(110).* Physical Review B, 2002. **65**(20): p. 201401.

(8) Ulrich, S.; Nilius, N.; Freund, H.-J., *Growth of thin alumina films on a vicinal NiAl surface.* Surface Science, 2007. **601**(19): p. 4603.

(9) Pradhan, N. A.; Liu, N.; Ho, W., *Vibronic Spectroscopy of Single C60 Molecules and Monolayers with the STM* The Journal of Physical Chemistry B, 2005. **109**(17): p. 8513.

(10) Libuda, J.; Winkelmann, F.; Baumer, M.; Freund, H. J.; Bertrams, T.; Neddermeyer, H.; Maller, K., *Structure and defects of an ordered alumina film on NiAl(110).* Surface Science, 1994. **318**: p. 61.

(11) Lay, T.; Yoshitake, M.; Mebarki, B., *Temperature effect on growth of well-ordered thin Al2O3 film on NiAl(110).* American Vacuum Society, 2002. **20**(6): p. 2027

(12) Stierle, A.; Renner, F.; Streitel, R.; Dosch, H.; Drube, W.; Cowie, B. C., *X-ray Diffraction Study of the Ultrathin Al2O3 Layer on NiAl(110).* Science, 2004. **303**(5664): p. 1652.

(13) Kelber, J. A., *Alumina surfaces and interfaces under non-ultrahigh vacuum conditions.* Surface Science Reports, 2007. **62**(7): p. 271.

(14) Kulawik, M.; Nilius, N.; Rust, H. P.; Freund, H. J., *Atomic Structure of Antiphase Domain Boundaries of a Thin Al2O3 Film on NiAl(110).* Physical Review Letters, 2003. **91**(25): p. 256101.

(15) Simon, G. H.; Koenig, T.; Rust, H. P.; Heyde, M.; Freund, H. J., *Atomic structure of the ultrathin alumina on NiAl(110) and its antiphase domain boundaries as seen by frequency modulation dynamic force microscopy.* New Journal of Physics, 2009. **11**.

(16) Jacobs, J. P.; Reijne, S.; Elfrink, R. J. M.; Mikhailov, S. N.; Brongersma, H. H.; Wuttig, M., *Quantification of the Composition of Alloy and Oxide Surfaces Using Low-Energy Ion-Scattering.* Journal of Vacuum Science & Technology A, 1994. **12**(4): p. 2308.

(17) Libuda, J.; Baumer, M.; Freund, H. J., *Structural Characterization of Platinum Deposits Supported on Ordered Alumina Films.* Journal of Vacuum Science & Technology a-Vacuum Surfaces and Films, 1994. **12**(4): p. 2259.

(18) Diebold, U.; Li, S.-C.; Schmid, M., *Oxide Surface Science.* Annual Review of Physical Chemistry, 2010. **61**(1): p. 129.

(19) Simon, G. H.; Heyde, M.; Freund, H. J., *Imaging and manipulation of adatoms on an alumina surface by noncontact atomic force microscopy.* Journal of Physics: Condensed Matter, 2012. **24**(8): p. 084007.

(20) Kovarik, L.; Bowden, M.; Genc, A.; Szanyi, J. n.; Peden, C. H. F.; Kwak, J. H., *Structure of Alpha-Alumina: Toward the Atomic Level Understanding of Transition Alumina Phases.* The Journal of Physical Chemistry C. **118**(31): p. 18051.

(21) Addepalli, S.; Magtoto, N. P.; Kelber, J. A., *Interactions at the Ni3Al(111)-S-Al2O3 interface at elevated temperatures: Ordering of Al2O3 on an S-modified substrate.* Langmuir, 2000. **16**(22): p. 8352.

(22) Jennison, D. R.; Bogicevic, A., *Ultrathin aluminum oxide films: Al-sublattice structure and the effect of substrate on ad-metal adhesion.* Surface Science, 2000. **464**(2-3): p. 108.

(23) Jaeger, R. M.; Libuda, J.; Baumer, M.; Homann, K.; Kuhlenbeck, H.; Freund, H. J., *Vibrational structure of excited states of molecules on oxide surfaces* Journal of Electron Spectroscopy and Related Phenomena, 1993. **64**-**5**: p. 217.

CHAPTER 4

Formation of $Pt/Al_2O_3/NiAl(110)$

4.1 Abstract

Platinum (Pt) nanoparticles formed on Al_2O_3/NiAl(110) were studied using scanning tunneling microscopy (STM) held under ultra-high vacuum (UHV) conditions. Pt nanoparticles were deposited onto the sample at room temperature for 1 minute at a deposition flux of 1200 nA. Pressures were maintained in low 10^{-10} Torr with no significant change in pressure during Pt evaporation. The sample was then flash annealed at 770 K for 5 minutes. The Pt nanoparticles were on average 13 ± 3.1 Å in width and 2.1 ± 0.64 Å in height, corresponding to approximately 20 atoms per cluster. Pt nanoparticles deposited only on the crystalline alumina. The nanoparticles did not selectively deposit onto domain boundaries.

4.2 Introduction

Catalytic nanoparticles have high catalyst activity and provide a larger surface area to volume ratio than bulk catalysts.[1] Nanoparticles tend to have different and often higher catalytic activity compared to their bulk counterparts due to their varying size, structure and shape.[1] Nanoparticles are very important to industry in that they can reduce the cost of production as less expensive catalyst material is needed.[1] With higher catalytic activity lower temperatures are needed for reactions to occur.[1] Pt nanoparticles are used in a wide variety of fields such as in fuel cells and automotive exhaust gas cleanup.[1] Oxide supports can help stabilize nanoparticles thermodynamically, prevent agglomeration or movement, and prevent catalyst poisoning during reaction.[2,3] Not all supports are created equal. Many support materials such as SiO_2 and TiO_2 are either too soft or highly temperature sensitive.[4,5] Al_2O_3 on the other hand, is stable and a comparatively strong surface making it an ideal catalyst support.[3]

Al_2O_3 is one of the most used supports in industry, such as fuel cell and oil refining.[6-8] It was found in the late 1990's that Pt particles can stick to Al_2O_3 via evaporation as the Pt was found not to be elastically scattered with a sticking probability slightly less than 1 due to some re-evaporation.[9,10] The deposited particles then diffuse on the surface, which is dependent on a variety of factors. The defects on the support can play a role in the nanoparticle properties.[11] Nanoparticles act differently depending on their support, as the support can change the particles electronic properties, shape and structure.[12] For example, in previous LEED studies it was found that annealing Pt nanoparticles to temperatures of 500 K produces crystalline Pt(111).[2,13] However, in a TEM study the crystallinity of Pt(111) nanoparticles were observed to be size dependent and do not appear until the particles are at least 2-5 nm.[14,15]

The goal of this project is to deposit Pt nanoparticles onto Al_2O_3. The Pt nanoparticles are to be fully analyzed via STM and compared to previous Pt/Al_2O_3 studies. The main goal is to develop a method for forming Pt nanoparticles in a standardized way that can allow for utility in future projects. In future projects, thermal dehydrogenation of olefins on Pt/Al_2O_3 will be performed and compared to bulk Pt and discussed in further detail in Chapter 5 and 6.

4.3 Experimental Section

In literature, little information is given on how much Pt is dosed onto the thin film alumina. This is in part due to the fact that very small amounts of Pt are evaporated. The Pt evaporation occurs under ultra high vacuum (UHV) conditions. The pressures in UHV are on the order of 10^{-10} Torr. The amount of Pt evaporated is so little that the UHV pressures do not rise. Therefore, monolayer information in terms of Lagmuirs cannot be derived from the pressure. Instead, measurements are often given by QCM and deposition flux values. Unfortunately, often these techniques are more qualitative than quantitative and cannot be repeated in another

experimental setup. For our experimental setup we monitored the deposition of Pt using a flux monitor (EBE-FC, SPECS).

The Al_2O_3/NiAl(110) sample was held 2-3 mm from the evaporator's (EBE-1, SPECS) shutter in Ultra High Vacuum (UHV) conditions. Pt nanoparticles were deposited onto the sample at room temperature for 1 minute at a deposition flux of 1200 nA. Pressures were maintained in low 10^{-10} Torr with no significant change in pressure during Pt evaporation. The sample was then flash annealed at 770 K for 5 minutes. The sample was then imaged using Scanning Tunneling Microscopy (STM, UHV 300 VT-STM, RHK Technology, Inc). Without flash annealing the Pt particles, we found that the sample was difficult to image. Furthermore, dosing ethylene onto the Pt without annealing did not produce any new particle formation. Figure 4.1 exemplifies the differing Pt evaporation parameters. Figure 4.1c shows that when dosing at 800 nA flux, not enough Pt nanoparticles were deposited and it was quite difficult to find particles when imaging. Dosing at 5 min and 2.5 min at 1500 nA as shown in Figures 4.1a and 4.1b, produced a large quantity of particles. We desired a surface with fewer particles for an easier analysis. We finally settled on a 1 min dosing as shown in Figure 4.1d. To note, the amount of Pt deposited on the surface was too low to resolve with AES.

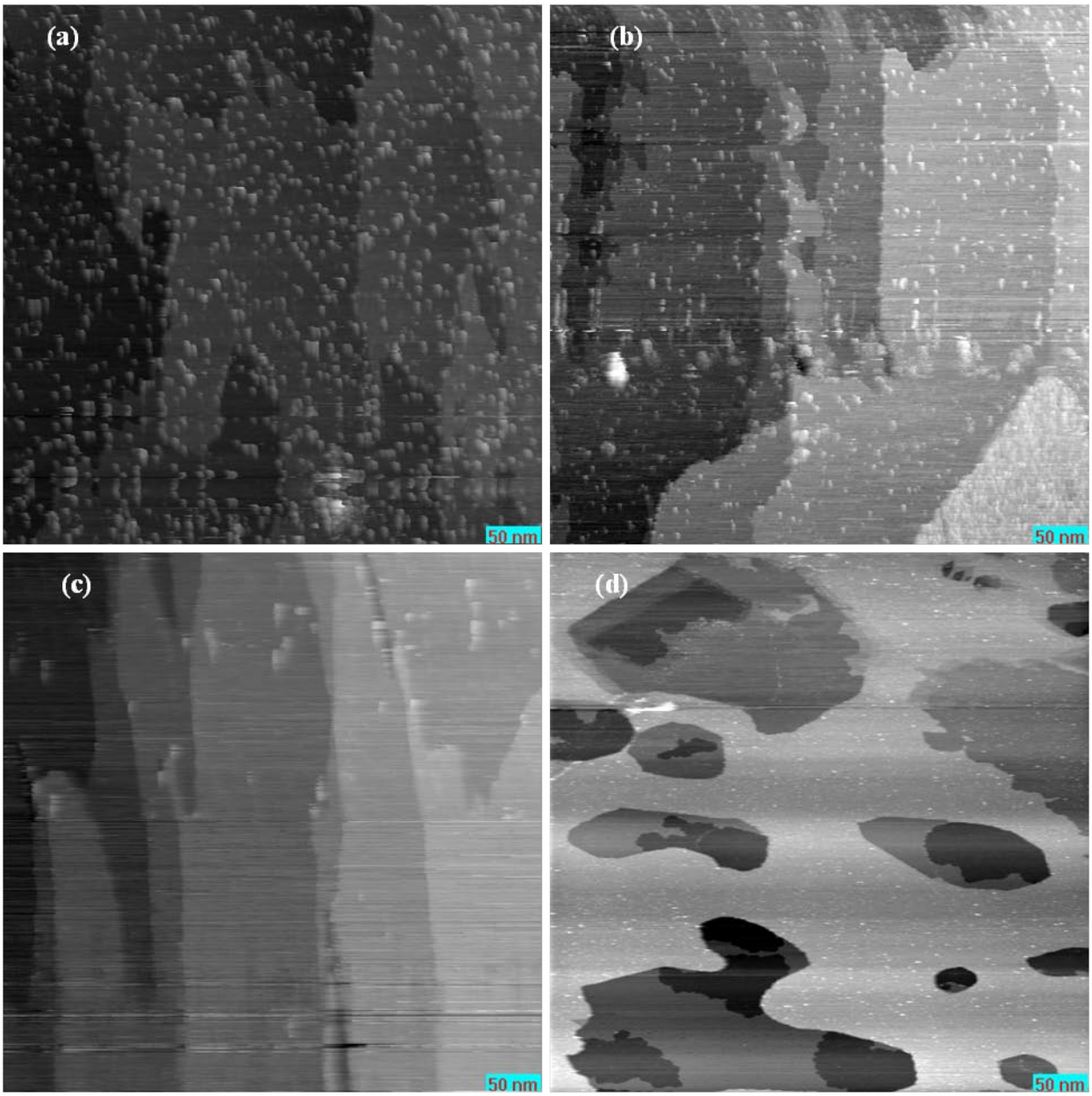

Figure 4.1 500 × 500 nm STM images of differing evaporating Pt conditions on Al_2O_3/NiAl(110). After evaporation, all samples were annealed to 770 K for 5 minutes before imaging. The evaporation conditions are as follows: (a) 5 minute evaporation with 1500 nA flux, (b) 2.5 minute evaporation with 1500 nA flux, (c) 1 minute evaporation with 1200 nA flux and (d) 1 minute evaporation with 1500 nA flux. The size differences between nanoparticles are due to tip differences and not actual particle size difference.

4.4 Results and Discussion

The evaporated Pt nanoparticles on Al_2O_3/NiAl(110) were analyzed using STM. It was observed that regardless of dosing time or quantity, the Pt nanoparticles remained constant in height and width. This is contradictory to a previous TEM study that found that with increased dosing, the Pt particles grew in size.[16] Interestingly, our study matched STM results of Pt on different alumina setup: Al_2O_3/NiAl(100).[17] With TEM the electron beam can modify the surface, including moving clusters around on the surface and changing their structure or shape – it was found with another study using higher current densities with TEM induced the Pt particles to coalesce.[18] Our Pt nanoparticles were on average 13 ± 3.1 Å in width and 2.1 ± 0.64 Å in height, as seen in Figures 4.2a-c. Based on this size parameter and using the estimation in a previous study, these Pt clusters contain approximately 20 atoms.[19]

Previously, it was reported in LEED studies that upon heating to temperatures up to 800 K[2,19] or even as low as 165 K[20] Pt diffused into the bulk or possibly moved along the surface. With continued annealing cycles, we did not observe a difference in height for the Pt nanoparticles, nor did it appear that the Pt particles reduced in number. Possibly, more annealing time is required for the Pt to diffuse into the bulk. Also, the Pt may have already diffused as we anneal at nearly 800 K before imaging. The Pt may not diffuse further after a certain point. It has been observed that high temperatures and/or pressures can affect the formation of Pt nanoparticles.[15] However, we found that our Pt nanoparticles are thermally stable up to temperatures of 1100 K.

In previous studies, at room temperature deposition with Ag[19], Pd[21], Pt[22] and Rh[21] on Al_2O_3/NiAl(110) the varying metals mainly deposited to the domain boundaries. This is believed to be the case as the evaporated metal binds strongly to the excess O at the defect

sites.[11] To the contrary, we observed that the Pt clusters deposited uniformly throughout the crystalline layer and have no preferential binding to step edges or grain boundaries, as can be seen in Figures 4.2a-c. This was observed in STM studies by *Klimenkov, et al.* and *Bertrams, et al.* and was explained as a possibility of a small diffusion length and a strong binding of the Pt to the Al_2O_3 surface.[16,23] This phenomena can be explained by a recent paper published in *Science* using ultrahigh magnetic field, solid-state magic-angle spinning nuclear magnetic resonance spectroscopy, and high-angle annular dark-field scanning transmission electron microscopy with density functional theory calculations. [24] This paper elucidates that the Al^{3+} pentahedral coordination sites on the Al_2O_3 are anchoring sites of the catalytically active Pt.[24] Similarly, in γ-Al_2O_3 bulk studies the Pt was found to be bound to the oxygen vacancy sites.[25,26]

Finally, we also observed that the Pt deposits only on the crystalline layer and not the amorphous layer, as shown in Figure 4.2b. This finding is consistent with a previous STM study with Pt on Al_2O_3/NiAl(100)[17] and a few studies of Co on Al_2O_3/NiAl(100).[27,28]

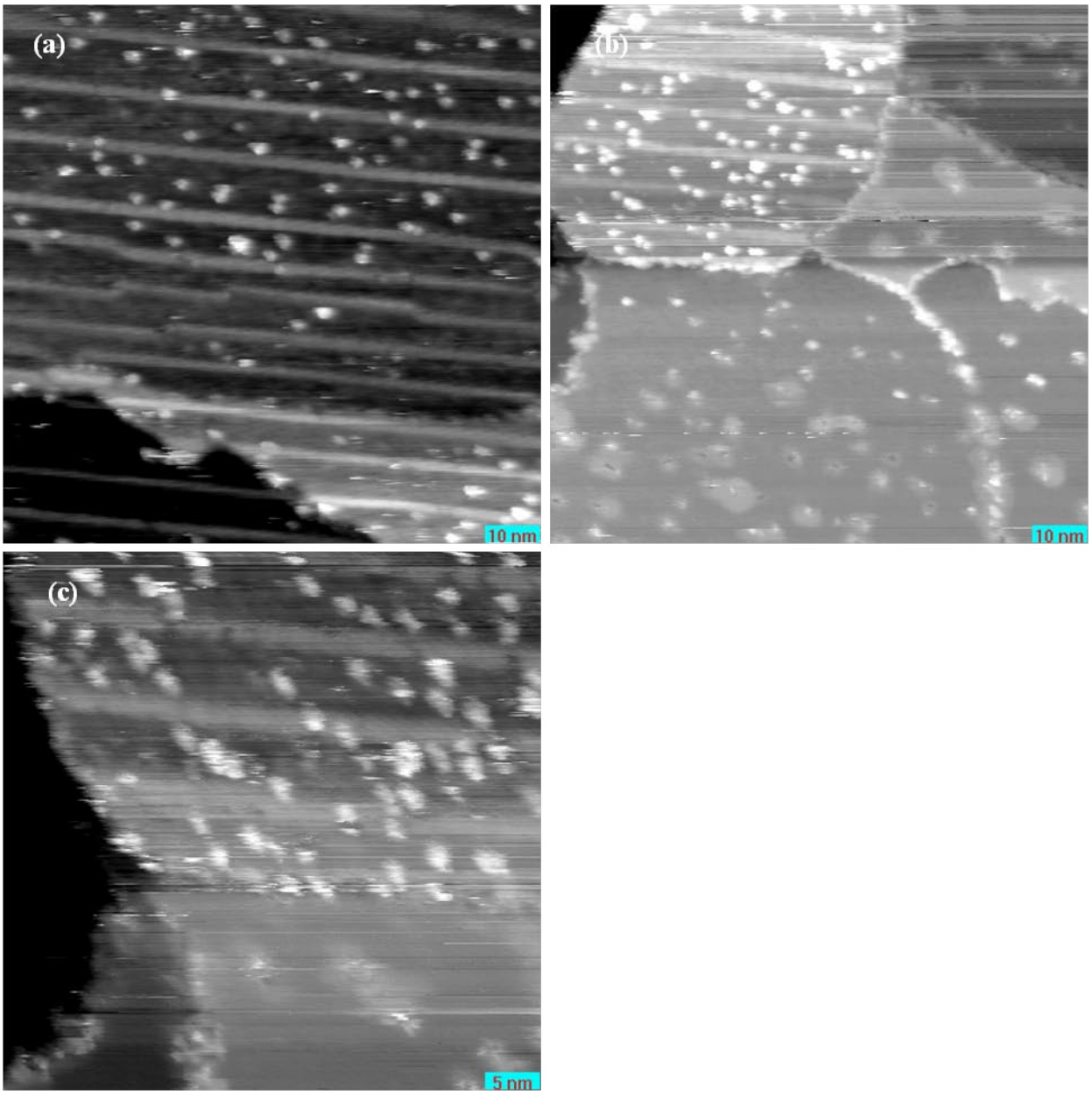

Figure 4.2 STM images of Pt evaporated onto Al_2O_3/NiAl(110). a) 100 × 100 nm image showing only crystalline Al_2O_3, b) 100 × 100 nm image showing two distinct regions of amorphous and crystalline Al_2O_3, c) 50 × 50 nm image exemplifying how Pt deposits only onto the crystalline Al_2O_3.

4.5 Conclusions

We studied Pt nanoparticles on Al_2O_3/NiAl(110) using STM. We found that the Pt nanoparticles were on average 13 ± 3.1 Å in width and 2.1 ± 0.64 Å in height. The Pt nanoparticles deposited uniformly throughout the crystalline alumina. It may be desirable in future studies to grow larger Pt nanoparticles, using varying deposition temperatures[17] to study size effects on dehydrogenation hydrocarbon chemistry.

4.6 References

(1) Applegate, J. R.; Pearlman, H.; Bakrania, S. D., *Catalysis of Methanol-Air Mixture Using Platinum Nanoparticles for Microscale Combustion.* Journal of Nanomaterials. **2012**: p. 8.

(2) Libuda, J.; Baumer, M.; Freund, H. J., *Structural Characterization of Platinum Deposits Supported on Ordered Alumina Films.* Journal of Vacuum Science & Technology a-Vacuum Surfaces and Films, 1994. **12**(4): p. 2259.

(3) Dandapat, A.; Jana, D.; De, G., *Synthesis of Thick Mesoporous Î³-Alumina Films, Loading of Pt Nanoparticles, and Use of the Composite Film as a Reusable Catalyst.* ACS Applied Materials & Interfaces, 2009. **1**(4): p. 833.

(4) Cortial, G.; Siutkowski, M.; Goettmann, F.; Moores, A.; Boissière, C.; Grosso, D.; Le Floch, P.; Sanchez, C., *Metallic Nanoparticles Hosted in Mesoporous Oxide Thin Films for Catalytic Applications.* Small, 2006. **2**(8-9): p. 1042.

(5) Yu, J. C.; Wang, X.; Fu, X., *Pore-Wall Chemistry and Photocatalytic Activity of Mesoporous Titania Molecular Sieve Films.* Chemistry of Materials, 2004. **16**(8): p. 1523.

(6) Jiang, C.; Hara, K.; Fukuoka, A., *Low-Temperature Oxidation of Ethylene over Platinum Nanoparticles Supported on Mesoporous Silica.* Chem. Int. Ed, 2013. **52**: p. 6265.

(7) Namgee Junga; Dong Young Chungb; Jaeyune Ryua; Sung Jong Yooa; Yung-Eun Sungb, *Pt-based nanoarchitecture and catalyst design for fuel cell applications.* NanoToday, 2014. **9**: p. 433.

(8) Lin, Y.-C.; Huber, G. W., *The critical role of heterogeneous catalysis in lignocellulosic biomass conversion.* Energy Environ. Sci., 2008. **2**: p. 68.

(9) Campbell, C. T., *Ultrathin metal films and particles on oxide surfaces: Structural, electronic and chemisorptive properties.* Surface Science Reports, 1997. **27**(1-3): p. 1.

(10) Henry, C. R., *Surface studies of supported model catalysts.* Surface Science Reports, 1998. **31**(7-8): p. 235.

(11) Diebold, U.; Li, S.-C.; Schmid, M., *Oxide Surface Science.* Annual Review of Physical Chemistry, 2010. **61**(1): p. 129.

(12) Cuenya, B. R., *Synthesis and catalytic properties of metal nanoparticles: Size, shape, support, composition, and oxidation state effects.* Thin Solid Films. **518**(12): p. 3127.

(13) Minvielle, T. J.; White, R. L.; Hildner, M. L.; Wilson, R. J., *Temperature dependence of the epitaxial growth of Pt on basal-plane sapphire.* Surface Science, 1996. **366**(3): p. L755.

(14) Zhang, Z.; Li, L.; Yang, J. C., *Adhesion of Pt Nanoparticles Supported on gamma-Al2O3 Single Crystal.* Journal of Physical Chemistry C. **117**(41): p. 21407.

(15) Rupprechter, G. n.; Freund, H.-J., *Adsorbate-induced restructuring and pressure-dependent adsorption on metal nanoparticles studied by electron microscopy and sum frequency generation spectroscopy.* Topics in Catalysis, 2000. **14**(1-4): p. 3.

(16) Klimenkov, M.; Kuhlenbeck, H.; Nepijko, S. A., *Growth mode of Pt clusters deposited on gamma-Al2O3(111)/NiAl(110): a TEM study.* Surface Science, 2003. **539**(1-3): p. 31.

(17) Luo, M. F.; Sartale, S. D.; Shiu, H. W.; Ten, M. H.; Huang, J. Y., *Scanning tunneling microscopy study of growth of Pt nanoclusters on thin film Al 2O 3/NiAl(100).* Surface Science, 2006. **600**(22): p. 4978.

(18) Nepijko, S. A.; Klimenkov, M.; Kuhlenbeck, H.; Freund, H. J., *Transmission electron microscopy study of platinum clusters on Al2O3/NiAl(110) under the influence of electron irradiation.* Journal of Vacuum Science & Technology a-Vacuum Surfaces and Films, 1999. **17**(2): p. 577.

(19) Freund, H. J.; Dillmann, B.; Ehrlich, D.; Hassel, M.; Jaeger, R. M.; Kuhlenbeck, H.; Ventrice, C. A.; Winkelmann, F.; Wohlrab, S.; Xu, C.; Bertrams, T.; Brodde, A.; Neddermeyer, H., *Adsorption and Reaction of Molecules on Surfaces of Metal-Metal Oxide Systems.* Journal of Molecular Catalysis, 1993. **82**(2-3): p. 143.

(20) Nilius, N.; Corper, A.; Bozdech, G.; Ernst, N.; Freund, H. J., *Experiments on individual alumina-supported adatoms and clusters.* Progress in Surface Science, 2001. **67**(1â€“8): p. 99.

(21) Kulawik, M.; Nilius, N.; Rust, H. P.; Freund, H. J., *Atomic Structure of Antiphase Domain Boundaries of a Thin Al2O3 Film on NiAl(110).* Physical Review Letters, 2003. **91**(25): p. 256101.

(22) Beniya, A.; Isomura, N.; Hirata, H.; Watanabe, Y., *Lateral displacement in soft-landing process and electronic properties of size-selected Pt7 clusters on the aluminum oxide film on NiAl.* Chemical Physics Letters. **576**(0): p. 49.

(23) Bertrams, T.; Brodde, A.; Hannemann, H.; Ventrice, C. A.; Wilhelmi, G.; Neddermeyer, H., *STM of Manipulated Structures - Characterization of metal-oxide films.* Applied Surface Science, 1994. **75**: p. 125.

(24) Kwak, J. H.; Hu, J.; Mei, D.; Yi, C.-W.; Kim, D. H.; Peden, C. H. F.; Allard, L. F.; Szanyi, J., *Coordinatively Unsaturated Al3+ Centers as Binding Sites for Active Catalyst Phases of Platinum on gamma-Al2O3.* Science, 2009. **325**(5948): p. 1670.

(25) Nellist, P. D.; Pennycook, S. J., *Direct imaging of the atomic configuration of ultradispersed catalysts.* Science, 1996. **274**(5286): p. 413.

(26) Sohlberg, K.; Rashkeev, S.; Borisevich, A. Y.; Pennycook, S. J.; Pantelides, S. T., *Origin of anomalous Pt-Pt distances in the Pt/alumina catalytic system.* Chemphyschem, 2004. **5**(12): p. 1893.

(27) Luo, M. F.; Wen, W. H.; Lin, C. S.; Chiang, C. I.; Sartale, S. D.; Zei, M. S., *Structures of Co and Pt nanoclusters on a thin film of Al2O3/NiAl(100) from reflection high-energy electron diffraction and scanning-tunnelling microscopy.* Surface Science, 2007. **601**(10): p. 2139.

(28) Luo, M.-F.; Wang, C.-C.; Chao, C.-S.; Ho, C.-Y.; Wang, C.-T.; Lin, W.-R.; Lin, Y.-C.; Lai, Y.-L.; Hsu, Y.-J., *Temperature-dependent structuring of Au-Pt bimetallic nanoclusters on a thin film of Al2O3/NiAl(100).* Physical Chemistry Chemical Physics, 2007. **13**(4): p. 1531.

CHAPTER 5

The Conversion of Small Hydrocarbons to Carbon Clusters on Platinum

5.1 Abstract

Thermal dehydrogenation of propylene and butylene adsorbed on Pt(111) has been studied under ultra-high vacuum (UHV) conditions using scanning tunneling microscopy (STM). After heating to 700 K the alkenes dehydrogenated to form flat, uniformly sized circular carbon clusters with less than a monolayer coverage. With cycles of continued adsorption and heating, particles grew in number but not in size. The catalytic activity stopped by the third saturation dose, leaving areas of bare Pt. Clusters of propylene and butylene were 12 ± 1.2 Å and 13 ± 1.0 Å in diameter, respectively. Propylene and butylene clusters contained an average of 44 and 51 carbon atoms per cluster, respectively.

5.2 Introduction

Metal-hydrocarbon complexes are important precursors or intermediates to a multitude of catalysis reactions[1] and they have a variety of applications including the manufacturing of microelectronic components via organometallic chemical vapor deposition (OMCVD).[1] Noble and transition metals, such as Pt(111) have been studied as catalysts for a variety of reactions;[1-4] including adsorbed olefins, such as ethylene, propylene and butylene for hydrogenation-dehydrogenation reactions in catalysis studies.[5] This report provides morphological information about the thermal interaction of propylene and butylene with Pt(111) by implementing a variable temperature scanning tunneling microscope (STM) under ultra-high vacuum (UHV) to reveal the surface morphology of the dehydrogenated olefins. STM is an ideal tool to study the reactivity, stability and catalytic site on the model surface.[6]

Most studies of olefins on Pt have used techniques that focus on chemical identity[7-22] and/or the reaction kinetics.[12,15-20,23-25] Previous studies of the small olefins: ethylene, propylene and butylene have shown to be converted to alkylidyne at room temperature.[7-10,12,16,17,19,20,25-29] The dehydrogenation pathway for ethylene is shown in Figure 5.1. At temperatures around 320 K the alkylidyne species begins to break down into numerous C_xH_y fragments, in the range of 400-450 K all of the alkylidyne species are completely decomposed.[12,15,20,26]

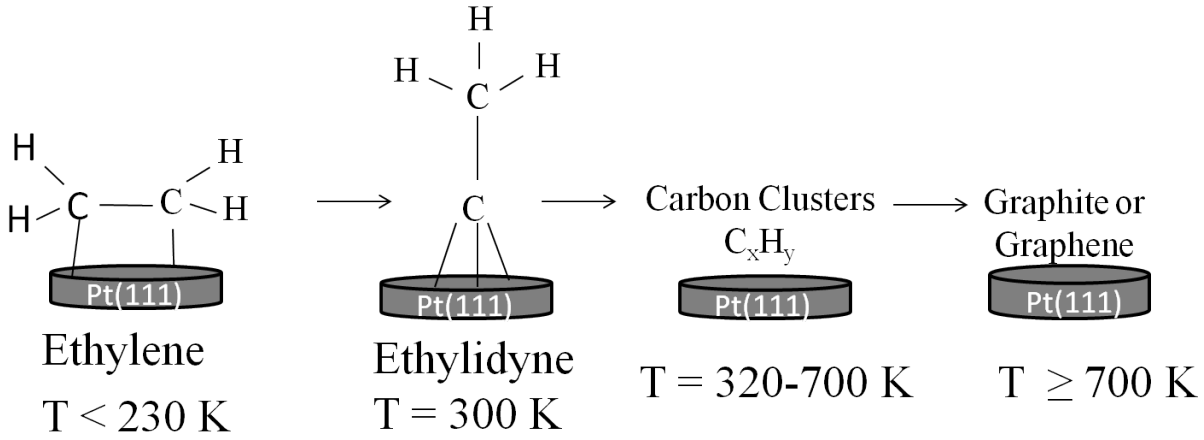

Figure 5.1 The temperature dependent pathway for ethylene adsorption and dehydrogenation on Pt(111).

Only a few STM studies of olefins on Pt have been performed.[30-32] Previous STM studies with ethylene and propylene have shown that the dehydrogenated fragments aggregate into well-defined clusters on open Pt areas when annealed above 400 K.[30-33] With additional adsorption and annealing cycles of ethylene, more clusters of the same size were formed; however, by the fourth cycle new cluster formation was negligible.[30] With continued annealing to higher temperatures, the olefins continued to dehydrogenate until only surface carbon remains at a temperature above 700 K.[12,15,27,33] At temperatures above 700-800 K graphite was formed from ethylene and propylene.[16,26,30-33] Previous studies have not determined if the adsorption and dehydrogenation of propylene and butylene will produce larger clusters or more clusters of the

same size in comparison to ethylene. Furthermore, no STM studies have been conducted to analyze the behavior of butylene during dehydrogenation, nor have there been any studies on the cluster growth with multiple cycles of adsorption/annealing with propylene and butylene.

In this work, the morphology of the dehydrogenation reactions of propylene and butylene occurring over Pt(111) is elucidated via STM imaging. Propylene and butylene gases were dosed onto Pt(111) at room temperature and subsequently annealed to 700 K. This process was repeated four times and the morphology was recorded by STM after each adsorption/annealing cycle. Annealing produced similar behavior as was previously seen with the smaller olefin, ethylene.[30] Flat circular cluster of uniform size were produced. The clusters do not change in size with subsequent dosing; however, the cluster density increases instead.

5.3 Experimental Section

A Pt(111) single crystal (MaTeck, 99.999% purity, ~9 mm in diameter by 1.5 mm thick) with average terrace widths of 100 nm was transferred into a UHV dual-chamber system with base pressure of less than 1×10^{-10} Torr. The size and morphology of molecular species adsorbed to the Pt single crystal were studied in a single chamber using a variable temperature STM (UHV 300 VT-STM, RHK Technology, Inc). A second chamber is equipped with both ion bombardment (ISE-10, Omicron) and Auger Electron Spectroscopy (AES, PHI model 10-155, single pass CMA) were used for sample cleaning and characterization.

The Pt single crystal sample was heated by electron beam via a tungsten wire ~2 mm beneath the sample in order to create a smooth surface. Surface temperatures were monitored using a chromel-alumel thermocouple attached to the sample. The Pt single crystal sample was cleaned by cycles of Ar^+ bombardment (I_{Ar+} = 5 μA at 600 eV, T_{sample} = 300 K, for 30 minutes), followed by oxygen treatment ($P = 5.0 \times 10^{-6}$ Torr, T_{sample} = 700 K for 30 minutes) and then

annealed (T_{sample} = 1100 K for 10 minutes). Cleaning cycles were repeated until AES confirmed a surface free of containments. STM images were obtained in constant current mode with tunneling currents of 1-2 nA and typical bias voltage of 500 mV applied to the tip. Images were calibrated in the z-dimension using the Pt crystal step height of 2.3 Å.[34]

Butylene (99.9% purity, Airgas) and propylene (99.95% purity, Matheson Tri-Gas) gas adsorbates were studied separately. The STM chamber was backfilled with the individual olefin gas through a leak valve, exposing the sample to a saturation exposure of 18 Langmuir[10] at 300 K (1 Langmuir = 10^{-6} Torr s). One cycle was completed by annealing to 700 K for 5 minutes, followed by STM imaging. Previous studies have indicated that by about 700 K complete dehydrogenation occurs for ethylene,[12,27] propylene,[15,26,27] and butylene.[20] This dosing/annealing cycle was repeated five times.

5.4 Results and Discussion

The terrace and morphology of a Pt(111) single crystal surface after cycles of cleaning is shown in Figure 5.2a. Straight steps with single atomic step height run across the surface, and the resulting terraces on Pt(111) are flat with an average width of ~100 nm. Olefin molecules are then introduced for adsorption onto the Pt(111) surface. Propylene and butylene dehydrogenate to propylidyne[9,10,16,17,26,28] and butylidyne[7,10,19,20] at room temperature. The adsorption and annealing of propylene and butylene in UHV on Pt(111) were examined using STM. STM images of a Pt(111) surface after saturation exposure of propylene at 300 K reveal a (2 × 2) structure of propylidyne (Figure 5.2). This is the first time that propylidyne has been imaged by STM.

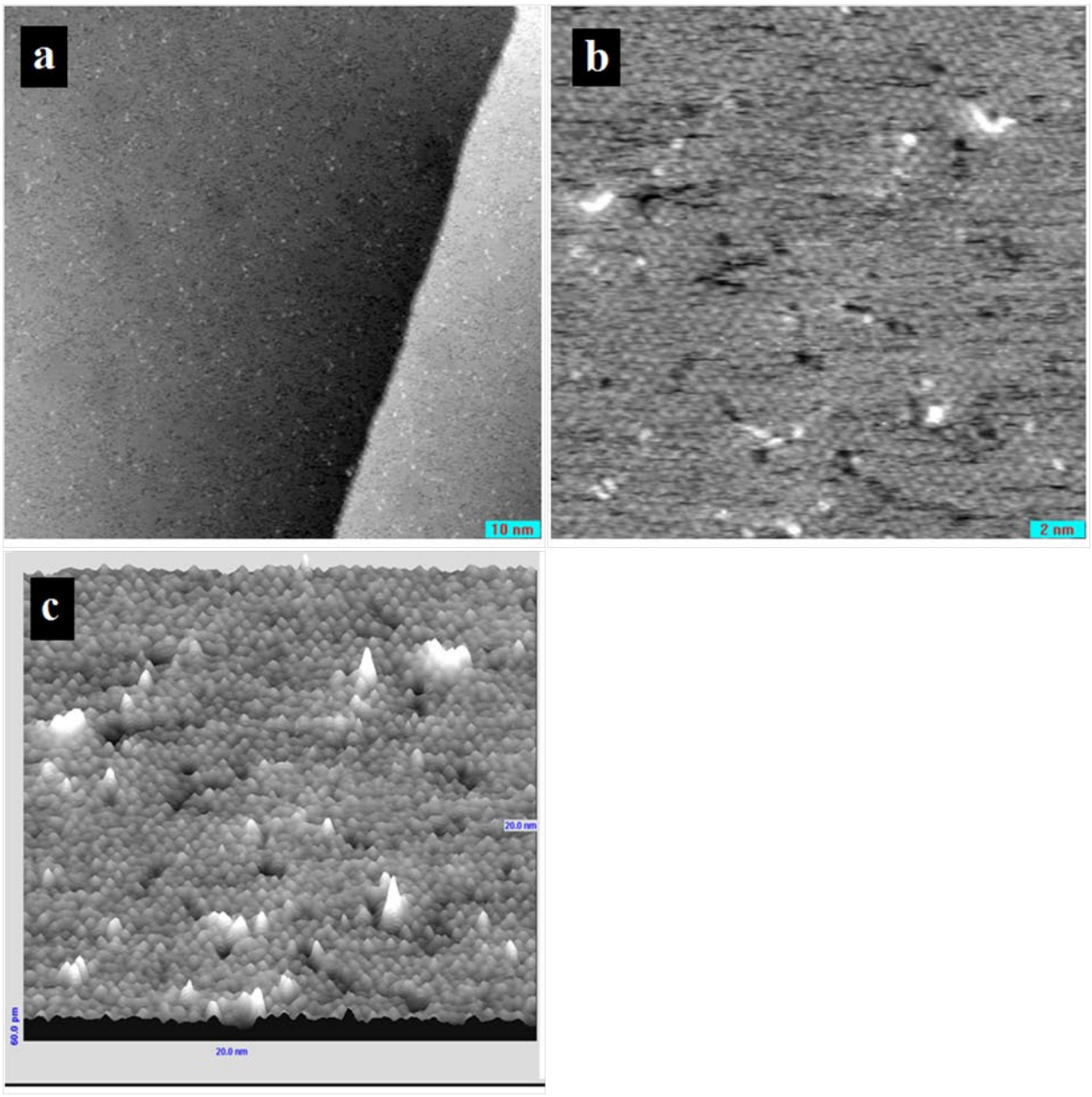

Figure 5.2 First dosing of propylene on Pt(111) before annealing. (2 × 2) structure is shown. (a) 100 nm × 100 nm (b) 20 nm × 20 nm (c) 3D view at 20 nm × 20 nm. STM images of a Pt(111) surface after saturation exposure of propylene at 300 K reveal a (2 × 2) structure of propylidyne.

STM images of butylene at 300 K did not resolve any discernible structures, which may be due to low frequency vibrations or high surface mobility.[32] Annealing to 700 K allows for the complete dehydrogenation of propylene[12,22] and butylene.[18] Figure 5.3b shows the morphology after one cycle of adsorption/annealing of propylene. We can see that carbon clusters form across the Pt(111) surface with no indication of step decorations.

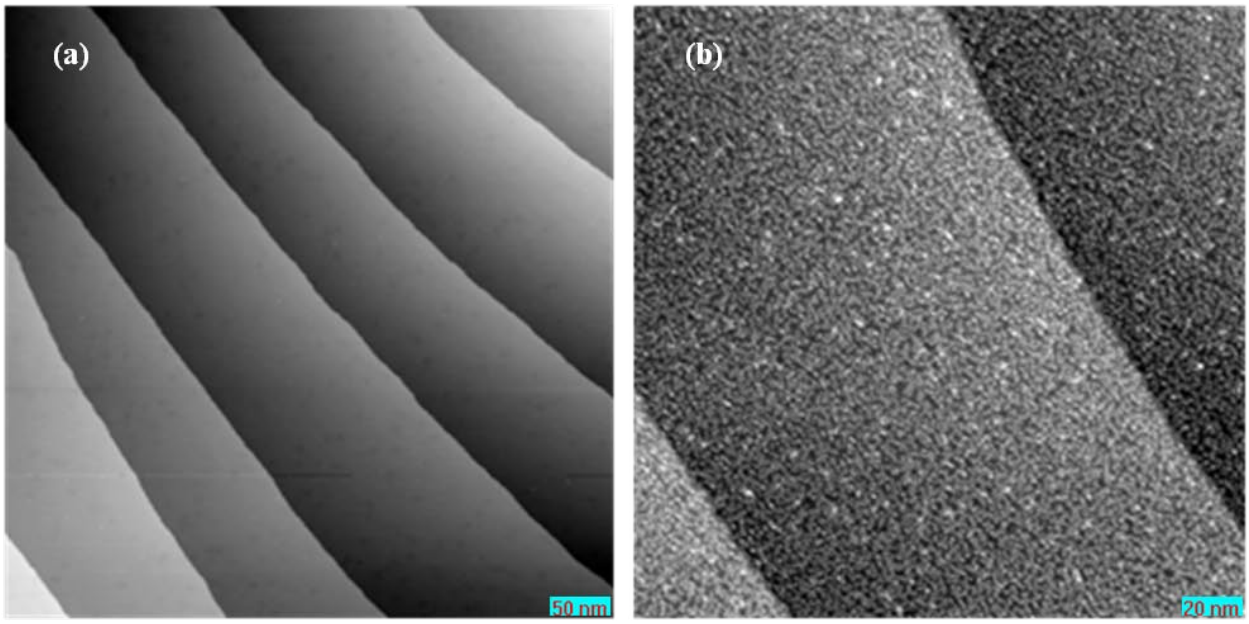

Figure 5.3 STM image of (a) clean Pt(111) surface with an average terrace width of ~100 nm (500 nm × 500 nm), and (b) Pt(111) surface covered with carbon clusters (200 nm × 200 nm) produced by adsorption of 20 Langmuir propylene at room temperature and subsequently flash-annealed at 700 K.

Figures 5.4a-d present higher resolution STM images of cycles of adsorption/annealing of propylene/butylene. After the first cycle, the dehydrogenation particles for both propylene and butylene appear to be flat, circular clusters, in a single atomic layer and uniform in size. With continued adsorption/annealing cycles, particle clusters continued to form on the empty Pt spaces.

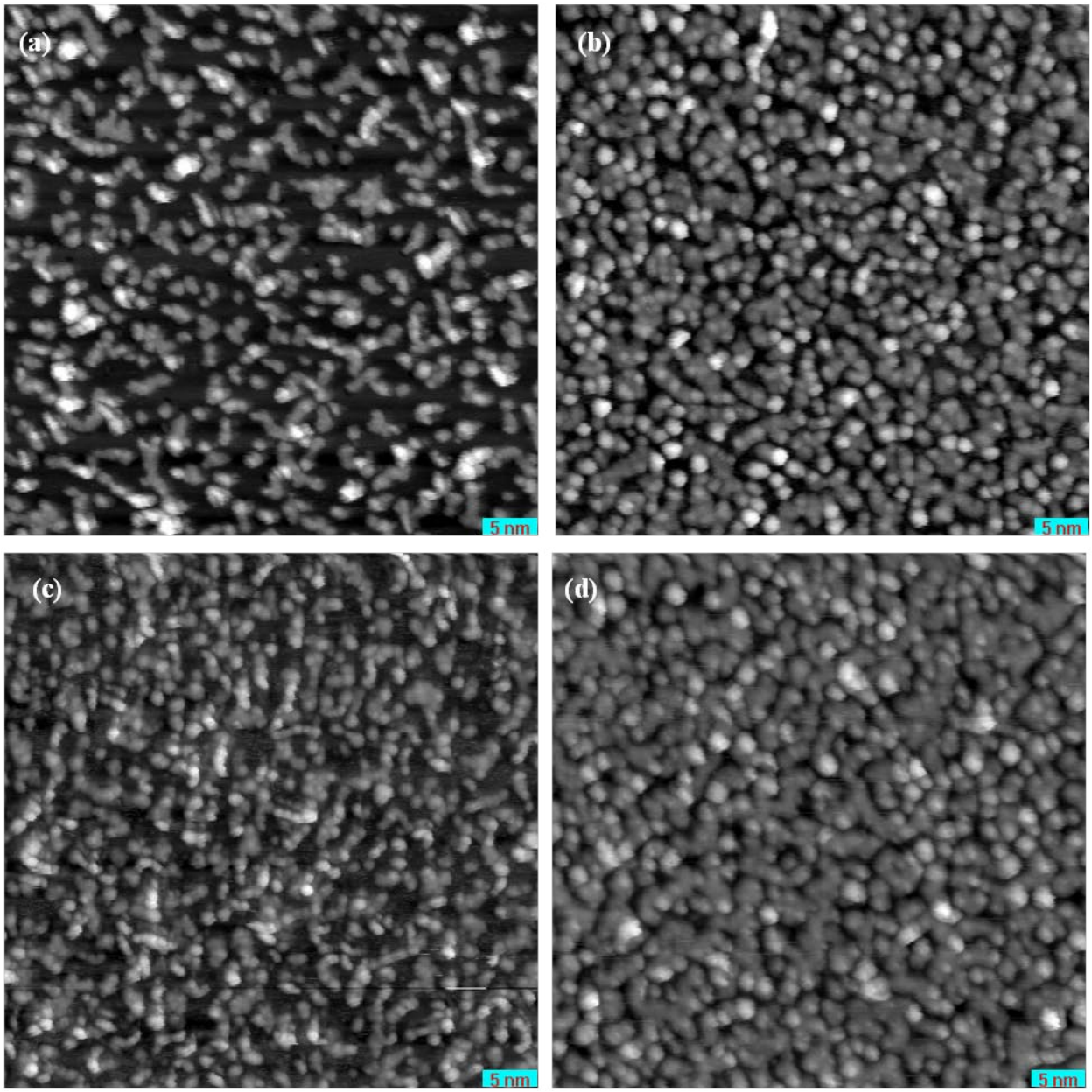

Figure 5.4 50 nm × 50 nm STM images of Pt(111) surface covered with carbon clusters after (a) 1 cycle of adsorption/annealing of propylene, (b) 4 cycles of adsorption/annealing of propylene, (c) 1 cycle of adsorption/annealing of butylene and (d) 4 cycles of adsorption/annealing of butylene. A cycle of adsorption/annealing is defined as adsorption of 20 Langmuir olefin at room temperature and subsequently flash-annealed to 700 K.

The evolution of the surface area coverage and particle density with the number of adsorption/annealing cycles is presented in Figure 5.5. The particle surface area coverage on Pt from the STM images was analyzed by using the ImageJ free software[35] to distinguish the background Pt from the particles. The program converts the images to a binary black/white format with pixels being grouped based on their grayscale.[35] In this manner, the Pt surface is distinguished from the particles and the program can then provide coverage data. Analysis of the images showed that the percent area coverage increased with dosing as seen in Figure 5.6. After the first cycle, over 40% of the Pt had non-bonded regions which could potentially be catalytically active. This data indicates that Pt catalytic activity is not quenched with the first saturation dosages of alkylidyne. By the third cycle the Pt surface was no longer catalytically active as the percent coverage leveled off. There was no new particle formation during the fourth cycle, even though only 80% of the Pt was covered. Similar results were previously seen with ethylene, where by the fourth adsorption/annealing cycle new cluster formation ceased.[30] The parameters of the ethylene study were essentially the same as this study.[30] It is interesting to note that the particle formation from ethylene ceased one cycle before propylene and butylene.[30] There may be a correlation between linear chain length and maximum surface coverage; whereby the formation of particles from larger reactants ceases earlier. Larger olefins may stop reacting sooner due to the greater amount of carbon presented to the surface at each saturation dose. By counting the number of particles manually in an area we estimated the density of the dehydrogenated particles (Figure 5.5). The carbon particle density from butylene is lower when compared with propylene, suggesting that the particle size for the longer olefin is larger.

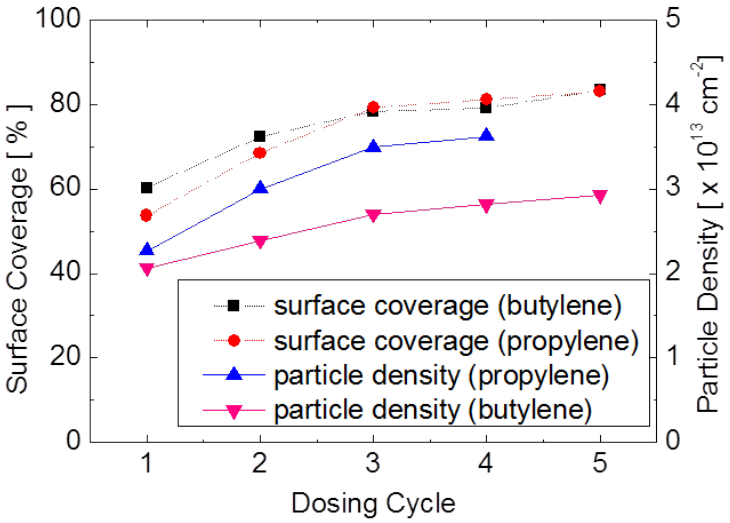

Figure 5.5 Evolution of surface coverage and density of carbon particles on Pt(111) surface.

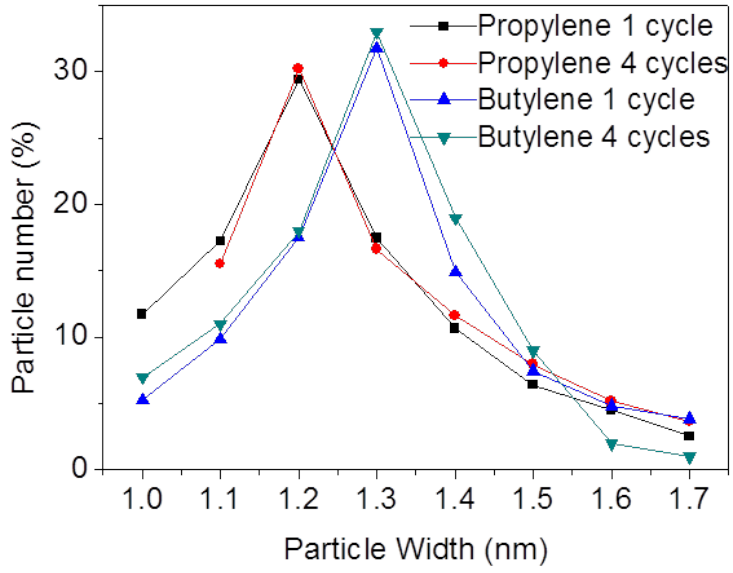

Figure 5.6 Size distribution of carbon particles on Pt(111) surface after several adsorption/annealing cycles of propylene/butylene.

The particle sizes were then analyzed using surface cross section analysis per standard STM methods. There was no significant change in particle size between the five dosings indicating that clusters did not act as nucleation sites. Instead of particles increasing in size, they increased in quantity. Johanek *et al.*[30] observed this same behavior with ethylene and postulated that this phenomenon is either due to: a) a space requirement for the hydrocarbon to undergo dehydrogenation; or b) that the catalytic properties of Pt are altered by carbon adsorption.[30] Figure 5.6 shows the distribution of particle sizes for cycles 1 and 4. The average widths of the propylene and butylene particles are 12 ± 1.2 Å and 13 ± 1.0 Å, respectively. This size difference may be due to tip-sample convolution. As the size difference between the dehydrogenated propylene and butylene particles is small, it is possible that the particles are in actuality the same size. Previous work on dehydrogenating ethylene over Pt(111) in our lab has shown that the dehydrogenated ethylene clusters have an average diameter of 15 ± 2 Å.[30] Another dehydrogenation study of ethylene in our lab gave the range for the clusters at 7-13 Å.[36] Previously, it was thought that particles formed from olefin dehydrogenation would create individual carbon atoms on the surface.[32] Other work has shown that particles formed from propylene and ethylene were actually much larger than individual carbon atoms.[30-33] Our results support the latter – that is, particles formed from propylene and butylene are larger than individual carbon atoms.

STM images are a convolution of sample, tip, and electron structure effects[37] – therefore an alternative method to estimate particle size is preferred.[32] Size can be estimated by determining the carbon atoms per particle from the surface density. The surface densities from the first adsorption/annealing cycle are 2.0×10^{13} particles cm^{-2} and 2.25×10^{13} particles cm^{-2} for butylene and propylene, respectively. Assuming that by annealing to 700 K all adsorbed

alkylidyne converted to carbon without desorption or dissolving, the number of carbon atoms in each particle can be estimated. With this in mind, the saturation surface coverage of propylidyne and butylidyne on Pt have been previously experimentally determined to be 0.22 ML[10,15] and 0.17 ML[7] respectively (ML = monolayer and is referred to here as a coverage of one molecule per surface Pt atom). Using the ratio of the known Pt surface atom density of 1.505×10^{15} atoms cm^{-2} (equivalent to 1.0 ML)[7] and the particle density, multiplied by the surface coverage and the number of carbon atoms per molecule we are able to deduce the number of carbon atoms. The carbon particles consist of an average of 51 carbon atoms for butylene and 44 carbon atoms for propylene. The previous study under the same conditions determined 34 ± 9 carbon atoms per cluster were formed from ethylene.[30] Particle size information shows a correlation of the particle size with the hydrocarbon's chain length. More detailed structure of the clusters is not resolved by STM.

To better determine the structure, an alternative method was used to determine the number of carbon atoms. In previous ethylene dehydrogenation studies graphite was formed.[30-32] Although STM images in this study did not reveal the atomic structure of the carbon particles, it is assumed these particles may have graphite-like structures with a round shape since they are all about 2 Å high with a flat top. Based on the diameter of the particles and the hexagonal structure of graphite, the areas of the individual dehydrogenated particles from propylene and butylene were determined respectively. By equating the quotient of the rhombus area and the 2 carbons of the graphite unit cell to that of the area of particles we are able to determine the carbon number per cluster. From this method we find that the carbon number per cluster is 43 ± 7 and 51 ± 8 C-atoms for propylene and butylene respectively. These numbers correspond well with our previous method, indicating that these particles are consistent with graphite. It is not understood

how graphite is created on Pt surfaces with olefins. From the above results, it is possible that graphite is formed from carbon clusters which were created from olefins reacting on Pt surfaces.

5.5 Conclusion

STM experiments in UHV have led to an understanding of olefin dehydrogenation on single crystals of Pt(111). Propylidyne was formed by dosing propylene onto Pt(111) at room temperature. Propylene and butylene behave in a similar manner to ethylene in that upon heating, they form flat circular and uniform particle clusters without preference for step edges or terraces. Heating the sample to 700 K may not have fully dehydrogenated propylene and butylene. Particle density increased with dosing - indicating that catalytic activity was not suppressed until the third cycle. With the third 18 Langmuir dosing cycle, the catalytic activity appeared to halt. The particles are consistent with graphite's structure.

It is difficult to make a definitive conclusion about the actual size of the individual particles. From two separate STM studies performed in our lab, clusters formed from ethylene were measured at either a range of 7-13 Å[36] or an average of 15 ± 2 Å.[30] The clusters formed from propylene and butylene were 12 ± 1.2 Å and 13 ± 1.0 Å in diameter respectively. By comparing the size of the clusters formed from the various olefins, there is no apparent size dependent value between the chain lengths. There may be a set size that the carbon clusters grow to on Pt(111) regardless of the initial molecules chain length. Based on their densities, saturation dosing, and initial particle size the carbon number in each cluster can be inferred. At 700 K propylene and butylene formed 44 and 51 carbon atom clusters respectively. Previously, it was inferred that ethylene formed 34 carbon atom clusters.[30] From this calculation, the carbon number in each cluster was linear with respect to chain length (e.g. $C_4 > C_3 > C_2$). The only true

conclusion that can be made from the size analysis is that the size of clusters remained constant and larger clusters were not formed from continuous dosing and annealing cycles for each olefin.

5.6 References

(1) Sivaramakrishna, A.; Clayton, H. S.; Mogorosi, M. M.; Moss, J. R., *Hydrocarbon (pi- and sigma-) complexes of nickel, palladium and platinum Synthesis, reactivity and applications.* Coordination Chemistry Reviews, 2010. **254**(23-24): p. 2904.

(2) Zaera, F., *Surface chemistry of hydrocarbon fragments on transition metals: towards understanding catalytic processes.* Catalysis Letters, 2003. **91**(1-2): p. 1.

(3) Ahmed, S.; Aitani, A.; Rahman, F.; Al-Dawood, A.; Al-Muhaish, F., *Decomposition of hydrocarbons to hydrogen and carbon.* Applied Catalysis a-General, 2009. **359**(1-2): p. 1.

(4) Samorjai, G.; Li, Y., *Introduction to Surface Chemistry and Catalysis*. 2nd ed. 2010, New Jersey: John Wiley and Sons, Inc.

(5) Sivaramakrishna, A.; Clayton, H. S.; Mogorosi, M. M.; Moss, J. R., *Hydrocarbon ([pi]- and [sigma]-) complexes of nickel, palladium and platinum: Synthesis, reactivity and applications.* Coordination Chemistry Reviews. **254**(23-24): p. 2904.

(6) Bonnell, D., *Introduction*, in *Scannning Tunneling Microscopy and Spectroscopy: Theory, Techniques, and Applications*, Bonnell, D., Editor. 1993, VCH Publishers, Inc: New York.

(7) Tsai, Y. L.; Koel, B. E., *Temperature-programmed desorption investigation of the adsorption and reaction of butene isomers on Pt(111) and ordered Pt-Sn surface alloys.* Journal of Physical Chemistry B, 1997. **101**(15): p. 2895.

(8) Lee, I.; Zaera, F., *Thermal Chemistry of C4 Hydrocarbons on Pt(111):â€‰ Mechanism for Double-Bond Isomerization.* The Journal of Physical Chemistry B, 2005. **109**(7): p. 2745.

(9) Valcarcel, A.; Ricart, J. M.; Clotet, A.; Illas, F.; Markovits, A.; Minot, C., *Theoretical study of dehydrogenation and isomerisation reactions of propylene on Pt(111).* Journal of Catalysis, 2006. **241**(1): p. 115.

(10) Koestner, R. J.; Frost, J. C.; Stair, P. C.; Vanhove, M. A.; Somorjai, G. A., *Evidence For The Formation Of Stable Alkylidyne Structures From C-3 And C-4 Unsaturated-Hydrocarbons Adsorbed On The Pt(111) Single-Crystal Surface.* Surface Science, 1982. **116**(1): p. 85.

(11) Yang, M.-L.; Zhu, Y.-A.; Fan, C.; Sui, Z.-J.; Chen, D.; Zhou, X.-G., *Density functional study of the chemisorption of C1, C2 and C3 intermediates in propane dissociation on Pt(1 1 1).* Journal of Molecular Catalysis A: Chemical, 2010. **321**(1-2): p. 42.

(12) Creighton, J. R.; White, J. M., *A Sims Study of the Dehydrogenation of Ethylene on Pt(111).* Surface Science, 1983. **129**(2-3): p. 327.

(13) Mittendorfer, F.; Thomazeau, C.; Raybaud, P.; Toulhoat, H., *Adsorption of Unsaturated Hydrocarbons on Pd(111) and Pt(111): A DFT Study.* The Journal of Physical Chemistry B, 2003. **107**(44): p. 12287.

(14) Delbecq, F.; Sautet, P., *The effect of substituents on the adsorption of alkenes on (111) Pt and Pd surfaces: a theoretical study.* Catalysis Letters, 1994. **28**(1): p. 89.

(15) Zaera, F.; Chrysostomou, D., *Propylene on Pt(111)II. Hydrogenation, dehydrogenation, and H-D exchange.* Surface Science, 2000. **457**(1-2): p. 89.

(16) Zaera, F.; Chrysostomou, D., *Propylene on Pt(111) I. Characterization of surface species by infra-red spectroscopy.* Surface Science, 2000. **457**(1-2): p. 71.

(17) Cremer, P. S.; Su, X.; Shen, Y. R.; Somorjai, G. A., *Hydrogenation and Dehydrogenation of Propylene on Pt(111) Studied by Sum Frequency Generation from UHV to Atmospheric Pressureâ€* The Journal of Physical Chemistry, 1996. **100**(40): p. 16302.

(18) Lee, A. F.; Wilson, K.; Goldoni, A.; Larciprete, R.; Lizzit, S., *A Fast XPS Study of Propene Decomposition over Clean and Sulphated Pt{111}.* Catalysis Letters, 2002. **78**(1): p. 379.

(19) Avery, N. R.; Sheppard, N., *On the structure of C4 hydrocarbon species resulting from the adsorption of linear butenes on a Pt(111) surface as studied by thermal desorption and electron energy loss spectroscopies.* Surface Science Letters, 1986. **169**(2-3): p. L367.

(20) Avery, N. R.; Sheppard, N., *The Use of Thermal Desorption and Electron Energy Loss Spectroscopy for the Determination of the Structures of Unsaturated Hydrocarbons Chemisorbed on Metal Single-Crystal Surfaces. II. Cis- and Trans-but-2-Ene, but-2-Yne and Buta-1,3-Diene on Pt(111).* Proceedings of the Royal Society of London. Series A, Mathematical and Physical Sciences, 1986. **405**(1828): p. 27.

(21) Bertolini, J. C.; Cassuto, A.; Jugnet, Y.; Massardier, J.; Tardy, B.; Tourillon, G., *A comparative study of 1,3-butadiene and 1-butene chemisorbed on Pt(111), and Pd(111).* Surface Science, 1996. **349**(1): p. 88.

(22) Cassuto, A.; Tourillon, G., *The Adsorption Of Butene-1, Isobutene, Cis-2-Butene And Trans-2-Butene On Pt(111) At 95-K - NEXAFS and UPS results.* Surface Science, 1994. **307**: p. 65.

(23) Enachescu, M.; Schleef, D.; Ogletree, D. F.; Salmeron, M., *Integration of point-contact microscopy and atomic-force microscopy: Application to characterization of graphite/Pt(111).* Physical Review B, 1999. **60**(24): p. 16913.

(24) Salmeron, M.; Somorjal, G. A., *Desorption, Decomposition, And Deuterium-Exchange Reactions Of Unsaturated-Hydrocarbons (Ethylene, Acetylene, Propylene, And Butenes) On The Pt(111) Crystal-Face.* Journal of Physical Chemistry, 1982. **86**(3): p. 341.

(25) Cremer, P.; Stanners, C.; Niemantsverdriet, J. W.; Shen, Y. R.; Somorjai, G., *The conversion of di-[sigma] bonded ethylene to ethylidyne on Pt(111) monitored with sum frequency generation: evidence for an ethylidene (or ethyl) intermediate.* Surface Science, 1995. **328**(1-2): p. 111.

(26) Lee, A. F.; Wilson, K.; Goldoni, A.; Larciprete, R.; Lizzit, S., *A Fast XPS study of propene decomposition over clean and sulphated Pt{111}.* Catalysis Letters, 2002. **78**(1-4): p. 379.

(27) Salmeron, M.; Somorjai, G. A., *Desorption, decomposition, and deuterium exchange reactions of unsaturated hydrocarbons (ethylene, acetylene, propylene, and butenes) on the platinum(111) crystal face.* The Journal of Physical Chemistry, 1982. **86**(3): p. 341.

(28) Yang, M.-L.; Zhu, Y.-A.; Fan, C.; Sui, Z.-J.; Chen, D.; Zhou, X.-G., *Density functional study of the chemisorption of C1, C2 and C3 intermediates in propane dissociation on Pt(1 1 1).* Journal of Molecular Catalysis A: Chemical, 2009. **321**(1-2): p. 42.

(29) Steininger, H.; Ibach, H.; Lehwald, S., *Surface-Reactions Of Ethylene And Oxygen On Pt(111).* Surface Science, 1982. **117**(1-3): p. 685.

(30) Johanek, V.; De la Ree, A. B.; Hemminger, J. C., *Scanning Tunneling Microscopy Investigation of the Conversion of Ethylene to Carbon Clusters and Graphite on Pt(111).* Journal of Physical Chemistry C, 2009. **113**(11): p. 4441.

(31) Land, T. A.; Michely, T.; Behm, R. J.; Hemminger, J. C.; Comsa, G., *STM investigation of the adsorption and temperature dependent reactions of ethylene on Pt(111).* Applied Physics A: Materials Science & Processing, 1991. **53**(5): p. 414.

(32) Land, T. A.; Michely, T.; Behm, R. J.; Hemminger, J. C.; Comsa, G., *Direct Observation Of Surface-Reactions By Scanning Tunneling Microscopy - Ethylene-]Ethylidyne-]Carbon Particles-]Graphite On Pt(111).* Journal of Chemical Physics, 1992. **97**(9): p. 6774.

(33) McIntyre, B. J.; Salmeron, M.; Somorjai, G. A., *Formation and morphology of hydrocarbon clusters on Pt(111) produced by the thermal decomposition (coking) of propylene under high pressures of H-2 and CO observed in situ by scanning tunneling microscopy.* Journal of Catalysis, 1996. **164**(1): p. 184.

(34) MacLaren, J. M.; Pendry, J. B.; Rous, P. J.; Saldin, D. K.; Somorjai, G. A.; Van Hove, M. A.; Vvedensky, D. D., *Surface crystallographic information service. A handbook of surface structures.* Surface crystallographic information service. A handbook of surface structures, 1987: p. viii+352.

(35) Rasband, W. S., *ImageJ*. 1997-2011, U. S. National Institutes of Health: Bethesda, Maryland, USA. p.

(36) Land, T. A.; Michely, T.; Behm, R. J.; Hemminger, J. C.; Comsa, G., *Stm Investigation Of The Adsorption And Temperature-Dependent Reactions Of Ethylene On Pt(111).* Applied Physics a-Materials Science & Processing, 1991. **53**(5): p. 414.

(37) Rohrer, G., *The Preparation of Tip and Sample Surfaces for STM Experiments*, in *Scannning Tunneling Microscopy and Spectroscopy: Theory, Techniques, and Applications*, Bonnell, D., Editor. 1993, VCH Publishers, Inc: New York.

CHAPTER 6

The Dehydrogenation of Ethylene on $Pt/Al_2O_3/NiAl(110)$

6.1 Abstract

A model catalyst system, $Pt/Al_2O_3/NiAl(110)$, was created to study ethylene dehydrogenation using scanning tunneling microscopy (STM) held under ultra-high vacuum (UHV) conditions. The sample was dosed at room temperature and then subsequently annealed to 700 K. It appeared that the ethylene only deposited onto the Pt nanoparticles, rather than the oxide layer. The Pt nanoparticles did not grow beyond the second dosing, as their catalytic capability was quenched. However, when the sample was dosed at high temperatures of 1100 K, the Pt acted as a nucleation site and carbon clusters were formed along the step edges. With cycles of continued adsorption and heating, more particles were formed on the oxide layer until it was completely covered. The Pt nanoparticles were 13 ± 3.1 Å in diameter before dosing. With the first dosing and annealing to 700 K, 40% of the Pt particles grew in size to 20 ± 1.8 Å in diameter. By the final dosing 70% grew to 20 Å ± 2.3 Å. New particle formation was not observed. At temperatures of 1100 K, particles of 20 ± 2.0 Å are formed, mostly along the crystalline and amorphous boundary. The particles did not change in height.

6.2 Introduction

Hydrocarbon chemistry over Platinum (Pt) surfaces are important to industry and science and are being utilized for a number of projects, such as pollution control, biodegradable detergents and chemical synthesis.[1,2] The Pt catalyst is deactivated during the dehydrogenation reaction and little is actually known about the byproducts left after dehydrogenation.[1] Therefore, studying the morphology of the Pt surface before and after dehydrogenation at various temperatures can help lead to better control of the surface. Pt is one of the most used and

important heterogeneous catalysts in industry. Pt has applications in a variety of settings from fuel cells and food storage to chemical refinery.[3-5] Pt nanoparticles deposited over a support material such as alumina to stabilize the particles can reduce the cost by using less precious metals.[6,7] Ultrathin oxide layers are ideal as they have similar physical properties to the bulk oxide, while the bulk oxide is problematic as it is insular and cannot used with techniques such as STM.[6,8] Nanoparticles have a higher surface area than single crystals, providing for more catalytic capability.[7] However, nanoparticles are known to often have completely different catalytic properties than its single crystal counterparts due to many factors, including metal-oxide interactions.[6] Therefore, reactions are in part dependent upon the support chosen. Al_2O_3 is an ideal support as it known to maintain a wide dispersion of Pt nanoparticles.[1] This paper analyzes the morphology of ethylene as it is dehydrogenated on Pt nanoparticles supported on Al_2O_3/NiAl(110). This dehydrogenation mechanism is compared to previous studies on Pt(111) single crystal with the same experimental conditions. A variable temperature STM is utilized in the experiments as it is held under ultra-high vacuum (UHV) to reveal the surface morphology of the dehydrogenated ethylene.

Previous research on ethylene on Pt nanoparticles have covered topics of adsorption,[9-12] oxidation,[3] and hydrogenation.[11,13-19] Few studies have used Pt/Al_2O_3[9,10,14,16,17,20] and none used imaging techniques. Previous studies of ethylene on Pt nanoparticles have shown that at room temperature, the ethylene absorbs onto the Pt surface and converts by a single dehydrogenation to ethylidene,[10] which is in contrast to the occurrence on Pt(111) where ethylene converts to ethylidyne instead as shown in Figure 6.1.[21-34] There have been no studies investigating the decomposition of ethylene at higher temperatures on Pt nanoparticles. For the Pt(111) single

crystal, the alkylidyne species is completely decomposed at 400-450 K[21,23,30,35] and only surface carbon remains at a temperature above 700 K.[22,23,35,36]

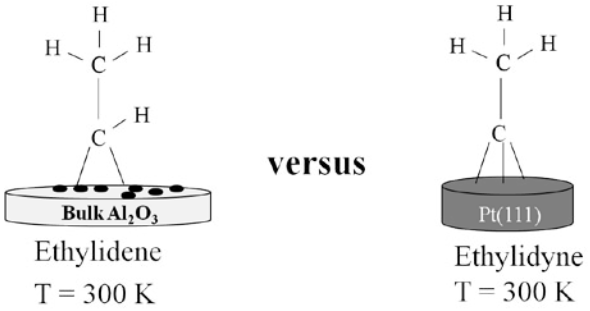

Figure 6.1 The difference in ethylene adsorption at room temperature between Pt bulk and Pt nanoparticles.

In our previous work, dehydrogenation studies of olefins on Pt(111) have been performed only on single crystals. Our STM studies with ethylene, propylene and butylene show that with annealing to 700 K, flat, uniform carbon clusters are formed.[37,38] Graphite begins to form at temperatures above 700-800 K.[21,26,36,38-40] One purpose of this study is to determine if a similar size carbon cluster forms on the oxide layer and if graphite can be created.

In this experiment, Al_2O_3 was formed on NiAl(110). Pt nanoparticles were deposited and then ethylene gas was dosed onto the sample at room temperature. The sample was subsequently annealed to 700 K. This dosing and heating cycle was performed a total of five times and the morphology was recorded by STM after each cycle. It was observed that the Pt nanoparticles grew slightly in size with the first dosing and then leveled off with no further size change with subsequent dosing. With dosings of ethylene, no additional particles were formed on the sample. The sample was then annealed to a higher temperature of 1100 K, where the particles moved to the step edges. With the same setup of $Pt/Al_2O_3/NiAl(110)$, ethylene was dosed at temperatures of 1100 K. Flat, circular clusters were formed at mostly the step edges, and as dosings increased more particles were formed until the entire Al_2O_3 layer was covered.

6.3 Experimental Section

The experiments have been performed in a UHV system equipped with two chambers. One chamber is kept relatively clean and is used only for imaging with a variable temperature STM (UHV 300 VT-STM, RHK Technology, Inc). A second chamber is used to prepare the sample and contains an Auger Electron Spectroscopy (AES, PHI model 10-155, single pass CMA), a platinum evaporator (EBE-1, SPECS) and a flux monitor (EBE-FC, SPECS). A NiAl(110) single crystal (MaTeck, 99.999% purity, ~9 mm in diameter by 1.5 mm thick) with average terrace widths of 100 nm was heated by electron beam via a tungsten wire ~2 mm beneath the sample in order to create a smooth surface. Surface temperatures were monitored using a chromel-alumel thermocouple attached to the sample. The NiAl single crystal sample was cleaned by cycles of oxygen dosing (P = 2 × 10^{-6} Torr, T_{sample} = 540 K, for 10 minutes), followed by annealing (T_{sample} = 1320 K for 15 minutes). Cleaning cycles were repeated until AES and STM confirmed a surface free of containments. STM images of the NiAl surface were obtained in constant current mode with tunneling currents of 1-2 nA and typical bias voltage of 0.5 V applied to the tip. Images were calibrated in the z-dimension using the NiAl crystal step height of 2.0 Å.[6]

A well ordered, thin film of Al_2O_3 was formed on the NiAl surface by backfilling the chamber with oxygen (99.9% purity, Airgas) through a leak valve, exposing the sample to a saturation exposure of 1200 Langmuir at 550 K (1 Langmuir = 10^{-6} Torr s) for 10 minutes. The sample was then annealed at 1200 K for 10 minutes. Due to Al_2O_3 having a wide band gap of 8 eV,[41] images were obtained with a bias voltage in the range of 4-6 V.

Pt nanoparticles were deposited onto the sample at room temperature, for 1 minute at a flux of 1200 nA. The sample was then flashed annealed at 770 K for 5 minutes and then imaged

before ethylene dosing. Ethylene gas was dosed with a directional doser, exposing the sample to 20 Langmuir at 300 K for 400 seconds. One cycle was completed by annealing to 700 K for 5 minutes, followed by STM imaging. Previous studies have indicated that by about 700 K complete dehydrogenation occurs for ethylene on a single Pt crystal.[22,23] A total of five cycles were completed per sample. After dosing a total of 100 L, the sample was then annealed to 1000 K. Previous studies on a Pt single crystal, showed that at 1000 K graphite was formed.[38-40]

A second series of experiments was performed on clean Pt nanoparticles by dosing ethylene gas with a directional doser, exposing the sample to 50 L at 1000 K for 500 seconds. The sample was then annealed to 1100 K. This dosing/annealing cycle was repeated a total of six times.

Furthermore, two blank samples were built. An oxide layer without Pt nanoparticles was dosed with ethylene at room temperature, 700 K, 1000 K and 1100 K. Another sample with Pt nanoparticles, without ethylene was annealed to 1100 K.

6.4 Results and Discussion

The terrace and morphology of a NiAl(110) single crystal surface after cycles of cleaning is shown in Figure 6.2a. Straight steps with single atomic step height run along the surface. The terraces on NiAl(110) are flat with an average width of ~200 nm. Oxygen is then introduced for adsorption onto the NiAl(110) surface, creating a thin crystalline Al_2O_3 layer approximately 5 Å thick (which corresponds to 2 layers).[41] The oxide layer was examined using STM and is shown in Figures 6.2b and 3.2b. The crystalline Al_2O_3 displays the characteristic grain boundaries over 50-60% of the surface. The remaining NiAl surface is covered with an unordered oxide layer. The step heights were approximately 2 Å and terrace widths ranged from 25-80 nm.

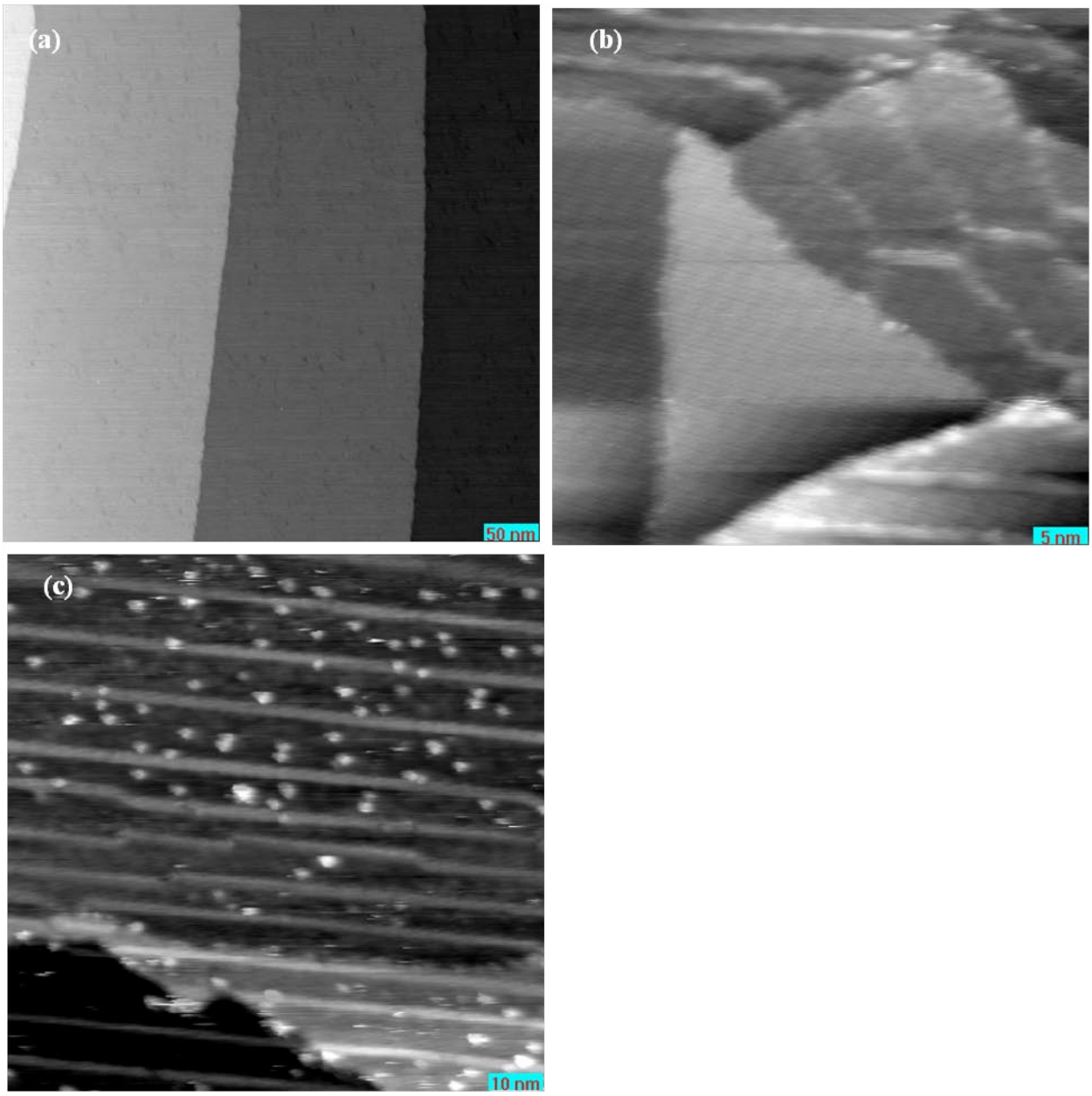

Figure 6.2 STM image of (a) clean NiAl(110) surface with an average terrace width of ~200 nm (500 nm × 500 nm), (b) Al_2O_3 produced by adsorption of 1200 Langmuir oxygen at 550 K and subsequently annealed at 1200 K (50 nm × 50 nm), (c) Pt nanoparticles adsorbed onto the Al_2O_3 layer (100 nm × 100 nm).

Pt is then deposited onto the oxide surface and is shown in Figures 6.2c and 4.2a. The Pt deposited onto the crystalline oxide layer and not on the unordered layer. The Pt deposited evenly throughout the crystalline layer and not preferentially to the step edges. The Pt nanoparticles were on average 13 ± 3.1 Å in width and 2.1 ± 0.64 Å in height.

We then dosed 20 Langmuir of ethylene onto the oxide layer. It is important to note that when ethylene is dosed without the Pt nanoparticles, they do not attach to the surface and it appears as if there is only Al_2O_3 on the surface. STM images of ethylene at 300 K did not resolve any discernible structures, which may be due to low frequency vibrations or high surface mobility.[40] Annealing to 1000 K completes one dosing/annealing cycle. Figure 6.2 shows the morphology after one cycle of adsorption/annealing. The unordered oxide is covered in a carbon layer and the crystalline layer contains clusters.

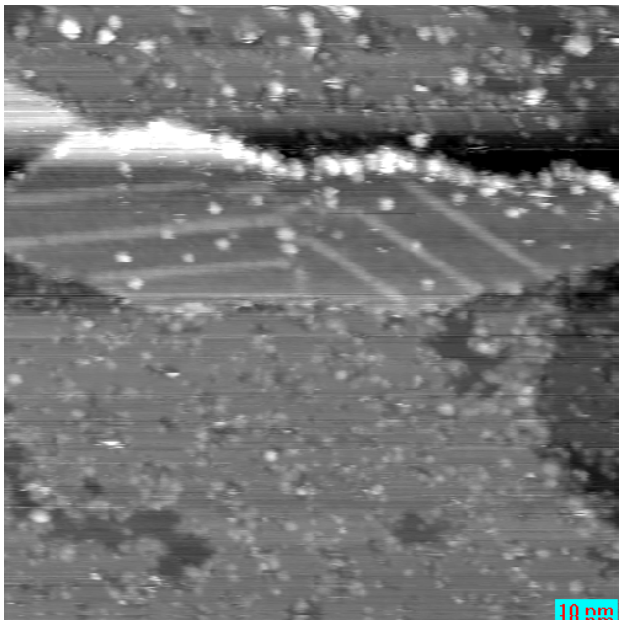

Figure 6.3 100 nm × 100 nm STM image of Pt/Al_2O_3 after a single cycle of adsorption of 20 Langmuir ethylene at room temperature and subsequently flash-annealed to 1000 K. The crystalline and unordered oxide reacted differently to the ethylene.

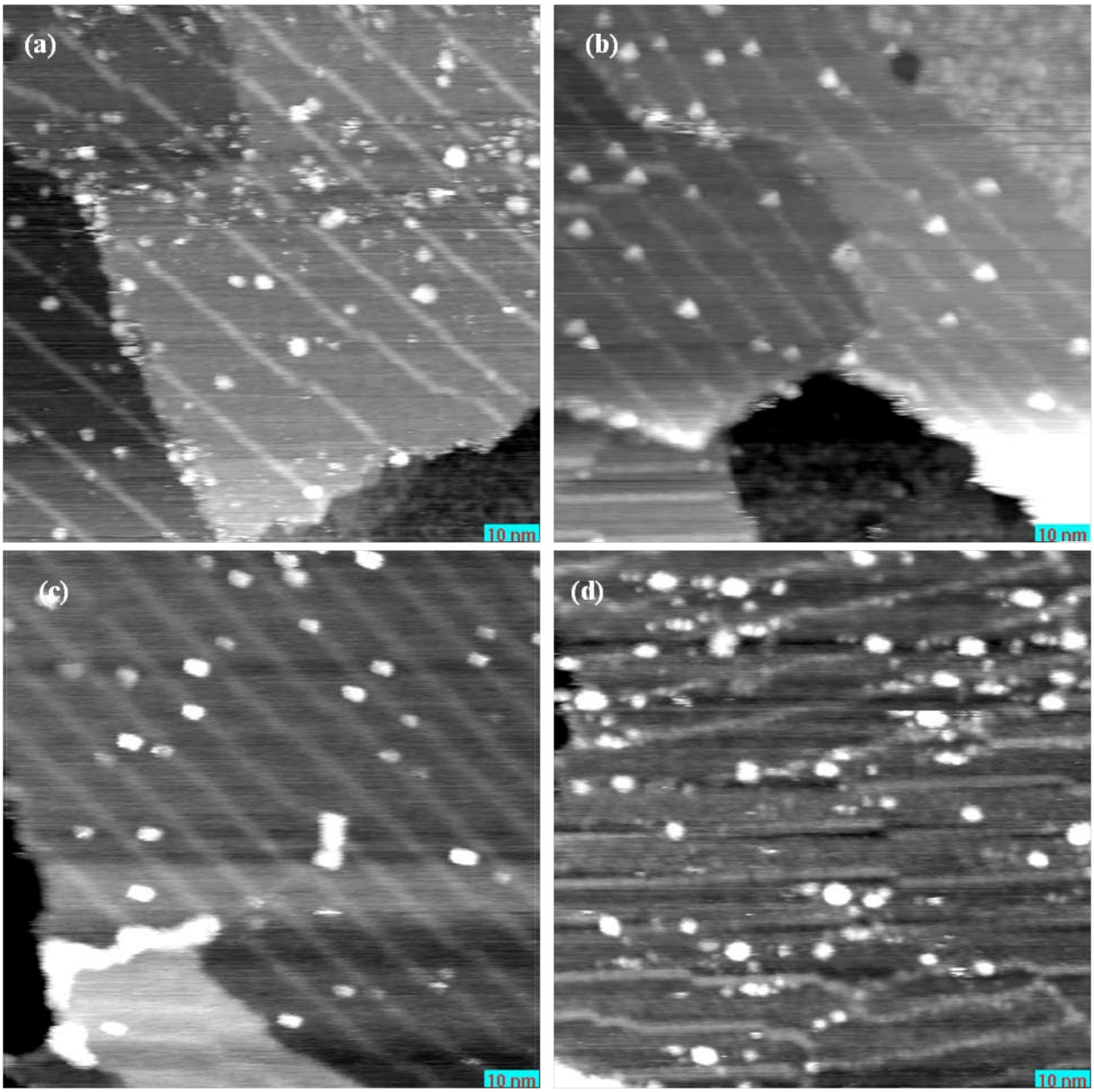

Figure 6.4 Each STM image (100 nm × 100 nm) is of Pt/Al_2O_3 after a cycle of adsorption of 20 Langmuir ethylene at room temperature and subsequently flash-annealed to 1000 K. (a) Total 40 Langmuir of ethylene dosed, (b) Total 60 Langmuir of ethylene dosed, (c) Total 80 Langmuir of ethylene dosed, (d) Total 100 Langmuir of ethylene dosed. The density of particles did not significantly change.

The particle sizes were analyzed using surface cross section analysis per standard STM methods. The heights of the particles do not change with dosing and remain the same as the un-dosed Pt nanoparticles. Approximately 60% of the particles are averaged to be 13 ± 3.0 Å, which is the same width as clean Pt nanoparticles. The other 40% are averaged at a larger width of 20 ± 2.6 Å. It is possible that we observed the above findings because ethylene only deposited onto 40% of the particles. With continued cycles of dosing/annealing, the 13 Å sized particles decrease in amount and the larger particles increase as shown in Table 6.1. By the third cycle, most particles are 20 Å in diameter and the amount of 13 Å particles leveled off to ~7%. We hypothesize that the Pt nanoparticles became encapsulated in carbon. Based on previous Pt(111) single crystal data for the ethylene saturation coverage and the density of Pt atoms and by assuming that the Pt nanoparticles are flat and circular, the amount of carbon atoms adsorbed onto the Pt surface can be estimated to be 8 carbon atoms. 8 carbon atoms is significantly smaller than the amount of carbon (~40 carbon atoms) in the clusters formed on Pt(111) single crystal. Figures 6.4(a-d) are of STM images after continued cycles of adsorption/annealing. There was no significant change in the density of particles on the crystalline layer from one cycle to the next. The average widths of particles for all other cycles (excluding the first) were 20.0 ± 2.0 Å.

Table 6.1 A histogram of the ethylene dosing/annealing cycles. The percent frequency of particles falls in to three ranges: 1-1.8, 1.9-2.5 and above 2.5. The Pt sized particles decrease with each dosing until 60 Langmuir where it levels off.

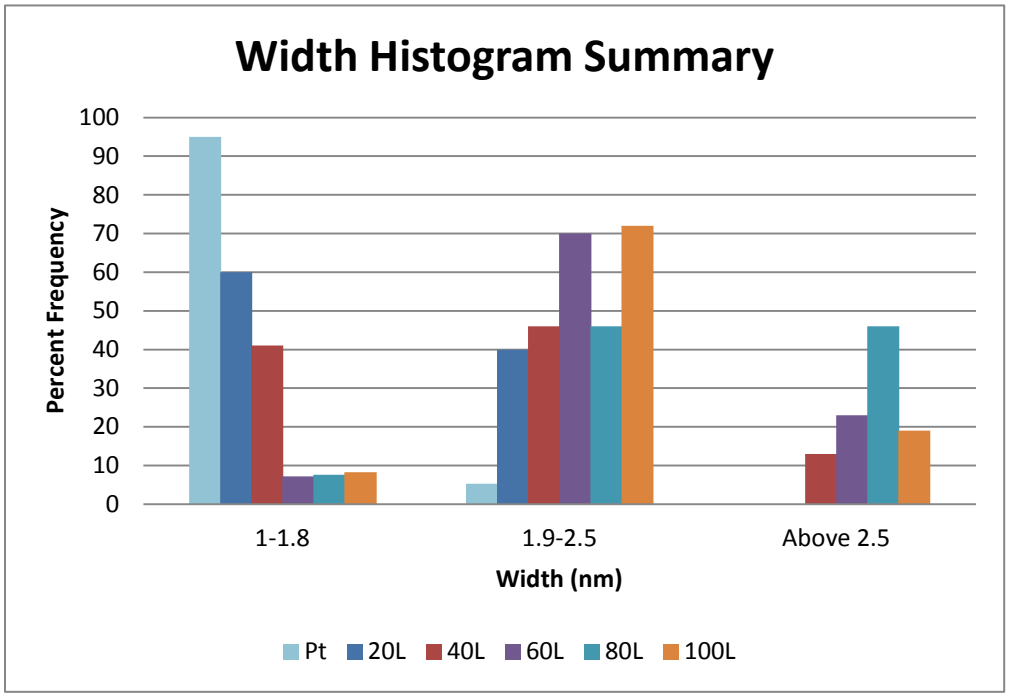

For the second set of experiments, 50 Langmuir of ethylene was dosed at 1000 K. At 1000 K large clusters are deposited to the surface. These large clusters were too large for high resolution imaging, as shown in Figure 6.5 with a 150 Langmuir sample. The surface was then annealed to 1100 K, which completes one cycle as shown in 250 nm × 250 nm STM images in Figures 6.6(a-d). After annealing to 1100 K, all of these large clusters on the oxide surface disappeared. Particles are deposited to the boundary between the crystalline and amorphous oxide layer. As the dosing/annealing cycles increase the quantity of particles increase along the boundary, until the entire crystalline oxide layer is completely covered. This process is further exemplified with STM images at 100 nm × 100 nm shown in Figures 6.7(a-d). Interestingly, when annealing at 1100 K, clean Pt nanoparticles without ethylene dosing gave a different result.

The clean Pt nanoparticles did not move to the step edges and appeared to have been unchanged. For the 50 Langmuir dosing, 63% of the particles were at the step edges and 38% were at the terraces. By the 250 Langmuir dosing, 76% of the particles were at the step edges and 23% were at the terraces. By the 450 Langmuir dosing, nearly the entire crystallized oxide layer was covered in particles. At 1100 K the surface began to lose the crystallized oxide layer. These small islands were fully covered with particles. The density of particles increased with each dosing until the crystallized Al_2O_3 was fully covered.

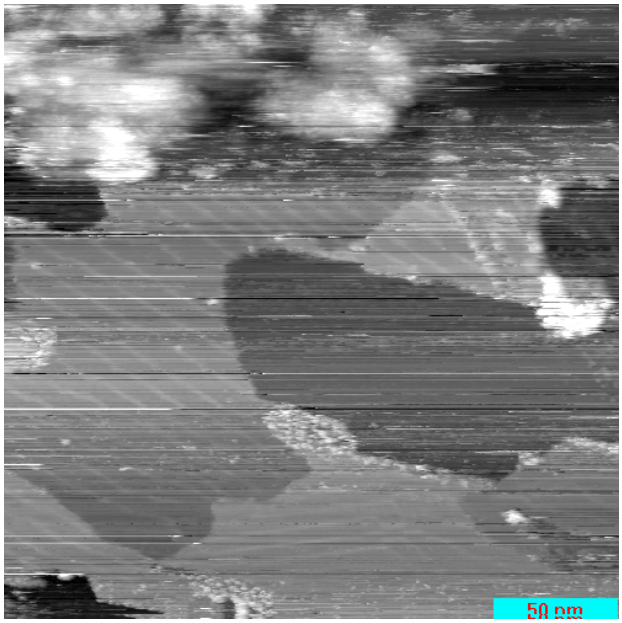

Figure 6.5 An STM image of Pt/Al_2O_3 after a two cycles of adsorption of 50 Langmuir ethylene at 1000 K and subsequently flash-annealed to 1100 K (250 nm × 250 nm). An additional 50 Langmuir has been deposited at 1000 K but has not been annealed. The top left corner is covered in larger clusters. These large clusters disappear after annealing to 1100 K.

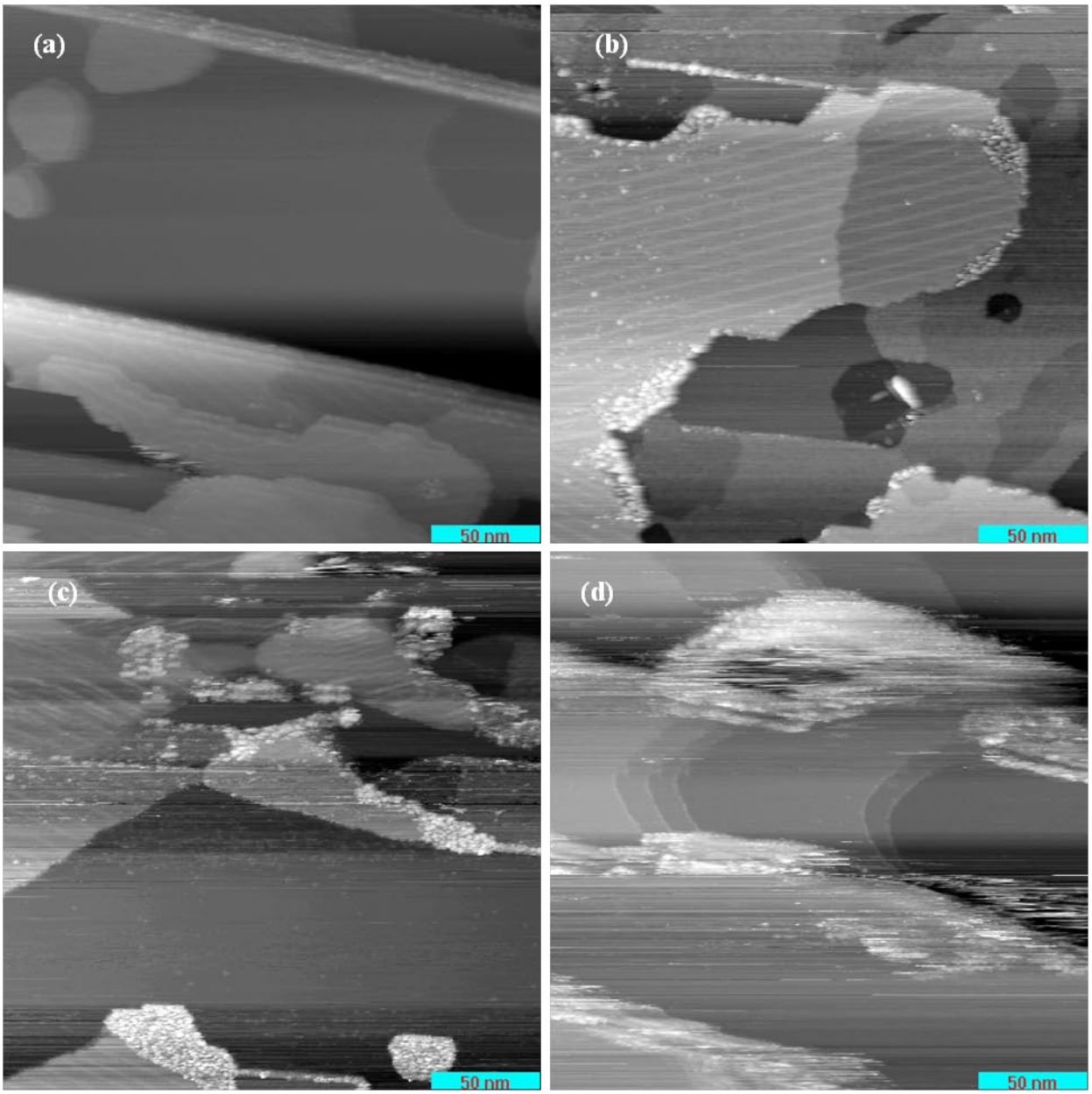

Figure 6.6 250 nm × 250 nm STM images of Pt/Al_2O_3 after cycles of adsorption of 50 L ethylene at 1000 K and subsequently flash-annealed to 1100 K. (a) Total 50 Langmuir of ethylene dosed, (b) Total 100 Langmuir of ethylene dosed, (c) Total 250 Langmuir of ethylene dosed, and (d) Total 450 Langmuir of ethylene dosed. Particles adsorb to the step edges of the crystalline oxide and increase in quantity until the entire crystalline oxide is covered.

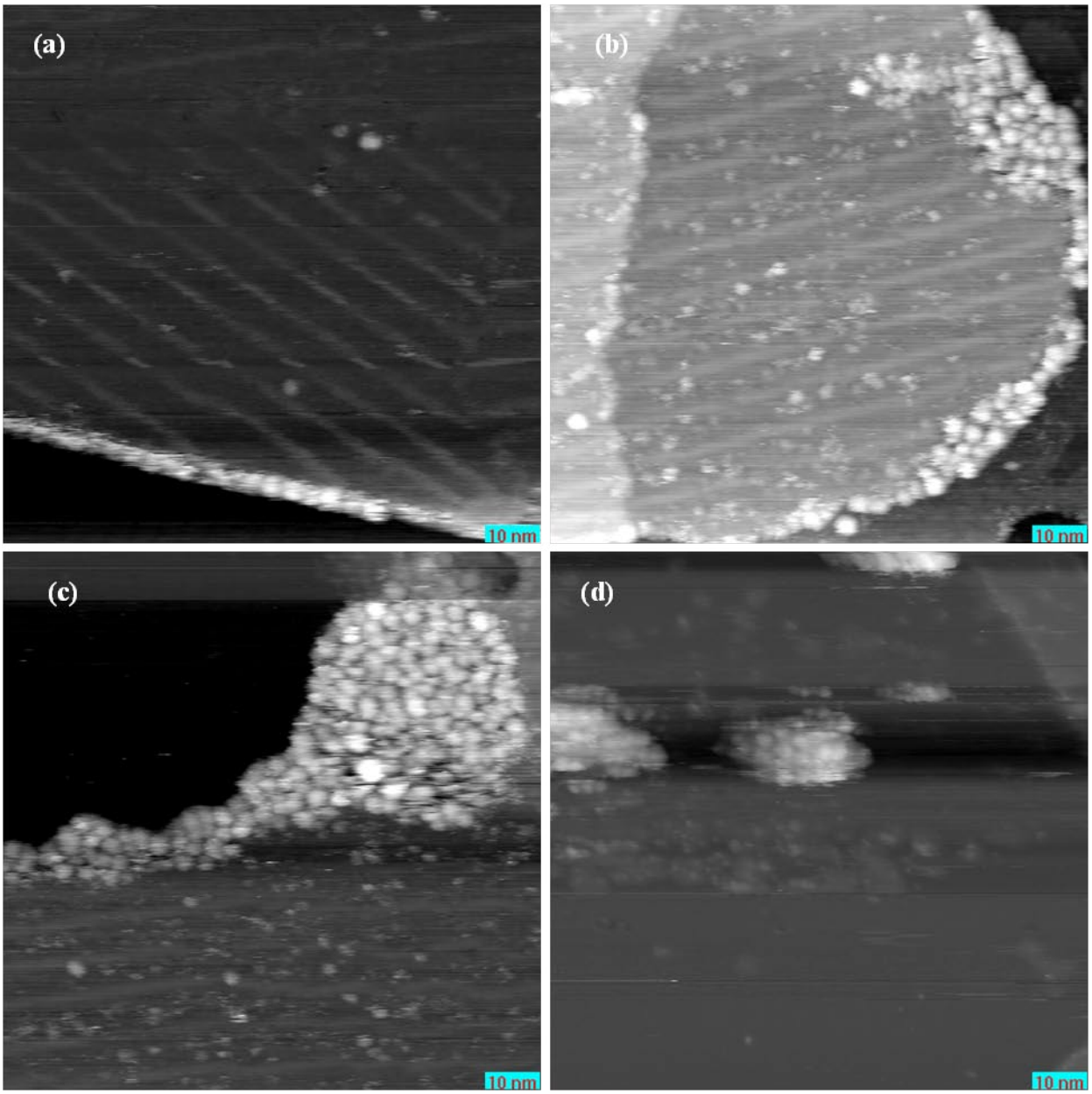

Figure 6.7 100 nm × 100 nm STM images of Pt/Al_2O_3 after cycles of adsorption of 50 Langmuir ethylene at 1000 K and subsequently flash-annealed to 1100 K. (a) Total 50 Langmuir of ethylene dosed, (b) Total 100 Langmuir of ethylene dosed, (c) Total 150 Langmuir of ethylene dosed, and (d) Total 450 Langmuir of ethylene dosed. Particles adsorb to the step edges of the crystalline oxide and increase in quantity until the entire crystalline oxide is covered.

There was no significant change in particle size between all dosings - indicating that clusters did not act as nucleation sites. The particles were 20 ± 1.8 Å wide and 2.1 ± 1.1 Å high. These sizes were the same for cycles performed at room temperature and annealed at 1000 K. The particles were wider than the Pt particles of 13 ± 3.0 Å, however their heights were similar. A similar behavior was seen with ethylene thermal dehydrogenation on Pt single crystal with a similar experimental setup of 20 Langmuir dosing at room temperature and flash annealing.[37-40] Instead of particles increasing in size, they increased in quantity.[37-40] It is observed that regardless of the size of the Pt catalyst (i.e. single crystal vs nanoparticle) the dehydrogenated ethylene particles have a set cluster size. The possible pathway that we hypothesize is occurring is shown in Figure 6.8. At room temperature ethylene adsorbs onto the supported Pt particles with a single dehydrogenation to ethylidene (as was previously seen in literature).[10] When the sample is annealed to 1000 K, the Pt activates the decomposition of ethylene and only carbon is left adsorbed to the Pt particle. When ethylene is dosed onto the Pt particles at 1000 K, ethylene is continuously dehydrogenated and carbon begins to spill over onto the alumina. When the sample is then annealed to 1100 K the carbon becomes mobile and clusters along the boundary between the crystalline and amorphous oxide layer. This process continues until the entire crystalline oxide layer is covered with 20 Å particles. The Pt particles remain immobile throughout the process.

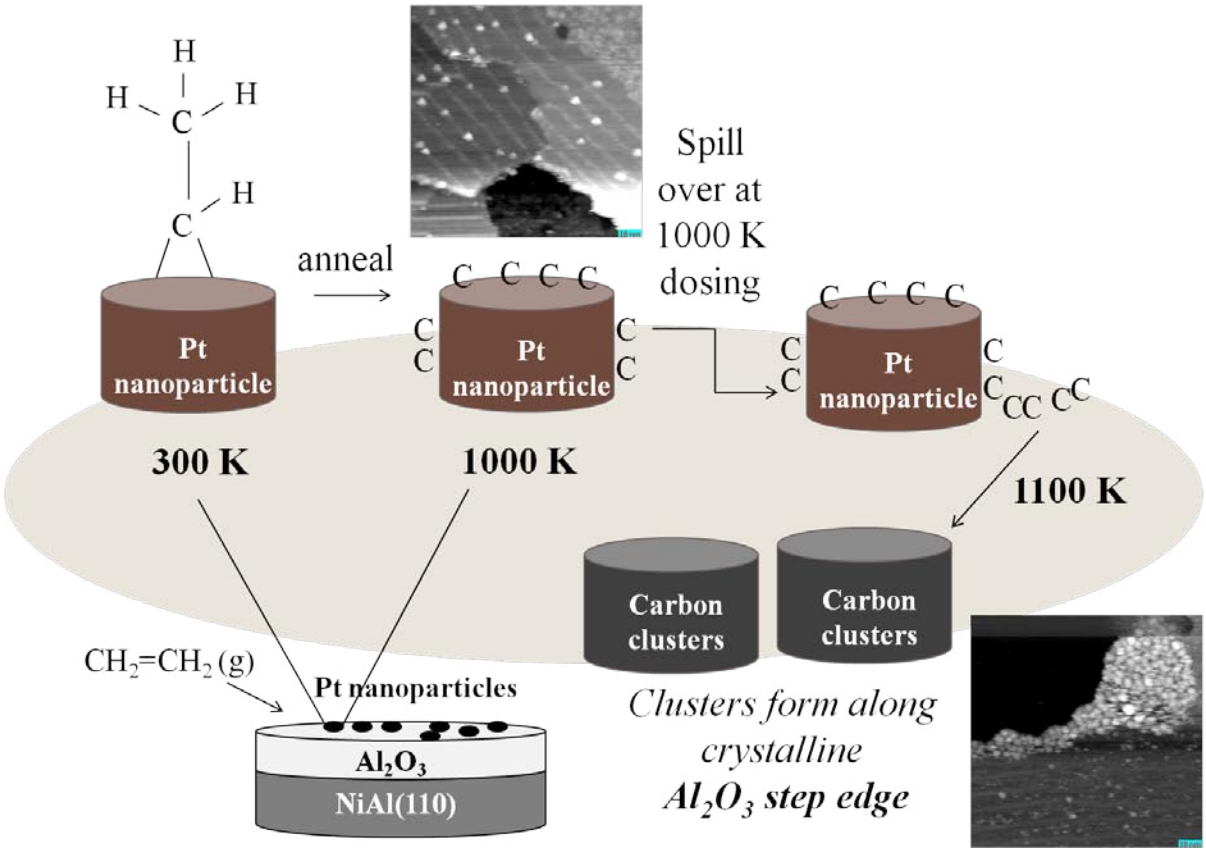

Figure 6.8 The hypothetical pathway for adsorption and dehydrogenation of ethylene on $Pt/Al_2O_3/NiAl(110)$ for two different conditions.

6.5 Conclusion

STM experiments in UHV have led to insights into ethylene dehydrogenation on Pt nanoparticles. The Pt nanoparticles formed herein were circular, flat and uniform in size (13 Å) and shape. Ethylene was dosed onto the Pt. The thermally dehydrogenated ethylene generated carbon covered the Pt nanoparticles and until the particles grew to a maximum of 20 Å. Particle density did not increase at the annealing temperature of 1000 K. When raising the dosing temperature to 1000 K and the annealing temperature to 1100 K, the density of particles increased. The particles formed at 1100 K decorated the boundary between the crystalline and amorphous oxide layer. Unlike, with single crystal Pt(111), graphite was never produced. In

future studies, larger Pt particles may provide for a better catalytic activity. It was found that when Pt nanoparticles are less than 18 Å their catalytic capability is lowered when oxidizing methanol and formic acid.[42] Specifically, this study found that in terms of catalytic activity Pt(111) was more active than Pt nanoparticles of any size.[42] Possibly larger Pt nanoparticles may help produce graphite with olefin dehydrogenation.

6.6 References

(1) Akia, M.; Alavi, S. M.; Yan, Z.-F., *Promoted Platinum Dehydrogentaion Catalyst on a Nano-Sized Gamma Alumina Support.* Petroleum and Coal, 2010. **52**(4): p. 280.

(2) Gawthrope, D. E.; Wilson, K.; Lee, A. F., *Propene combustion over a model Pt/Al2O3/NiAl{110} catalyst.* Physical Chemistry Chemical Physics, 2003. **5**(15): p. 3299.

(3) Jiang, C.; Hara, K.; Fukuoka, A., *Low-Temperature Oxidation of Ethylene over Platinum Nanoparticles Supported on Mesoporous Silica.* Chem. Int. Ed, 2013. **52**: p. 6265.

(4) Namgee Junga; Dong Young Chungb; Jaeyune Ryua; Sung Jong Yooa; Yung-Eun Sungb, *Pt-based nanoarchitecture and catalyst design for fuel cell applications.* NanoToday, 2014. **9**: p. 433.

(5) Lin, Y.-C.; Huber, G. W., *The critical role of heterogeneous catalysis in lignocellulosic biomass conversion.* Energy Environ. Sci., 2008. **2**: p. 68.

(6) Cuenya, B., *Synthesis and catalytic properties of metal nanoparticles: Size, shape, support, composition, and oxidation state effects.* Thin Solid Films, 2010. **518**: p. 3127.

(7) Samorjai, G., *Introduction to Surface Chemistry and Catalysis.* 2nd ed. 2010, Honoken, New Jersey: John Wiley & Sons.

(8) R.M. Jaeger; H. Kuhlenbeck; Freund, H.-J., *Formation of a well-ordered aluminium oxide overlayer by oxidation of NiAl(110).* Surface Science, 1991. **259**: p. 235.

(9) Celio, H.; Trenary, M.; Robota, H. J., *Comparative IR Study of Ethylene Adsorption on a PtRh Alloy and Monometallic Pt and Rh Catalysts Supported on Al2O3. Identification of Alloy-Specific Binding Sites.* The Journal of Physical Chemistry, 1995. **99**(16): p. 6024.

(10) Griffiths, J. M.; Bell, A. T.; Reimer, J. A., *Magnetic-resonance Studies of Ethene Adsorption on Alumina-Supported Platinum Surfaces* Journal of Physical Chemistry, 1993. **97**(36): p. 9161.

(11) Palazov, A.; Bonev, C.; Shopov, D.; Lietz, G.; SÃ¡rkÃ¡ny, A.; VÃ¶lter, J., *Adsorption and hydrogenation of ethylene, 1-hexene, and benzene and CO adsorption on PtAl2O3andPtî—¸SnAl2O3 catalysts.* Journal of Catalysis, 1987. **103**(2): p. 249.

(12) Mohsin, S. B.; Trenary, M.; Robota, H. J., *Infrared identification of the low-temperature forms of ethylene adsorbed on platinum/alumina.* The Journal of Physical Chemistry, 1988. **92**(18): p. 5229.

(13) Ghosh, A.; Hsu, B. B.; Dougal, S. M.; Afeworki, M.; Stevens, P. A.; Yeganeh, M. S., *Effects of Gas Feed Ratios and Sequence on Ethylene Hydrogenation on Powder Pt Catalyst Studied by Sum Frequency Generation and Mass Spectrometry.* Acs Catalysis. **4**(6): p. 1964.

(14) Pazmino, J.; Bai, C.; Miller, J.; Ribeiro, F.; Delgass, W. N., *Effects of Support on Sulfur Tolerance and Regeneration of Pt Catalysts Measured by Ethylene Hydrogenation and EXAFS.* Catalysis Letters. **143**(11): p. 1098.

(15) Dominguez, F.; Carruyo, G.; Andrade, R.; Solano, R.; RodrÃguez, D.; SÃ¡nchez, J.; Arteaga, G., *Ethylene Hydrogenation over Pt/Ga2O3/Al2O3 Catalysts*. Catalysis Letters, 2008. **123**(3-4): p. 207.

(16) Ko, M. K.; Frei, H., *Millisecond FT-IR spectroscopy of surface intermediates of C2H4 hydrogenation over Pt/Al2O3 catalyst under reaction conditions.* Journal of Physical Chemistry B, 2004. **108**(6): p. 1805.

(17) Grunes, J.; Zhu, J.; Yang, M. C.; Somorjai, G. A., *CO poisoning of ethylene hydrogenation over Pt catalysts: a comparison of Pt(111) single crystal and Pt nanoparticle activities.* Catalysis Letters, 2003. **86**(4): p. 157.

(18) Prairie, M. R.; Bailey, J. E., *Experimental and Modeling Investigations of Steady-State and Dynamic Characteristics of Ethylene Hydrogenation on Pt/Al2O3.* Chemical Engineering Science, 1987. **42**(9): p. 2085.

(19) Cider, L.; Schoon, N. H., *Competition Between Ethyne, Ethene, and Carbon-monoxide for the Active-Sites During Hydrogenation at Transient Conditions Over Supported Metal-Catalysts* Applied Catalysis, 1991. **68**(1-2): p. 191.

(20) Wasylenko, W.; Frei, H., *Direct Observation of Surface Ethyl to Ethane Interconversion upon C2H4 Hydrogenation over Pt/Al2O3 Catalyst by Time-Resolved FT-IR Spectroscopy.* The Journal of Physical Chemistry B, 2005. **109**(35): p. 16873.

(21) Lee, A. F.; Wilson, K.; Goldoni, A.; Larciprete, R.; Lizzit, S., *A Fast XPS study of propene decomposition over clean and sulphated Pt{111}.* Catalysis Letters, 2002. **78**(1-4): p. 379.

(22) Salmeron, M.; Somorjai, G. A., *Desorption, decomposition, and deuterium exchange reactions of unsaturated hydrocarbons (ethylene, acetylene, propylene, and butenes) on the platinum(111) crystal face.* The Journal of Physical Chemistry, 1982. **86**(3): p. 341.

(23) Creighton, J. R.; White, J. M., *A SIMS STUDY OF THE DEHYDROGENATION OF ETHYLENE ON PT(111).* Surface Science, 1983. **129**(2-3): p. 327.

(24) Koestner, R. J.; Frost, J. C.; Stair, P. C.; Vanhove, M. A.; Somorjai, G. A., *Evidence For The Formation Of Stable Alkylidyne Structures From C-3 And C-4 Unsaturated-Hydrocarbons Adsorbed On The Pt(111) Single-Crystal Surface.* Surface Science, 1982. **116**(1): p. 85.

(25) Yang, M.-L.; Zhu, Y.-A.; Fan, C.; Sui, Z.-J.; Chen, D.; Zhou, X.-G., *Density functional study of the chemisorption of C1, C2 and C3 intermediates in propane dissociation on Pt(1 1 1).* Journal of Molecular Catalysis A: Chemical, 2009. **321**(1-2): p. 42.

(26) Zaera, F.; Chrysostomou, D., *Propylene on Pt(111) I. Characterization of surface species by infra-red spectroscopy.* Surface Science, 2000. **457**(1-2): p. 71.

(27) Cremer, P. S.; Su, X.; Shen, Y. R.; Somorjai, G. A., *Hydrogenation and Dehydrogenation of Propylene on Pt(111) Studied by Sum Frequency Generation from UHV to Atmospheric Pressureâ€* The Journal of Physical Chemistry, 1996. **100**(40): p. 16302.

(28) Valcarcel, A.; Ricart, J. M.; Clotet, A.; Illas, F.; Markovits, A.; Minot, C., *Theoretical study of dehydrogenation and isomerisation reactions of propylene on Pt(111).* Journal of Catalysis, 2006. **241**(1): p. 115.

(29) Avery, N. R.; Sheppard, N., *On the structure of C4 hydrocarbon species resulting from the adsorption of linear butenes on a Pt(111) surface as studied by thermal desorption*

and electron energy loss spectroscopies. Surface Science Letters, 1986. **169**(2-3): p. L367.

(30) Avery, N. R.; Sheppard, N., *The Use of Thermal Desorption and Electron Energy Loss Spectroscopy for the Determination of the Structures of Unsaturated Hydrocarbons Chemisorbed on Metal Single-Crystal Surfaces. II. Cis- and Trans-but-2-Ene, but-2-Yne and Buta-1,3-Diene on Pt(111).* Proceedings of the Royal Society of London. Series A, Mathematical and Physical Sciences, 1986. **405**(1828): p. 27.

(31) Lee, I.; Zaera, F., *Thermal Chemistry of C4 Hydrocarbons on Pt(111):â€‰ Mechanism for Double-Bond Isomerization.* The Journal of Physical Chemistry B, 2005. **109**(7): p. 2745.

(32) Tsai, Y. L.; Koel, B. E., *Temperature-programmed desorption investigation of the adsorption and reaction of butene isomers on Pt(111) and ordered Pt-Sn surface alloys.* Journal of Physical Chemistry B, 1997. **101**(15): p. 2895.

(33) Steininger, H.; Ibach, H.; Lehwald, S., *Surface-Reactions Of Ethylene And Oxygen On Pt(111).* Surface Science, 1982. **117**(1-3): p. 685.

(34) Cremer, P.; Stanners, C.; Niemantsverdriet, J. W.; Shen, Y. R.; Somorjai, G., *The conversion of di-[sigma] bonded ethylene to ethylidyne on Pt(111) monitored with sum frequency generation: evidence for an ethylidene (or ethyl) intermediate.* Surface Science, 1995. **328**(1-2): p. 111.

(35) Zaera, F.; Chrysostomou, D., *Propylene on Pt(111)II. Hydrogenation, dehydrogenation, and H-D exchange.* Surface Science, 2000. **457**(1-2): p. 89.

(36) McIntyre, B. J.; Salmeron, M.; Somorjai, G. A., *Formation and morphology of hydrocarbon clusters on Pt(111) produced by the thermal decomposition (coking) of*

propylene under high pressures of H-2 and CO observed in situ by scanning tunneling microscopy. Journal of Catalysis, 1996. **164**(1): p. 184.

(37) Khan, S.; Sun, G.; De La Ree, A.; Hemminger, J., *The Conversion of Small Hydrocarbons to Carbon Clusters on Platinum.* In progress.

(38) Johanek, V.; De la Ree, A. B.; Hemminger, J. C., *Scanning Tunneling Microscopy Investigation of the Conversion of Ethylene to Carbon Clusters and Graphite on Pt(111).* Journal of Physical Chemistry C, 2009. **113**(11): p. 4441.

(39) Land, T. A.; Michely, T.; Behm, R. J.; Hemminger, J. C.; Comsa, G., *STM investigation of the adsorption and temperature dependent reactions of ethylene on Pt(111).* Applied Physics A: Materials Science & Processing, 1991. **53**(5): p. 414.

(40) Land, T. A.; Michely, T.; Behm, R. J.; Hemminger, J. C.; Comsa, G., *Direct Observation Of Surface-Reactions By Scanning Tunneling Microscopy - Ethylene-]Ethylidyne-]Carbon Particles-]Graphite On Pt(111).* Journal of Chemical Physics, 1992. **97**(9): p. 6774.

(41) Libuda, J.; Winkelmann, F.; Baumer, M.; Freund, H. J.; Bertrams, T.; Neddermeyer, H.; Maller, K., *Structure and defects of an ordered alumina film on NiAl(110).* Surface Science, 1994. **318**: p. 61.

(42) Rhee, C. K.; Kim, B.-J.; Ham, C.; Kim, Y.-J.; Song, K.; Kwon, K., *Size Effect of Pt Nanoparticle on Catalytic Activity in Oxidation of Methanol and Formic Acid: Comparison to Pt(111), Pt(100), and Polycrystalline Pt Electrodes.* Langmuir, 2009. **25**(12): p. 7140.

CHAPTER 7

The Investigation of Ethylenediamine Conversion to Cyanogen on Nickel

7.1 Abstract

Thermal dehydrogenation of ethylenediamine on Ni(111) at 300-500 K to possibly form cyanogen has been studied under ultra-high vacuum (UHV) conditions and using scanning tunneling microscopy (STM). Unfortunately, cyanogen formation was not observed by STM and the end result was not discernible.

7.2 Introduction

Nano-filters are important for the elimination of contaminants in the air and water.[1] Cyanogen is theorized to form mesh-like structures that can act as an air filter to catch various hydrocarbons and other toxic gases.[2] In this study, imaging was used to investigate if cyanogen can be formed from the dehydrogenation of ethylenediamine on a Ni crystal. This is the first time that we know of that this hypothetical reaction on Ni has been studied. Previously, Kingsley *et al* demonstrated that cyanogen was formed with ethylenediamine on a Pt single crystal with x-ray photoelectron spectroscopy (XPS).[2] Assuming the structure of ethylenediamine on fcc(111) metals should be similar (such as Pt(111)), this experiment will use the Pt reaction as a model for the expected reaction using Ni as a catalyst. By imaging the end product of cyanogen using STM, the fundamental atomic reaction can be better understood.

The Ni surface was promptly imaged after dosing of ethylenediamine at room temperature. Previous studies have shown that at room temperature ethylenediamine adsorbs without dissociation on Ni.[3-6] Between the temperature range of 80-300 K, it is postulated that ethylenediamine is bound to the surface by the lone pair electrons on nitrogen and is not

dehydrogenated.[4,5] No experimental studies that we know of have been carried out on the ordered overlayer of ethylenediamine on Ni or other fcc(111) surfaces. The goal of this experiment was to investigate if an ordered overlayer was formed by imaging.

After imaging at room temperature the sample was annealed. Previous experimental studies have shown that heating ethylenediamine on Pt to temperatures above 445 K result in its complete dehydrogenation to cyanogen.[4,5] STM images were taken to verify the expected ordered overlayer of cyanogen. Cyanogen has a (6×6) ordered overlayer on Ni.[7]

7.3 Experimental Section

Ethylenediamine (99.5%, Sigma-Aldrich), a liquid at room temperature, was subjected to several "freeze-pump-thaw" cycles to purify the chemical. The crystal was approximately 9 mm in diameter and 1.5 mm thick. The size and morphology of molecular species were studied using a variable temperature STM (UHV 300 VT-STM, RHK Technology, Inc). Auger Electron Spectroscopy (AES, PHI model 10-155, single pass CMA) was used to identify and quantify surface atoms. STM imaging was used to observe atomic morphology of the reactants on the surface. All STM images were obtained in constant current mode with tunneling currents of 1-2 nA and a typical bias voltage of 0.5 V applied to the tip.

Before each experiment the Ni crystal was cleaned by multiple cycles of Argon bombardment (Table 1). Ion bombardment (ISE-10, Omicron) was used to clean the surface from elements that cannot be removed by oxygen cleaning, such as sulfur. Each cycle was marked by the annealing of the sample which produces a smooth surface with sharp step edges. The samples were heated and annealed by using electron bombardment (e-beam) heating by a tungsten filament approximately 2 mm below the sample. The temperature was monitored using a chromel-alumel thermocouple sitting on the sample.

The chamber was backfilled with ethylenediamine vapor exposing the sample to 3 Langmuir (1 Langmuir = 1×10^{-6} Torr s). 3 L was chosen as previous studies have indicated that high doses are not required to form cyanogen on Pt(111).[5] The sample was imaged at room temperature. The sample was exposed to the following temperatures: 400K, 450K and 500K. A previous study found that cyanogen was formed by 445 K.[5] At each temperature stage, STM imaging was completed. The z-dimension of the STM images were recalibrated using the step height on the Ni crystal at 2.3 Å.[8-11]

7.4 Results and Discussion

AES and STM confirmed a clean surface with flat terraces and sharp step edges as illustrated in Figure 7.1. The average terrace width was 100 nm. Ethylenediamine was then introduced for adsorption onto the Ni(111) surface at room temperature. The resultant surface was analyzed using STM.

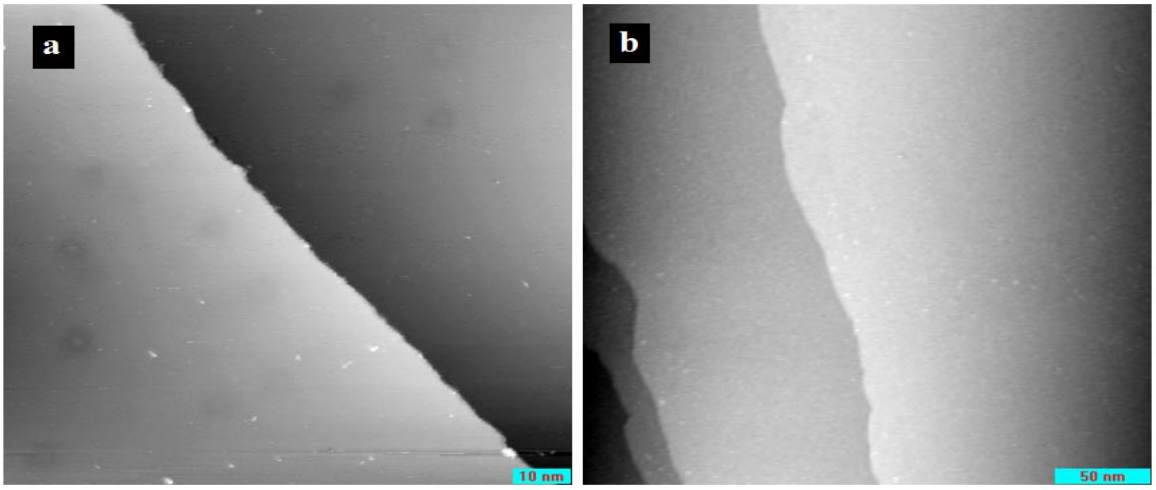

Figure 7.1 STM images of clean Ni(111) a) 1 µm × 1 µm and b) 500 nm × 500 nm.

No ordered structure or repeating pattern was observed, as seen in Figure 7.2. It is possible that other parameters (e.g. lower gas exposure) or other chemicals such as silver cyanide are needed to create a cyanogen. It is also possible that Ni itself is not a good catalyst for this

specific reaction. Other studies that have successfully made cyanogen have indeed used silver cyanide as a reactant, albeit on different catalysts.[7,8] This experiment was unsuccessful in creating cyanogen. This may be due to numerous factors explained herein. Imaging was difficult and thus the end product was all together not discernible.

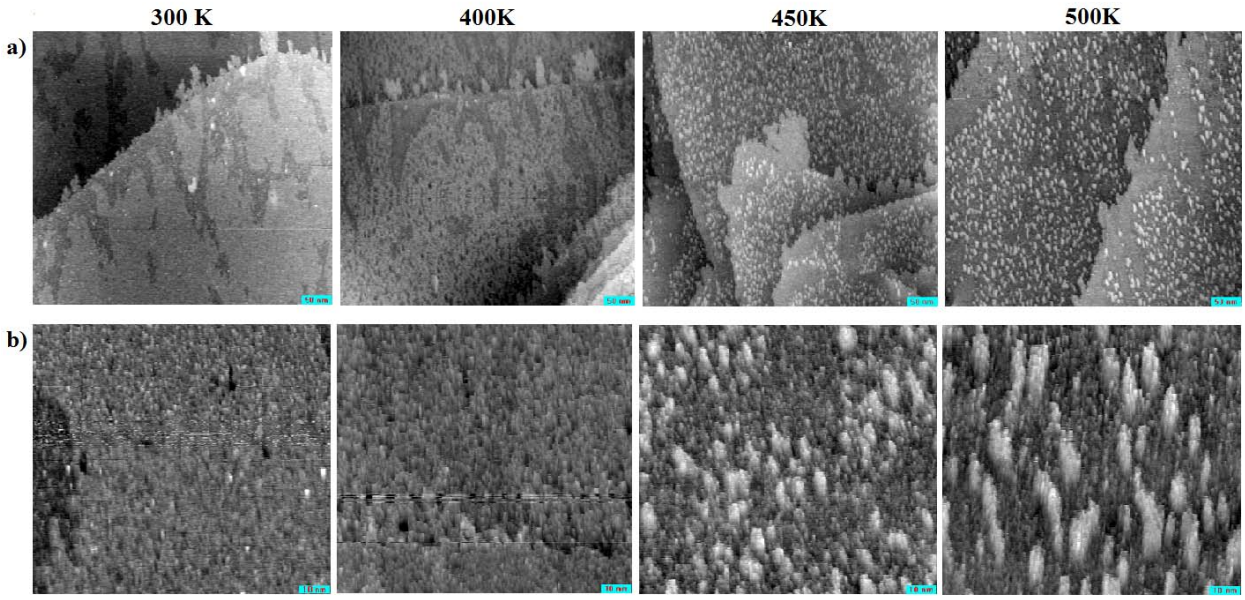

Figure 7.2 STM images of ethylenediamine on Ni(111) increasing in temperature. a) is a 500 nm × 500 nm image and b) is a 100 nm × 100 nm image.

7.5 Conclusion

The ethylenediamine experiment was unsuccessful in creating cyanogen. This may be due to numerous factors explained herein. Imaging was difficult and thus the end product was all together unidentifiable.

7.6 References

(1) Balamurugan, R.; Sundarrajan, S.; Ramakrishna, S., *Recent Trends in Nanofibrous Membranes and Their Suitability for Air and Water Filtrations.* Membranes. **1**(3): p. 232.

(2) Kingsley, J. R.; Dahlgren, D.; Hemminger, J. C., *Coadsorption Chemistry Of H-2 And C2n2 On Pt(111) - A Common Intermediate In The Hydrogenation Of Cyanogen And The Dehydrogenation Of Ethylenediamine On Pt(111).* Surface Science, 1984. **139**(2-3): p. 417.

(3) Kishi, K.; Ehara, Y., *Interaction of acetic acid with ethylenediamine on a Ni(111) surface studied by XPS.* Surface Science, 1986. **176**(3): p. 567.

(4) Kang, D. H.; Trenary, M., *Surface chemistry of ethylenediamine (NH2CH2CH2NH2) on Pt(111).* Surface Science, 2000. **470**(1-2): p. L13.

(5) Lindquist, J. M.; Ziegler, J. P.; Hemminger, J. C., *Photoelectron spectroscopy studies of the hydrogenation of cyanogen on Pt(111): Comparison with HCN and ethylenediamine.* Surface Science, 1989. **210**(1-2): p. 27.

(6) Kishi, K.; Ikeda, S., *X-Ray Photoelectron Spectroscopic Study For The Adsorption Of Acetic-Acid And Ethylenediamine On Iron And Nickels.* Applied Surface Science, 1980. **5**(1): p. 7.

(7) Hemminger, J. C.; Muetterties, E. L.; Somorjai, G. A., *A coordination chemistry study of a nickel surface. The chemistry of nickel (111) with triply bonded molecules.* Journal of the American Chemical Society, 1979. **101**(1): p. 62.

(8) Van De Walle, G. F. A.; Van Kempen, H.; Wyder, P.; Flipse, C. J., *Scanning tunneling microscopy and (scanning) tunneling spectroscopy on stepped Ni(111)/H.* Surface Science, 1987. **181**(1-2): p. 27.

(9) Johanek, V.; De la Ree, A. B.; Hemminger, J. C., *Scanning Tunneling Microscopy Investigation of the Conversion of Ethylene to Carbon Clusters and Graphite on Pt(111).* Journal of Physical Chemistry C, 2009. **113**(11): p. 4441.

(10) Terada, S.; Yokoyama, T.; Saito, N.; Okamoto, Y.; Ohta, T., *Growth and moiré superstructure of palladium films on Ni(111) studied by STM.* Surface Science, 1999. **433-435**: p. 657.

(11) Cao, G. X.; Nabighian, E.; Zhu, X. D., *Diffusion of hydrogen on Ni(111) over a wide range of temperature: Exploring quantum diffusion on metals.* Physical Review Letters, 1997. **79**(19): p. 3696.

CHAPTER 8

Conclusion

8.1 Summary of the Thesis

This thesis has provided a morphological analysis of the formation of the model catalyst system $Pt/Al_2O_3/NiAl(110)$. A fundamental understanding about the interaction of various olefins on $Pt/Al_2O_3/NiAl(110)$ has been elucidated. These results have been compared to thermal dehydrogenation studies of olefins on a Pt(111) single crystal. The morphology of the sample surfaces were studied using scanning tunneling microscopy (STM).

We formed Al_2O_3 thin films which stabilize and support Pt nanoparticles. Al_2O_3 thin films were created by dosing a clean NiAl(110) single crystal with 1200 Langmuir of oxygen at 550 K (1 Langmuir = 10^{-6} Torr s) for 10 minutes. The sample was then annealed at 1200 K for 10 minutes. STM imaging revealed a patchy oxide film that contained areas of both amorphous and crystalline Al_2O_3. The annealing temperature was critical to forming a crystalline thin film. Higher annealing temperatures resulted in loss of the oxide layer, while lower temperatures resulted in an amorphous oxide surface. Imaging of the crystalline layer inferred two directional domain boundaries running 24^o from each other. The average terrace width for the domain boundaries was 60 Å. The step height between crystallized oxide layers was observed at 2.5 Å. Dosing olefins at various temperatures to the bare alumina did not result in any change to the surface.

A model catalyst system of Pt/Al_2O_3 was created by evaporating Pt onto the Al_2O_3 thin film at room temperature for 1 minute with a deposition flux of 1200 nA. The sample was then annealed to 770 K for 5 minutes. STM studies elucidated the size, shape, and binding pattern of the Pt nanoparticles. The Pt nanoparticles selectively bind to the crystalline Al_2O_3. The Pt

particles were evenly spread, without any binding preference to surface defects such as step edges or domain boundaries. We found that the Pt nanoparticles were flat and circular with an average width of 13 ± 3.1 Å and an average height of 2.1 ± 0.64 Å. Annealing up to 1100 K did not change the binding arrangement, size, or shape of the Pt particles.

Olefins dosed onto the model catalysts $Pt/Al_2O_3/NiAl(110)$ and Pt(111) were studied and compared using STM imaging. In previous research in our lab, it was found that ethylene heated to 700 K on Pt(111) produces flat, circular carbon clusters that were 7-13 Å in range of width.[1] The clusters formed without preference for step edges or terraces.[1,2] Further dosing/annealing cycles did not produce larger particles.[1,2] Heating the clusters to 1000 K on Pt(111) produces graphite.[1,2] We found that propylene and butylene behave in a similar manner to ethylene in that upon heating, they form flat, circular, and uniform particle clusters that were 12 ± 1.2 Å and 13 ± 1.0 Å in diameter, respectively. The size difference between the dehydrogenated ethylene, propylene, and butylene clusters is not significant and may only correspond to tip-sample convolution. The carbon particles are very similar in size, indicating that there is a preferential formation size for carbon particles on Pt. The carbon particles are consistent with graphite.

The Pt(111) results were compared to Pt nanoparticles on Al_2O_3. Ethylene was dosed at room temperature over the $Pt/Al_2O_3/NiAl(110)$ and then annealed to 1000 K. The thermally dehydrogenated ethylene covered the Pt nanoparticles and grew from a pre-dosing value of 13 ± 3.1 Å to a maximum of 20 Å. Particle density did not increase at annealing temperature of 1000 K. By increasing the ethylene dosing temperature to 1000 K and annealing to 1100 K, the density of particles increased. The particle diameter on average was 20 ± 2.0 Å. These particles are similar in shape and size to the particles formed on the Pt single crystal. The new particles formed along the boundary between the crystalline and amorphous oxide layer. This behavior is

similar to what was previously seen in our lab with ethylene dehydrogenation on Pt single crystal, where with temperatures above 1100 K the carbon clusters and graphite moved to the step edges.[1] We found that with continued ethylene dosing/annealing cycles on Pt/Al_2O_3 the crystalline oxide layer became fully covered with very little spacing between particles. Unlike with the Pt single crystal, graphite is never formed on the Al_2O_3. We hypothesize that the interaction between the C-C bond may be stronger than the C-alumina bond, preventing the carbon particles from separating into graphite on Al_2O_3. While with the Pt single crystal the C-Pt bond is stronger, allowing for the carbon cluster to essentially fall apart and wet the metallic Pt surface as graphene. Furthermore, we hypothesize that the following pathway occurs. Ethylene binds to the Pt particles at room temperature and upon heating to 1100 K the Pt nanoparticles activate the decomposition of the ethylene and cause a spill-over of carbon onto the alumina surface. The carbon is then mobile enough to aggregate to the step edges.

8.2 Future Work

The experiments described within this thesis have led to many exciting fundamental property questions. Studying the model catalysts Pt(111) and $Pt/Al_2O_3/NiAl(110)$ can provide elemental knowledge that may help improve theoretical studies and the formation of nanotechnology. A wise proverb states that *hindsight vision is always 20/20*. In hindsight the experiments described herein can be enhanced and expanded as described below:

1) It is advantageous to improve the Al_2O_3 support by trying to create a surface free of the patchy, amorphous oxide. This will allow for more surface area to study. Furthermore, the carbon particle binding to step edges between the crystalline and amorphous layers may be due to some inherent property between the two. *Kulawik, et al.* found that by performing a second cycle of oxidation, all of the patchy areas were filled with crystalline Al_2O_3.[3]

2) In future studies, larger Pt particles may provide for a better catalytic activity. It was found that when Pt nanoparticles are less than 18 Å, their catalytic capability is lowered when oxidizing methanol and formic acid.[4] Specifically, this study found that in terms of catalytic activity, Pt(111) was more active than Pt nanoparticles of any size.[4] Possibly larger Pt nanoparticles may help produce graphite with olefin dehydrogenation. It would be interesting to determine size dependency of olefin reaction on Pt nanoparticles.

3) We could utilize other techniques available in our lab and collaborate with a theoretical group to simulate anticipated reactions. Low-energy electron diffraction (LEED) coupled with theoretical simulations can elucidate the structure of the Pt nanoparticles and their bonding to the Al_2O_3 surface.

4) We could consider continued dosing of olefins onto the Pt nanoparticles to provide for a more comprehensive comparison to our previous studies on Pt(111).

5) Finally, other metal catalysts should also be studied in a similar manner as performed herein to determine a pattern for olefin thermal dehydrogenation over both nanoparticles and single crystals.

8.3 References

(1) Land, T. A.; Michely, T.; Behm, R. J.; Hemminger, J. C.; Comsa, G., *STM investigation of the adsorption and temperature dependent reactions of ethylene on Pt(111).* Applied Physics A: Materials Science & Processing, 1991. **53**(5): p. 414.

(2) Johanek, V.; De la Ree, A. B.; Hemminger, J. C., *Scanning Tunneling Microscopy Investigation of the Conversion of Ethylene to Carbon Clusters and Graphite on Pt(111).* Journal of Physical Chemistry C, 2009. **113**(11): p. 4441.

(3) Kulawik, M.; Nilius, N.; Rust, H. P.; Freund, H. J., *Atomic Structure of Antiphase Domain Boundaries of a Thin Al2O3 Film on NiAl(110).* Physical Review Letters, 2003. **91**(25): p. 256101.

(4) Rhee, C. K.; Kim, B.-J.; Ham, C.; Kim, Y.-J.; Song, K.; Kwon, K., *Size Effect of Pt Nanoparticle on Catalytic Activity in Oxidation of Methanol and Formic Acid: Comparison to Pt(111), Pt(100), and Polycrystalline Pt Electrodes.* Langmuir, 2009. **25**(12): p. 7140.